

COMPUTER AIDED ANALYSIS OF PERIODIC SOLUTIONS IN
TWELVE-PULSE HVDC CONVERTERS :
A SEMI-ANALYTICAL APPROACH

by

GERALD ROGER BÉRUBÉ, B.Eng. (McGill University)

A thesis submitted to the Faculty of Graduate
Studies and Research in partial fulfillment
of the requirements for the degree of
Master of Engineering

Department of Electrical Engineering,
McGill University
Montreal, Canada.

© August, 1982

COMPUTER AIDED ANALYSIS OF HVDC CONVERTERS

ABSTRACT

The twelve-pulse bridge converter is treated as a piece-wise linear network, allowing for the use of linear circuit theory in its analysis. Explicit solutions are obtained for the converter operating in a variety of different modes, as specified by the valve commutation angles. The complexities of the final mathematical formulations are greatly reduced by fully exploiting a number of properties of the time-varying topology including: periodicity in T , transposed periodicity in $T/6$, and balanced three-phase symmetrical AC network components.

Based on these equations a digital algorithm is developed which converges rapidly on the steady-state solution. Post-processing routines are produced which render this method a useful tool in the design and analysis of the twelve-pulse converter.

RESUME

La théorie des circuits linéaires permet l'analyse de convertisseurs à douze impulsions, dont les paramètres sont continus et à segments linéaires.

Des solutions explicites sont obtenues pour le convertisseur opérant dans plusieurs modes en fonction des angles de commutation des valves.

Les complexités de la formulation mathématique sont grandement réduites lorsque les propriétés simplificatrices suivantes sont exploitées: la périodicité en T , la périodicité transposée en $T/6$, et la symétrie du circuit triphasé équilibré.

De ces équations, un algorithme est construit qui converge rapidement vers la solution en régime permanent.

Des programmes utilisant cette méthode sont développés pour l'analyse détaillée du convertisseur à douze impulsions.

ACKNOWLEDGEMENTS

The author wishes to express his gratitude to Dr.B.T. Ooi for his constant supervision. His enthusiasm and friendly attitude have been inspirations during the course of this work.

The author wishes also to thank Dr.H.Banakar for his helpful suggestions and encouragement.

Thanks are also due to Mr.R.Zhen for proof-reading the thesis and helping in making corrections.

Finally I wish to thank my parents for their continual support, patience and understanding.

TABLE OF CONTENTS

	<u>Page</u>
ABSTRACT	i
RESUME	ii
ACKNOWLEDGEMENTS	iii
TABLE OF CONTENTS	iv
NOMENCLATURE	vi
CHAPTER 1 INTRODUCTION	1
1.1 History of HVDC Systems	1
1.2 Basic Graetz Bridge Configuration	2
1.3 Overview of Digital Analysis Methods Applied to Switching Circuits	3
1.4 Thesis Justification and Outline	4
CHAPTER 2 BASIC CONVERTER OPERATION	7
2.1 Introduction	7
2.2 Operation of Graetz Bridge Circuit	7
2.2.1 Delay Angle	9
2.2.2 Commutation Angle	9
2.2.3 Typical Output Waveforms	10
2.3 Multibridge Connections	12
2.3.1 DC Line Voltage	13
2.3.2 AC Phase Currents	15
2.4 Harmonic Analysis of Bridge Converter Waveforms	20
2.4.1 Analysis of DC Line Voltage	20
2.4.2 Analysis of AC Phase Currents	22
2.5 Summary	26
CHAPTER 3 NETWORK ANALYSIS OF TWELVE-PULSE CONVERTER	27
3.1 Introduction	27
3.2 Digital Representation of Converter Valves	29
3.3 Network Model of Twelve-Pulse Converter	30
3.4 Linear Circuit Analysis	31
3.5 Properties of Periodic Solution in Periodically Triggered Three-Phase Bridge Configurations	32
3.5.1 Periodicity in T	33
3.5.2 Periodicity in T/6	33
3.6 State Analysis Applied to Piece-Wise Linear Problems	34
3.6.1 Iterative Determination of Initial Conditions	37
3.6.2 Closed-Form Solution	37
3.6.3 Unknown Boundaries in Closed-Form Solution	41

3.7	Application of T/6 Periodicity Property	42
3.8	Summary	43
CHAPTER 4	FORMULATION OF SOLUTION ALGORITHMS	45
4.1	Introduction	45
4.2	Classification According to Commutation Angles	46
4.3	Selection of State Variables for Sub-Networks	51
4.3.1	Case 1, $\omega\mu_2 < 30^\circ$	51
4.3.2	Case 2, $30^\circ \leq \omega\mu_2 < 60^\circ$	58
4.4	Solution Algorithm. Case 1	59
4.4.1	Case 1(i), $\omega\mu_1 < 30^\circ$	59
4.4.2	Case 1(ii), $30^\circ \leq \omega\mu_1 < 60^\circ$	66
4.5	Solution Algorithm. Case 2	69
4.5.1	Case 2(i), $\omega\mu_1 < 30^\circ$	69
4.5.2	Case 2(ii), $30^\circ \leq \omega\mu_1 < 60^\circ$	74
4.6	Determination of Commutation Times	75
4.7	Summary	76
CHAPTER 5	OUTPUT IN TIME AND FREQUENCY DOMAIN	78
5.1	Introduction	78
5.2	Time Domain Output	79
5.3	Frequency Domain Output	80
5.3.1	Calculation of Fourier Coefficients in Piece-Wise Linear Problem	81
5.3.2	Application of T/6 Periodicity	83
5.4	Summary	86
CHAPTER 6	SIMULATION EXAMPLES	87
6.1	Introduction	87
6.2	Time Domain Results	87
6.2.1	Converter with Shunt AC Filters	88
6.2.2	Converter with HP AC Filter	95
6.3	Frequency Decomposition of Full Filtering Scheme	99
6.4	Numerical Aspects of Results	102
CHAPTER 7	CONCLUSIONS	104
7.1	Conclusions	104
7.2	Suggestions for Further Investigation	105
BIBLIOGRAPHY		107
APPENDIX 1	FORMATION OF SYSTEM MATRICES AND STATE SOLUTIONS	110
APPENDIX 2	COMPUTER SUBROUTINES	112

NOMENCLATURE

α	Firing delay angle
I_d	DC line current
E_m	Generator peak emf
T	Period
ω	Angular frequency
μ_1	Wye-wye bridge commutation time
μ_2	Wye-delta bridge commutation time
i_{c1}	Wye-wye bridge commutation current
i_{c2}	Wye-delta bridge commutation current
i_a^Y, i_b^Y, i_c^Y	Wye-wye bridge phase currents
$i_a^\Delta, i_b^\Delta, i_c^\Delta$	Wye-delta secondary bridge line currents
i_x, i_y, i_z	Wye-delta bridge winding currents
v_{dy}	Wye-wye bridge output voltage
$v_{d\Delta}$	Wye-delta bridge output voltage
k	Harmonic order index
θ	Delay angle incorporated in source emf modelling
R_{T1}, L_{T1}	Wye-wye transformer impedance
R_{T2}, L_{T2}	Wye-delta transformer impedance
R_{HP}, L_{HP}, C_{HP}	High-pass filter impedances
R_{11}, C_{11}, L_{11}	11-th harmonic tuned filter impedances
R_{13}, C_{13}, L_{13}	13-th harmonic tuned filter impedances
n	Sub-interval index
N	Total number of sub-intervals encountered in one period of operation

$\underline{x}_n(t)$	State vector for n-th sub-network
$[A_n]$	Constant coefficient matrix of the system of linear differential equations for n-th sub-network
$[B_n]$	Constant coefficient matrix of the system of linear differential equations for n-th sub-network
$[\Phi_n(t)]$	State transition matrix for n-th sub-network
$\underline{\xi}_n$	Vector of integration constants for n-th sub-network
$\underline{x}_n^{ZSR}(t), \underline{x}_n^s(t)$	Zero-state response for n-th sub-network
$[C_n]$	Compatibility matrix
\underline{R}	Intermediate result vector in analytical formulation of initial condition vector
$[S]$	Intermediate result matrix in analytical formulation of initial condition vector
\underline{F}	Final result vector derived in formulation of initial condition vector
$[G]$	Final result matrix derived in formulation of initial condition vector
$[I]$	Identity matrix
$[P_{ij}]$	Partition of state transition matrix for first sub-network
$[Q_{ij}]$	Partition of state transition matrix for third sub-network
$[M_{ij}]$	Partition of state transition matrix for fifth sub-network
Δ	Step size used in numerical approximations, to derivatives in Newton algorithm

ε Tolerance on maximum admissible value of
 commutation currents evaluated at the iterate
 commutation time values

ABBREVIATIONS

ZIR Zero-input response
ZSR Zero-state response

CHAPTER 1

INTRODUCTION

1.1 History of HVDC Systems

The first practical electric power systems consisted of DC generators connected to lighting loads. Despite this historical precedent direct current was almost entirely replaced by alternating current as the standard mode of electric power generation, distribution and utilization. One of the main reasons for the wider usage of AC power was the lack of a DC counterpart for the transformer. Also the AC machines, and in particular the induction machine, proved more reliable and had wider applicability than machines with commutators.

Recently DC systems have made a resurgence in certain applications including:

- 1) Long transmission lines
- 2) Cable transmission
- 3) Frequency Converters

In these areas AC system implementations have a number of important dis-advantages. The main drawback encountered with AC transmission lines is the need for reactive compensation. The compensation requirements increase with increasing ~~line~~ length thus setting practical limitations on the distances across which AC transmission is possible. The

difficulties associated with attaching shunt compensators to underground or underwater cables make AC connections impractical for these transmission applications.

The solution to both these problems is found in the interconnection of AC systems through AC/DC converters to DC transmission lines. DC lines do not suffer from the same problems as the AC lines and are therefore better suited for many transmission applications.

Recent developments which have led to higher power capabilities in thyristors, make the DC transmission alternative more attractive.

1.2 Basic Graetz Bridge Configuration

The Graetz Bridge is used for the bulk of three-phase AC to DC conversion. The basic valve connection is shown in Fig. 1.1(a) with the standard symbol for the bridge shown in Fig. 1.1(b).

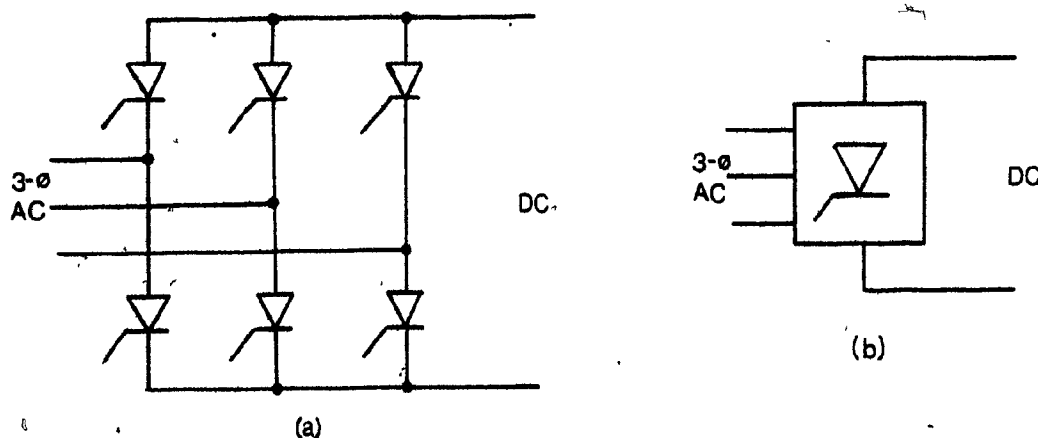


FIGURE 1.1 (a) Valve connection of Graetz Bridge Circuit
(b) Symbol for Graetz Bridge Circuit

Whereas in AC systems limitations are set by the transmission lines and the need for reactive compensation, in DC systems the converters pose the main restrictions. Two of the chief concerns involved in the design of these converters is their varying reactive power requirements and the limited over-voltage and over-current capabilities of the valves.

1.3 Overview of Digital Analysis Methods Applied to Switching Circuits

Because the DC converters set limitations on the overall operation of the DC transmission systems, it is important to gain a full understanding of their characteristics. In the past, the bulk of research done on the operation of the HVDC converters made use of analog simulation techniques [1-5]. More recently however, studies have been directed towards making the digital computer a more useful tool in the simulation of HVDC system operation.

Numerous papers dedicated to HVDC systems and converter circuits [6-15] have been chiefly interested in the valve modelling and the computer-aided automatic compilation of the network topologies produced using these models. The system differential equations produced by these methods have been solved using numerical integration. In general these programs are flexible in terms of allowing the study of transient and faulted conditions. Unfortunately, the solution methods used are time consuming and expensive when

applied to problems requiring convergence on steady state solutions.

A number of authors have presented papers which describe the achievement of analytical descriptions for switching network problems. In 1971 Lipo [16] produced a paper outlining an algorithm used in the study of a thyristor speed control for an induction motor. An analytical solution to the problem was achieved, through the use of state space techniques. Similar methods were used in the formulations included in a paper presented in 1972 by Liou [17] dealing with networks containing periodically operated switches.

Based on these general techniques, Ooi, Menemenlis and Nakra [18] studied the steady-state operation of a six-pulse inverter acting as a series tap.

1.4 Thesis Justification and Outline

This thesis is a presentation of the continuing work based on the paper [18] "Fast Steady-State Solution for HVDC Analysis" by Ooi, Menemenlis and Nakra, and the thesis "A Semi-Analytical Method for Steady-State Solution in HVDC Analysis" [21] by N. Menemenlis. The results developed for the six-pulse converter, while dramatically demonstrating the advantages of the piece-wise linear formulation, have limited practical applications. Because of the more extensive utilization of twelve-pulse converters, the

material presented in this thesis has much wider applicability.

The introduction of a second bridge, and therefore a second independent commutation time leads to a number of problems not encountered in the analysis of the six-pulse bridge. The topics discussed in this thesis include:

Chapter 2 presents an outline of the operating characteristics of the six-pulse and twelve-pulse bridge. Included in this chapter is a discussion of the winding current distributions in the converter transformers during the twelve-pulse converter operation. A harmonic analysis of the converter waveforms is used to compare the six- and twelve-pulse systems.

Chapter 3 demonstrates how the converter simulation may be treated as a piece-wise linear problem. The use of network analysis and the linear state description in the solution of piece-wise linear problems is then described. The symmetries of the network configuration and desired solution are exploited in reducing the manipulations required to achieve the final result.

Chapter 4 presents the actual network configurations and algorithms required to determine the solution. It is demonstrated that the algorithms required are functions of the commutation times and therefore must be selected concurrent with the solutions. The numerical techniques required to solve the final non-linear equations are also described.

Chapter 5 describes the manner in which the results of the algorithms of Chapter 4 may best be presented to convey the most information pertaining to the system operation. Included in this chapter is a derivation of the equations yielding the Fourier coefficients for state variable solutions in piece-wise linear problems. These equations are used to generate a frequency description of the converter currents for varying operating conditions.

Chapter 6 presents results based on the algorithms of the previous two chapters. Frequency and time domain output are presented as well as numerical information pertaining to the computer programs.

CHAPTER 2

BASIC CONVERTER OPERATION

2.1 Introduction

The analysis of converter circuits is well documented [22] and in particular, the application of three-phase bridge converters in HVDC systems has been the subject of extensive study [23]. This chapter, therefore, is not intended to serve as an extensive review of the operation of these converters. Instead, it will introduce the reader to common network configurations, waveforms, and nomenclature associated with the Graetz Bridge Circuit. Particular attention is paid to multi-bridge converters. Fourier Series analysis is applied to demonstrate the motivation behind their common use.

2.2 Operation of Graetz Bridge Circuit

Fig. 2.1 illustrates a six pulse Graetz Bridge connection. The AC side of the bridge is connected to a balanced three-phase sinusoidal generator. The positive sequence line-to-neutral emfs of the wye connected machine are,

$$\begin{aligned}
 e_a(t) &= E_M \sin(\omega t + \pi/6) \\
 e_b(t) &= E_M \sin(\omega t - \pi/2) \\
 e_c(t) &= E_M \sin(\omega t + 5\pi/6)
 \end{aligned}
 \tag{2.1}$$

where E_M is the generator peak voltage and ω is the angular frequency.

The generator sub-transient inductance and transformer leakage inductance are lumped together and shown as L . Stator and transformer winding resistances are omitted in the analysis of this section.

The DC line side of the bridge is modelled as a constant DC current source I_d .

The six controlled valves which make up the bridge are numbered in the relative order in which they receive gate pulses. This firing sequence produces:

- 1) positive-sequence balanced distribution of currents on the AC side
- 2) DC line open circuit voltage consisting of six identical sections of the line-to-line emfs.

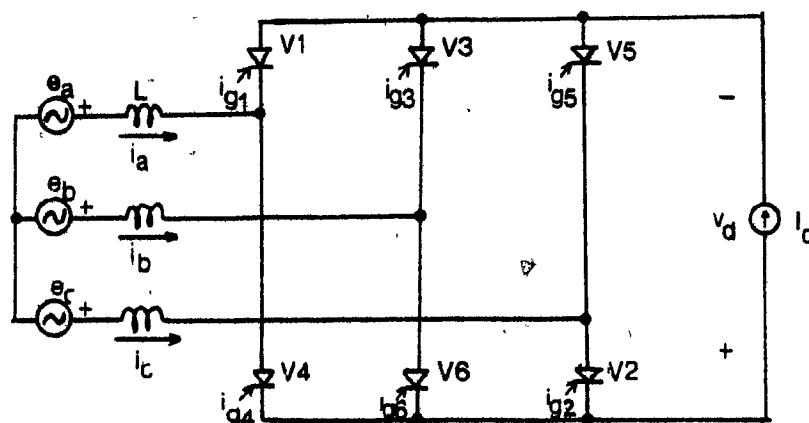


FIGURE 2.1 Six-pulse Graetz Bridge connection

2.2.1 Delay Angle

If the valves receive gate pulses at the instant they are forward biased the fundamental component of the stator phase currents will be exactly in phase with the generator emfs. To allow for the control of the bridge power factor, the valves gating signals may be delayed. For a delay angle between forward biasing and valve firing, denoted α , in the range $0^\circ < \alpha < 90^\circ$ real power is transferred from the AC side to the DC side and the bridge acts as a rectifier. For a delay angle, $90^\circ < \alpha < 180^\circ$, real power is delivered to the AC circuit by the DC line. In this mode the bridge acts as an inverter. Under both conditions the bridge absorbs reactive power.

2.2.2 Commutation Angle

Conducting valves are blocked by voltage line commutation. A valve is reverse-biased when another valve in the same row of the bridge is fired. For instance in Fig. 2.1 V1 is commutated when V3 is fired. The current in the commutating valve requires a finite time to reach zero due to the series inductance L through which it flows. This commutation time is denoted by μ with corresponding angle $\omega\mu$. Since the AC network is balanced and the valves receive gate pulses at equally spaced times each valve requires the same amount of time μ to complete its commutation.

In the normal steady state operation of practical bridge networks the commutation angle does not exceed 60° .

Bridge operation with $\omega\mu > 60^\circ$ is considered a faulted condition since line-to-line short circuits exist across both the AC generator and the DC line. The analysis of this thesis will be restricted to studying bridge operation with $\omega\mu < 60^\circ$.

2.2.3 Typical Output Waveforms.

In Fig. 2.2, typical waveforms [24] associated with operation of the bridge of Fig. 2.1 are depicted for a delay angle, $\alpha = 120^\circ$, and a commutation angle in the range $0^\circ \leq \omega\mu < 30^\circ$. The negative value of average direct voltage, V_d , clearly indicates that power is transferred from the DC line to the AC network. This direction of power flow is also implied by the phase relationship between the fundamental components of the stator currents and the three-phase generator emfs.

The flow of current from commutating valves to incoming valves takes place during the angular interval $\omega\mu$. Throughout these intervals the total current carried by each row of the bridge equals I_d . The bridge circuit is sketched in Fig. 2.3 for the first commutation interval where, for clarity, non-conducting valves have been removed from the diagram. Particular emphasis is placed on the current relationship between the incoming and outgoing valve.

Analysis of the Graetz Bridge is further complicated if circuit resistances and shunt elements on the AC side are included in the model. However, if the operating conditions

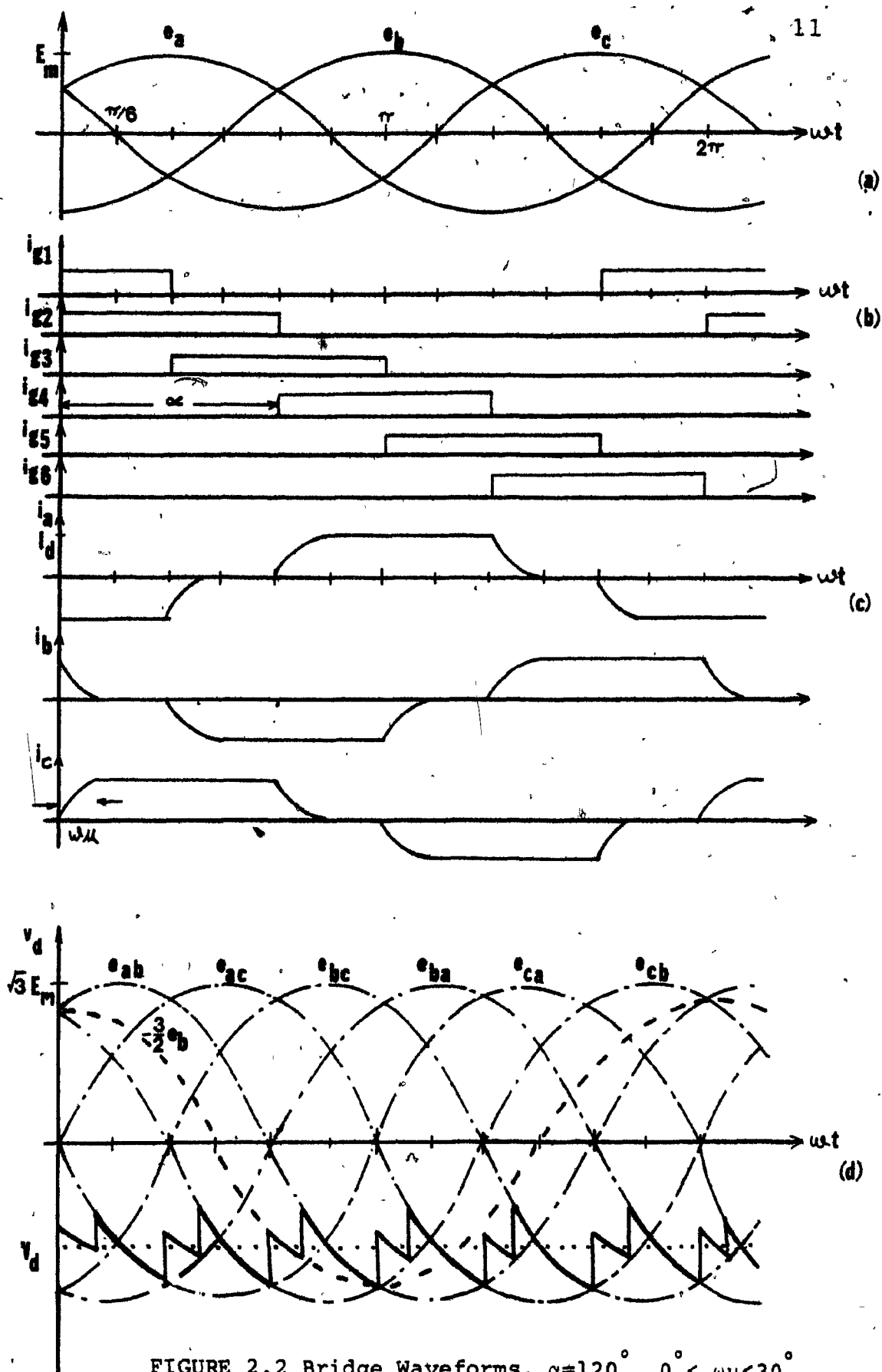


FIGURE 2.2 Bridge Waveforms, $\alpha = 120^\circ$, $0^\circ \leq \omega t < 30^\circ$

- (a) Sinusoidal emfs
- (b) Gate currents
- (c) AC phase currents
- (d) DC Voltage

of the bridge are such that the bulk of the alternating current is carried in the stator phases, Figs. 2.2(c), (d) and 2.3(b) approximately depict the variations of current and voltage in the bridge.

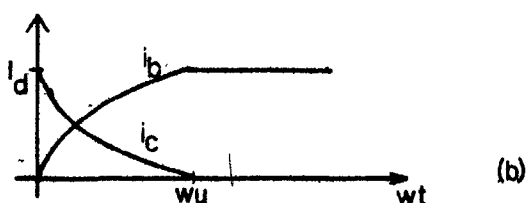
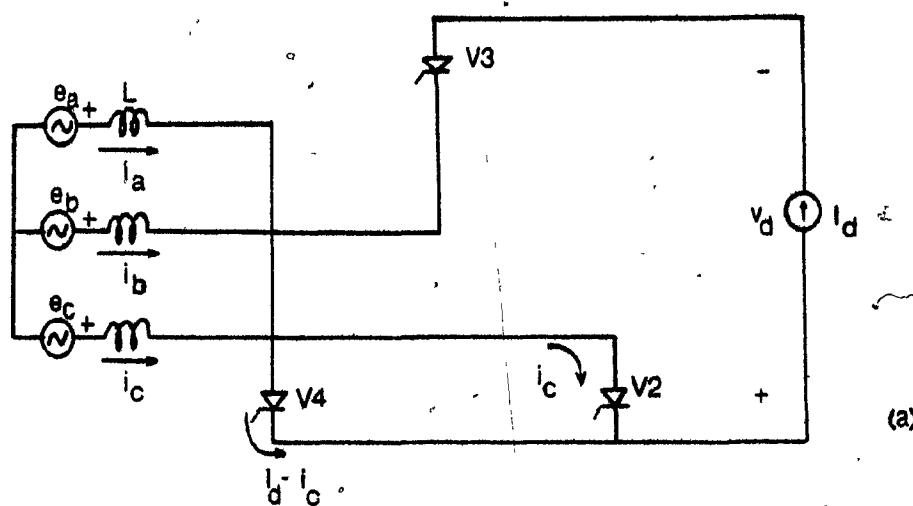


FIGURE 2.3 Valve commutation

- (a) Conducting valves during commutation of V2
 (b) Phase currents i_a and i_c during commutation

2.3 Multibridge Connections

In the converter model of Fig. 2.1 the DC line current is assumed to be completely constant while the AC emfs are modelled as perfect sinusoidal sources. Inspection of Fig. 2.2(c), (d) indicates that even under these operating

conditions the AC stator phase currents are clearly non-sinusoidal while the DC line voltage contains a high ripple content. These conditions indicate high harmonic contents in both the DC line voltage and AC phase currents. Harmonics have a number of undesirable effects including excessive heating in generators and interference on telephone lines. Because of these serious implications two of the chief criteria used in assessing the performance of a particular converter design are:

- 1) ripple or harmonic content of the DC line voltage
- 2) magnitudes of current harmonics with respect to fundamental current in the AC phases.

In HVDC applications multibridge connections are often used to reduce both harmonic contents. These connections consist of pairs of bridges connected in series on the DC side and in parallel on the AC side. While permitting harmonic reduction, the series DC connection also allows for increasing the DC line voltage to transmission levels.

2.3.1 DC Line Voltage

The multibridge configuration to be studied in this thesis is shown in Fig. 2.4. From Fig. 2.5(a), which depicts the phase relationships between the generator emfs and the open circuit secondary line-to-line voltages for the two transformers, it is clear that the wye-delta bridge voltages lead those of the wye-wye bridge by 30° . As the valve gating pulses are referenced with respect to the a,b,c

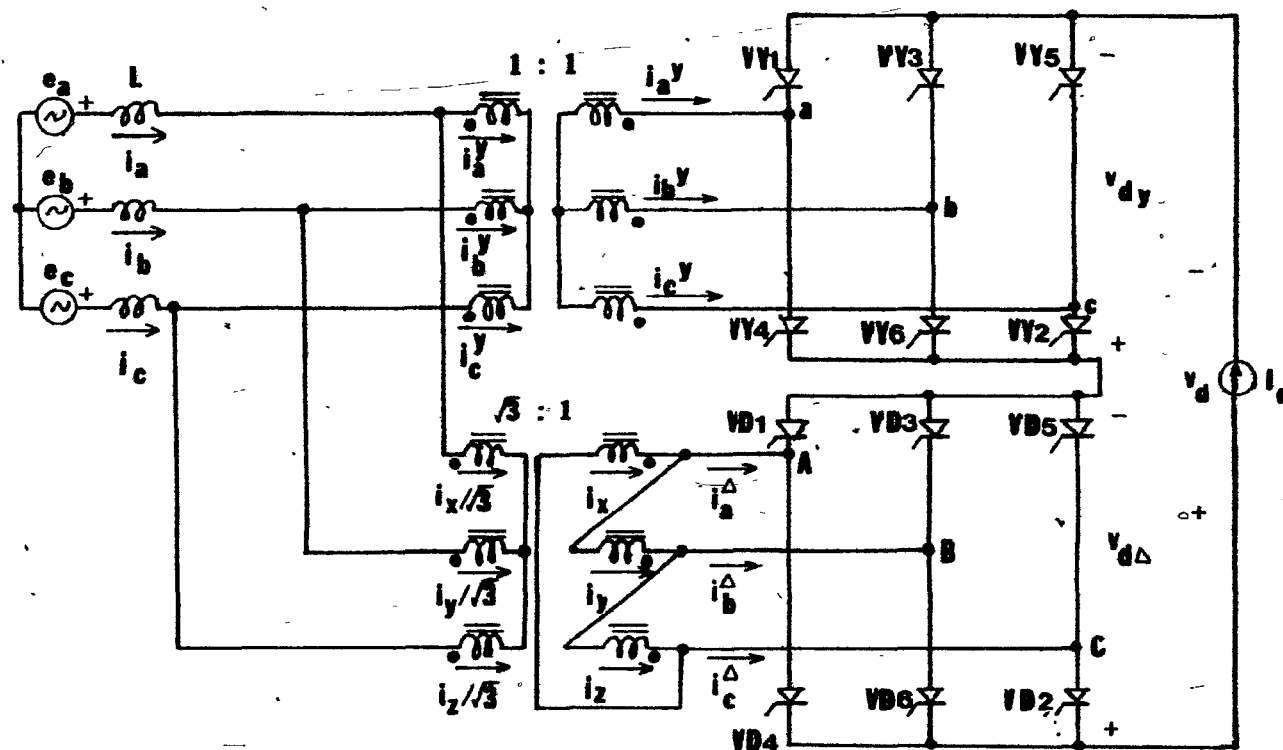
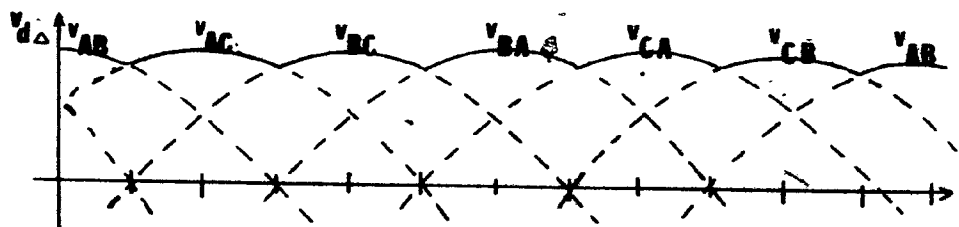
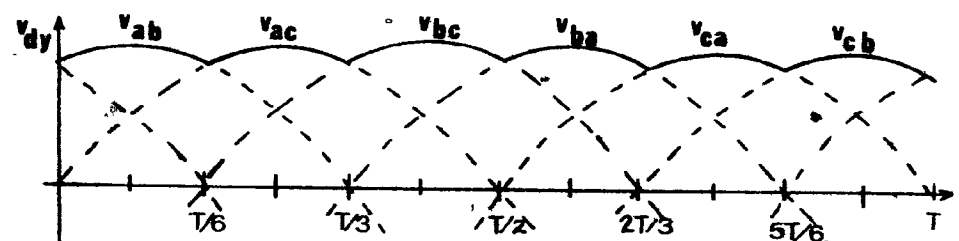
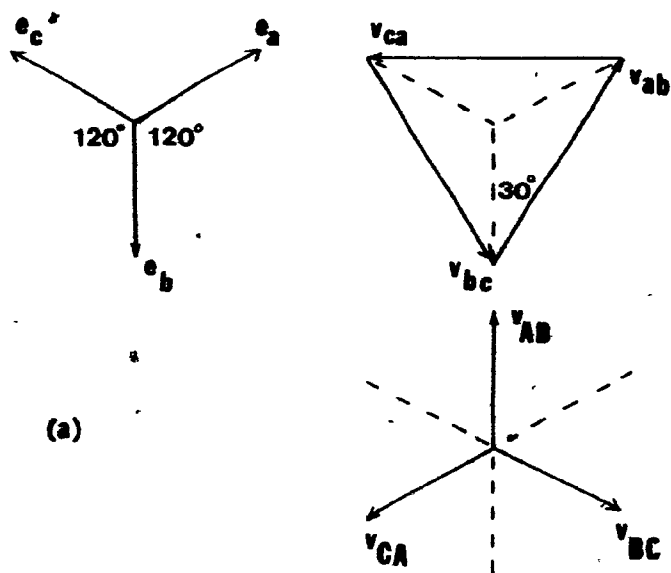


FIGURE 2.4 Twelve-pulse bridge converter

terminal voltages for the upper bridge and to the voltages at terminals A,B,C for the lower bridge, the secondary currents i_a^Δ , i_b^Δ , i_c^Δ and output voltage v_d^Δ are identical to the upper bridge waveforms i_a^Y , i_b^Y , i_c^Y and v_d^Y except advanced by 30° . Fig. 2.5(b) depicts graphically the addition of the DC line voltages of the two bridges, under the operating conditions $\alpha=0^\circ$, $\omega_1=0^\circ$. From Fig. 2.5 it is clear that the $\sqrt{3}:1$ turns ratio of the wye-delta transformer bank is required to match the secondary line-to-line voltage magnitudes for the two bridges. The sum of the two bridge output voltages yields the overall DC line voltage, which consists of twelve identical pulses per cycle. For this reason the multibridge connection of Fig. 2.4 is often referred to as a twelve-pulse converter, while the single Graetz Bridge circuit is known as a six-pulse converter. An exact analysis of the DC voltage ripple for the six and twelve-pulse converters is made in Section 2.4.

2.3.2 AC Phase Currents

Before the overall stator phase currents may be constructed, the wye-delta transformer winding currents i_x , i_y and i_z must be determined. Since the form of the wye-delta bridge currents i_a^Δ , i_b^Δ and i_c^Δ are known, the winding current distribution may be derived [19] by satisfying the dot convention and ampere-turns law for the transformer. The secondary line currents of the wye-delta transformer may be constructed using superposition, from the



(b)

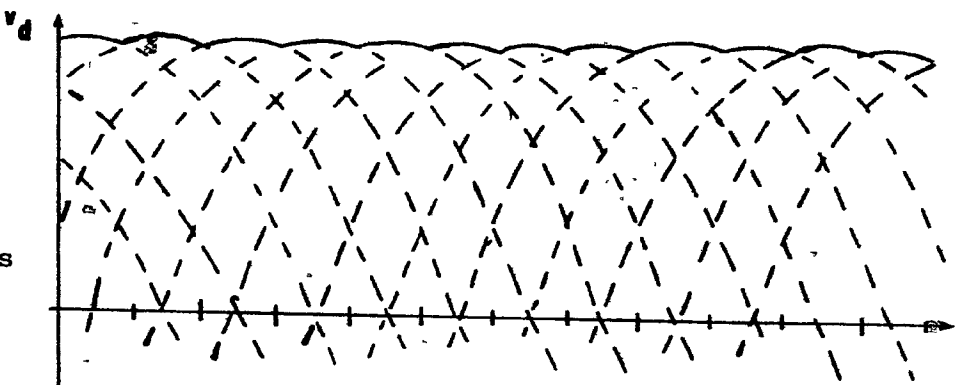


FIGURE 2.5

Twelve-pulse converter bridge voltages

- (a) Phase relationship of open circuit emfs in secondaries of wye-wye and wye-delta transformers
 (b) DC line voltages for wye-wye bridge, wye-delta bridge and overall combination. $\alpha=0^\circ$, $\omega\mu=0^\circ$

three basic distributions given in Table 2.1.

DISTRIBUTION	i_a^Δ	i_b^Δ	i_c^Δ
1	i_Δ	$-i_\Delta$	0
2	$-i_\Delta$	0	i_Δ
3	0	i_Δ	$-i_\Delta$

TABLE 2.1 THREE BASIC SECONDARY LINE CURRENT DISTRIBUTIONS FOR WYE-DELTA TRANSFORMER IN TERMS OF GENERAL CURRENT i_Δ

The equations relating the winding currents and the general current, i_Δ , for the first distribution of Table 2.1 are written as,

$$\begin{aligned} i_x - i_y &= i_\Delta \\ i_x &= i_z \\ (i_x + i_y + i_z) / \sqrt{3} &= 0 \end{aligned} \quad (2.2)$$

where the third equation represents the ampere-turns requirement on the primary side. Manipulating these three equations yields the delta winding current distributions,

$$\begin{aligned} i_x &= i_\Delta / 3 \\ i_y &= -2i_\Delta / 3 \\ i_z &= i_\Delta / 3 \end{aligned} \quad (2.3)$$

The two other winding current distributions may be derived in a similar manner. Table 2.2 lists the winding currents for the three basic cases of Table 2.1.

DISTRIBUTION	i_x	i_y	i_z
1	$i_{\Delta}/3$	$-2i_{\Delta}/3$	$i_{\Delta}/3$
2	$-2i_{\Delta}/3$	$i_{\Delta}/3$	$i_{\Delta}/3$
3	$i_{\Delta}/3$	$i_{\Delta}/3$	$-2i_{\Delta}/3$

TABLE 2.2 DELTA WINDING CURRENTS FOR THE THREE SECONDARY LINE CURRENT DISTRIBUTIONS OF TABLE 2.1

Given the constraints of Table 2.1 on the delta line currents a general relation for the winding currents may be derived. These equations are written in matrix form as,

$$\begin{bmatrix} i_x \\ i_y \\ i_z \end{bmatrix} = \begin{bmatrix} 1 & 2/3 & 1/3 \\ 1/3 & 1 & 2/3 \\ 2/3 & 1/3 & 1 \end{bmatrix} \begin{bmatrix} i_a^{\Delta} \\ i_b^{\Delta} \\ i_c^{\Delta} \end{bmatrix} \quad (2.4)$$

To illustrate the use of Eqn. 2.4 in determining the winding current distribution during normal bridge operation, a typical conduction interval will be studied. Fig. 2.6(a) illustrates the conduction interval involving valves VD3 and VD4 where the winding distribution is determined by substitution of,

$$i_a^{\Delta} = I_d, \quad i_b^{\Delta} = -I_d$$

into Eqn. 2.4.

Fig. 2.6(b) shows the flow of commutation current between valves VD3 and VD5. Eqn. 2.2 is employed with,

$$i_c^{\Delta} = i_{com}, \quad i_b^{\Delta} = -i_{com}$$

Combining these two cases, using superposition, yields the operating conditions for the wye-delta transformer during the commutation of valve VD3 by valve VD5. This overall distribution is shown in Fig. 2.6(c).

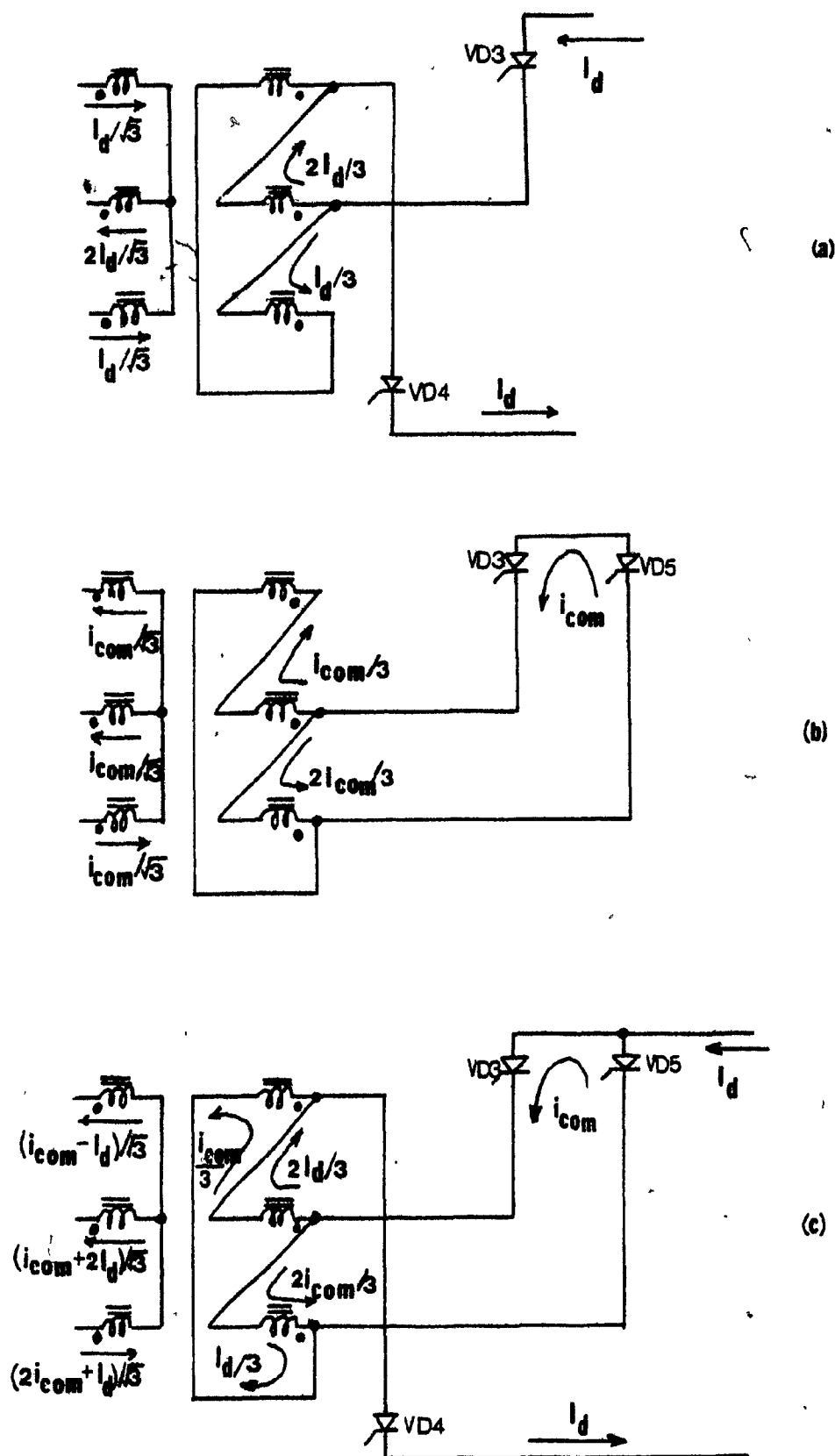


FIGURE 2.6 Application of superposition in determination of delta bridge winding currents

- (a) Current distribution with VD3, VD4 conducting
- (b) Commutation current distribution for VD3 commutating
- (c) Overall current distribution during commutation sub-interval

By following this procedure, the delta bridge primary currents are determined for an entire period and are sketched in Fig. 2.7(a). The wye-wye bridge primary currents shown in Fig. 2.7(b) are added to the wye-delta currents to yield the overall stator currents, sketched in Fig. 2.7(c). The resultant alternating currents achieved using this connection approximate the desired sinusoidal distribution better than the AC currents of a single Graetz Bridge.

2.4 Harmonic Analysis of Bridge Converter Waveforms

To evaluate the exact effect the 12-pulse converter connection has on reducing AC and DC harmonic content, Fourier Series analysis is employed. The Fourier coefficients for the DC line voltage and AC stator phase currents are calculated for both the six and twelve-pulse configuration with operating conditions, $\omega\mu = 0^\circ$ and $\alpha = 0^\circ$. The coefficients derived under these operating conditions are the simplest to evaluate and allow for a useful comparison of the characteristics of the two connections. The effect of commutation overlap and firing delay on the DC voltage and AC current harmonics will be discussed qualitatively at the end of the section.

2.4.1 Analysis of DC Line Voltage

The Fourier series describing the wye-wye bridge DC

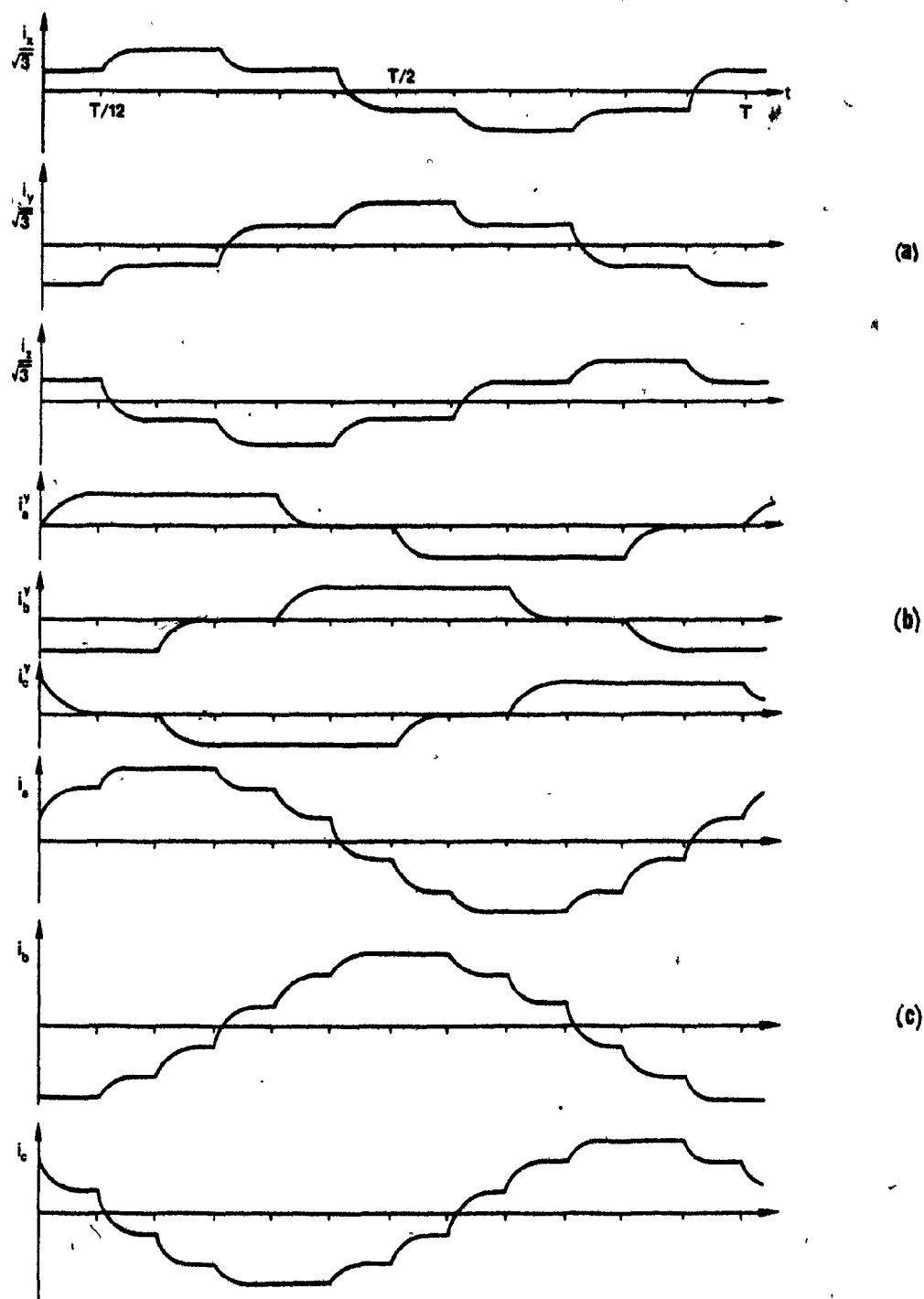


FIGURE 2.7 Bridge currents ; $\alpha=120^\circ, \omega\mu_1 < 30^\circ, \omega\mu_2 < 30^\circ$
 (a) Wye-delta transformer primary currents
 (b) Wye-wye transformer primary currents
 (c) Overall stator currents

line voltage waveform shown in Fig.2.5(b), is given by Eqn. 2.5

$$v_d^Y = (3\sqrt{3}E_m/\pi) (1 + \sum_{k=1}^{\infty} (1/(6k+1) - 1/(6k-1)) \cos 6k\omega t) \quad (2.5)$$

The series representation for the wye-delta bridge DC line voltage is obtained by advancing Eqn. 2.5 by 30° .

$$v_d^\Delta = (3\sqrt{3}E_m/\pi) (1 + \sum_{k=1}^{\infty} (1/(6k+1) - 1/(6k-1)) (-1)^k \cos 6k\omega t) \quad (2.6)$$

The overall DC line voltage is derived by adding the two series of Eqns. 2.5 and 2.6.

$$v_d = (6\sqrt{3}E_m/\pi) (1 + \sum_{k=1}^{\infty} (1/(12k+1) - 1/(12k-1)) \cos 12k\omega t) \quad (2.7)$$

2.4.2 Analysis of AC Phase Currents

For the operating conditions $\omega t = 0^\circ$ and $\alpha = 0^\circ$, i_a^Δ , i_a^Y and i_a are sketched in Fig. 2.8.

The Fourier series describing Fig. 2.8(b) is

$$i_a^Y = (2\sqrt{3}I_d/\pi) \{ \cos \omega t - \sum_{k=1}^{\infty} \cos(6k-1)\omega t / (6k-1) + \sum_{k=1}^{\infty} \cos(6k+1)\omega t / (6k+1) \} \quad (2.8)$$

The series for the wye-delta primary current of Fig. 2.8(a) may be written as

$$i_a^\Delta = (2\sqrt{3}I_d/\pi) \{ \cos \omega t - \sum_{k=1}^{\infty} (-1)^k \cos(6k-1)\omega t / (6k-1) + \sum_{k=1}^{\infty} (-1)^k \cos(6k+1)\omega t / (6k+1) \} \quad (2.9)$$

Direct addition of the two currents i_a^Y and i_a^Δ yields a series expression for the overall stator phase current.

$$i_a = (4\sqrt{3}I_d/\pi) \{ \cos \omega t + \sum_{k=1}^{\infty} (-1)^k \cos(12k-1)\omega t / (12k-1) - \sum_{k=1}^{\infty} (-1)^k \cos(12k+1)\omega t / (12k+1) \} \quad (2.10)$$

Fourier series expansions for the b and c phases may be calculated by shifting Eqns. 2.8, 2.9 and 2.10 by 120° and 240° respectively.

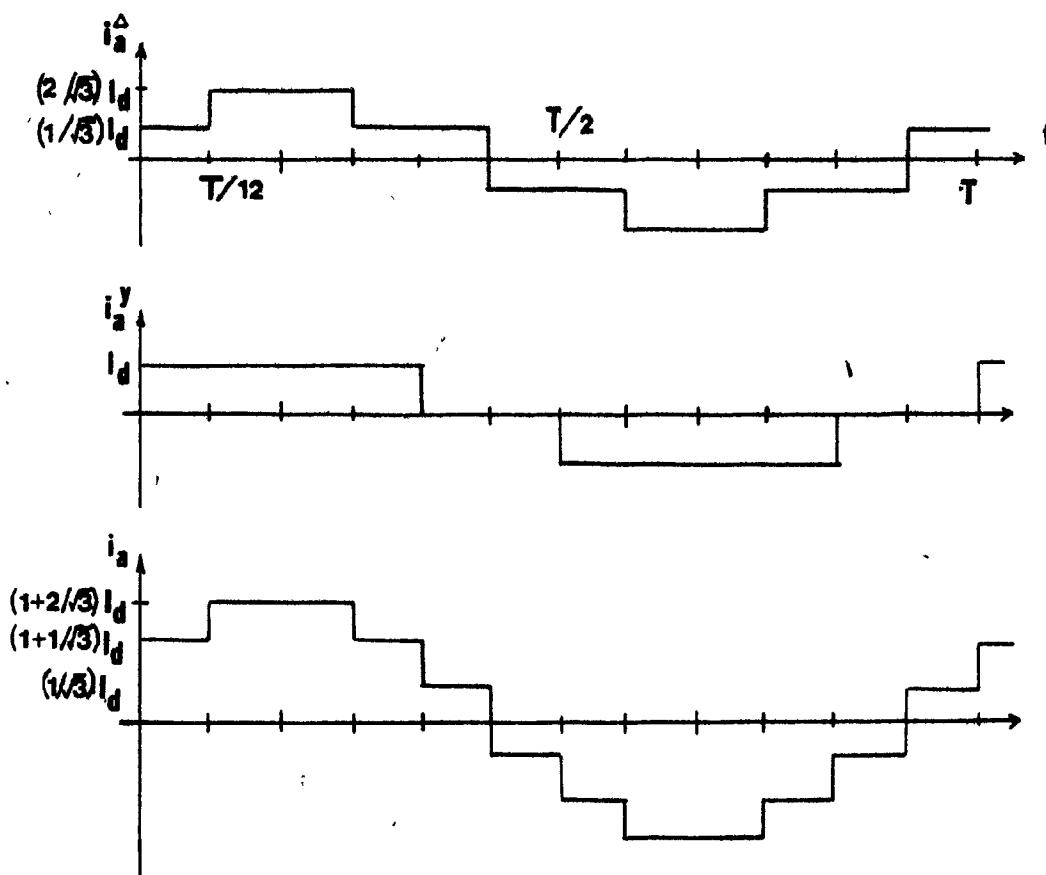


FIGURE 2.8 Bridge currents ; $\alpha=0^\circ$, $\omega\mu=0^\circ$

- (a) Wye-delta transformer primary current
- (b) Wye-wye transformer primary current
- (c) Total AC stator line currents

The results of this section are given in Tables 2.3 and 2.4 for the characteristic harmonics which are of practical interest in most engineering applications.

k	SIX-PULSE BRIDGE		TWELVE-PULSE BRIDGE	
	$*(2\sqrt{3}I_d/\pi)$	% OF FUNDAMENTAL	$*(2\sqrt{3} I_d/\pi)$	% OF FUNDAMENTAL
1	1	100.0	2	100.0
5	1/5	20.0	0	0.0
7	1/7	14.3	0	0.0
11	1/11	9.1	2/11	9.1
13	1/13	7.7	2/13	7.7

TABLE 2.3 MAGNITUDE OF HARMONICS OF AC LINE CURRENTS FOR BRIDGE OPERATION WITH $\omega\mu = 0^\circ$ AND $\alpha = 0^\circ$

k	SIX-PULSE BRIDGE		TWELVE-PULSE BRIDGE	
	$*(3\sqrt{3}E_M/\pi)$	% OF DC VALUE	$*(3\sqrt{3}E_M/\pi)$	% OF DC VALUE
DC	1	100.0	2	100.0
6	1/5-1/7	5.7	0	0.0
12	1/11-1/13	1.4	2/11-2/13	1.4
18	1/17-1/19	.6	0	0.0
24	1/23-1/25	.4	2/23-2/25	.4

TABLE 2.4 MAGNITUDE OF HARMONICS OF DC LINE VOLTAGE FOR BRIDGE OPERATION WITH $\omega\mu = 0^\circ$ AND $\alpha = 0^\circ$

From these tables it may be seen that the effect of the twelve-pulse connection is to remove specific current and voltage harmonics without changing the ratio of the

remaining harmonic magnitudes to their fundamental and DC components respectively.

Further pairs of bridges may be added to the connection, each with an appropriate phase shift, to yield a converter with characteristic AC current harmonics of order $pk+1$ and DC voltage harmonics of order pk , where p is the converter's pulse number. Although complex arrangements have been built and studied, it is generally accepted that for HVDC applications filtering is the most economical means of removing AC current harmonics of order $k=11$ and above, and DC voltage harmonics of order greater than or equal to $k=12$.

For practical 12-pulse configurations, tuned filters are generally employed to remove the $k=11$ and $k=13$ harmonics while a high-pass filter is employed to remove harmonics of order $k=23$ and above. Since the bridges absorb reactive power under all operating conditions, the filters also serve the function of injecting needed reactive power into the system.

The magnitudes of the DC voltage harmonics of practical 12-pulse bridge networks have lower per-unit values than their AC counterparts. The harmonics appearing on the DC line are further reduced by the insertion of a large choke inductance between the bridges and the DC system. In many applications, such as underground cable transmission, DC side filters are not required and are therefore not included in the general analysis of this thesis.

The analysis of this section has intentionally omitted the effect of both the delay angle and commutation overlap, to allow for simplifications in the calculations of the Fourier coefficients. Delay angle has no effect on the AC current harmonic content, while the valve commutation overlaps tend to reduce the harmonic content of the alternating currents below their $\omega_{\mu}=0$ level of $1/k$ [25]. However, calculations also indicate that most non-zero combinations of ω_{μ} and α tend to greatly increase the level of DC voltage harmonics. Despite this, the values of Tables 2.3 and 2.4 serve as useful upper limits for the analysis carried out in system simulations.

2.5 Summary

The higher power capabilities and reduced harmonic content of the twelve-pulse bridge connection described in this chapter make it a useful tool in HVDC conversion applications. Based on the simple analysis of this chapter the remainder of the thesis will study the means by which linear state analysis and computer techniques may be applied to the study of the twelve-pulse bridge converter.

CHAPTER 3

NETWORK ANALYSIS OF TWELVE-PULSE CONVERTER

3.1 Introduction

The first step in applying the digital computer to the study of the twelve-pulse converter is the selection of an appropriate network model. Figure 3.1 illustrates the network components included in the bridge converter of this thesis.

Having selected a suitable mathematical model for the network, the next step in the analysis is the determination and accurate description of the required solution. This allows for the full exploitation of any desirable properties of the solution in the formation of the numerical algorithm. In networks containing periodically switched elements careful consideration must be given to the nature of the periodic solution.

Once a complete study of the network properties has been made, the appropriate mathematical and numerical analysis tools may be selected and the computer algorithm prepared.

This chapter endeavours to describe the first two steps in the analysis procedure. Particular attention is focussed on the history of the application of state space techniques to periodically switched networks. The solution algorithms



of Chapter 4 follow as a direct progression of the concepts herein described.

3.2 Digital Representation of Converter Valves

In power switching analysis programs intended for use with differing topologies [6-15], the valves are generally modelled as variable resistances. When the valve is in its conducting state the resistance value is small. When the valve is reverse-biased and enters its blocking state the resistance value is made very large. The advantage of such a model is that the system equations need not be re-arranged to represent changes in circuit topology due to normal switching operations.

For programs dedicated to the simulation of specific switching circuits, [6-18], a Boolean (ON or OFF) representation is generally chosen for the valves. Such a representation is used for the valves of the twelve-pulse converter in this thesis. Eliminating non-conducting branches leads to a reduction in the number of equations and variables required to describe the system. However, separate systems of equations are required to represent each topology encountered in the process of normal switching operations. Symmetry properties are generally exploited to reduce the number of topologies required to fully define the network operation.

3.3 Network Model of Twelve-Pulse Converter

The twelve-pulse bridge converter model, shown in Fig. 3.1 consists of:

(1) The DC transmission line, represented by a constant direct current source of value I_d

(2) AC components

(a) Three-phase synchronous generator modelled in each phase by an emf in back of its sub-transient impedance R_s, L_s . To include the bridge firing delay in the analysis a variable angle is incorporated into the emfs:

$$\begin{aligned} e_a(t) &= E_M \sin(\omega t + \pi/6 + \theta) \\ e_b(t) &= E_M \sin(\omega t - \pi/2 + \theta) \\ e_c(t) &= E_M \sin(\omega t + 5\pi/6 + \theta) \end{aligned} \quad (3.1)$$

By using the unbiased emfs of Eqn. 2.1 to determine the bridge switchings, the desired delay α between forward biasing and firing may be obtained by controlling θ .

(b) The wye-wye and wye-delta transformers are modelled by ideal transformers connected to the winding leakage impedances R_{T1}, L_{T1} and R_{T2}, L_{T2} respectively.

(c) AC shunt filters labelled high-pass (HP), 11-th and 13-th, used to remove characteristic harmonics generated by the converter.

This model is sufficient for analysis of the steady state performance of the converter under normal operating conditions.

3.4 Linear Circuit Analysis

Linear networks containing periodically operated switching elements are often referred to as being piece-wise linear. Each circuit obtained by replacing the valves of the bridges in Fig. 3.1 with their Boolean models, is linear and time-invariant and thus amenable to linear circuit analysis [26].

The collection of circuits which are formed by replacing the bridge valves with open or short circuits will be referred to as sub-networks. The time interval during which any particular sub-network serves as the working model of the overall network, as determined by the valve states, is referred to as its sub-interval. The gating sequence applied to the network determines which sub-networks are required to model a complete cycle of operation, and in which order they will appear.

The dynamic variables of each sub-network may be described by a set of first order differential equations.

$$\dot{\underline{x}}_n(t) = [A_n] \underline{x}_n(t) + [B_n] u(t) \quad (3.2)$$

The vector $\underline{x}_n(t)$ is the state vector and generally consists of the minimum number of current and voltage variables which allow for a complete description of the n-th sub-network. Since the sub-networks are linear, $[A_n]$ and $[B_n]$ are constant matrices.

The solution for the state vector of Eqn. 3.2 is of the general form,

$$\underline{x}_n(t) = [\phi_n(t)] \underline{\xi}_n + \underline{x}_n^{ZSR}(t), \quad t_n \leq t < t_{n+1} \quad (3.3)$$

where t_n and t_{n+1} are the n -th sub-interval boundary times.

The first part of the solution is the zero-input response (ZIR), where $[\phi_n(t_n)]$ is the state transition matrix and ξ_n is a vector of integration constants. This part of the solution represents the response of the network to the initial capacitor voltages and inductor currents.

The second part of the solution, the zero-state response (ZSR) depends on the network forcing functions and topology. Appendix 1 elaborates on the formation of the ZSRs and state transition matrices for the sub-networks.

If $t=t_n$ is substituted into Eqn. 3.3, the unknown vector integration constant may be written in terms of the general solution. The overall solution may now be written

$$\underline{x}_n(t) = \underline{x}_n^{\text{ZSR}}(t) + [\phi_n(t-t_n)](\underline{x}_n(t_n) - \underline{x}_n^{\text{ZSR}}(t_n)) \quad (3.4)$$

The collection of sub-network solutions may be utilized to form a complete description of the circuit operation when combined with an understanding of the general nature of the overall solution.

3.5 Properties of Periodic Solution in Periodically Triggered Three-Phase Bridge Configurations

This section introduces two properties of the desired solution which will be used in conjunction with linear circuit theory to form the numerical algorithm.

3.5.1 Periodicity in T

The periodic solutions of the differential equations associated with the steady state operation of the bridge converter and other switching networks differ from the classical steady-state solutions in linear networks. In physical linear networks the periodic solution consists entirely of the ZSR, and is reached only after the ZIR or transient solution has been damped to an insignificant value.

For networks containing switching elements the ZIR of each sub-network is re-excited in each period by the switching process. Thus the overall periodic solution contains both the ZIR and ZSR in each sub-interval. The periodicity requirement which the solution must satisfy may be written in terms of the sub-interval state vectors $\underline{x}_n(t)$ and the overall switching period, denoted T, as

$$\underline{x}_n(t+T) = \underline{x}_n(t) \quad (3.5)$$

3.5.2 Periodicity in T/6

It was pointed out in Section 2.2 that the sequence of gating currents applied to the valves of the Graetz Bridge are chosen so as to produce balanced positive-sequence currents on the AC side. Since the AC network is balanced, superposition may be employed to show that the combined effect of the injected currents and generator emfs is to produce positive-sequence currents and voltages throughout the AC network.

()

Due to the balanced, positive-sequence nature of all AC variables, the $T/6$ periodicity property may be exploited. Simply stated, any $T/6$ segment of the three-phase solution is sufficient to reconstruct the entire solution.

As an example, Fig. 3.2 shows the transpositions required to reconstruct a full period of the three-phase emfs from a $T/6$ section commencing at $t=0$.

All currents and voltages on the AC side of the network may be reconstructed in exactly the same manner, and the entire problem may be reduced to studying any $T/6$ section of the bridge operation.

3.6 State Analysis Applied to Piece-Wise Linear Problems

The matrix handling capabilities of the digital computer make state space techniques very attractive for use in the computer-aided analysis and design of electronic circuitry. Despite this, the full advantages of this mathematical description have rarely been applied to the analysis of switching circuitry.

()

In numerous instances sophisticated methods have been applied to the compilation of defining equations of switching networks only to have these equations solved by slow and expensive numerical integration techniques [6-15]. These methods seem particularly inappropriate when applied to circuits where variable resistors are used to model the thyristors. In such network models, large order-of-magnitude

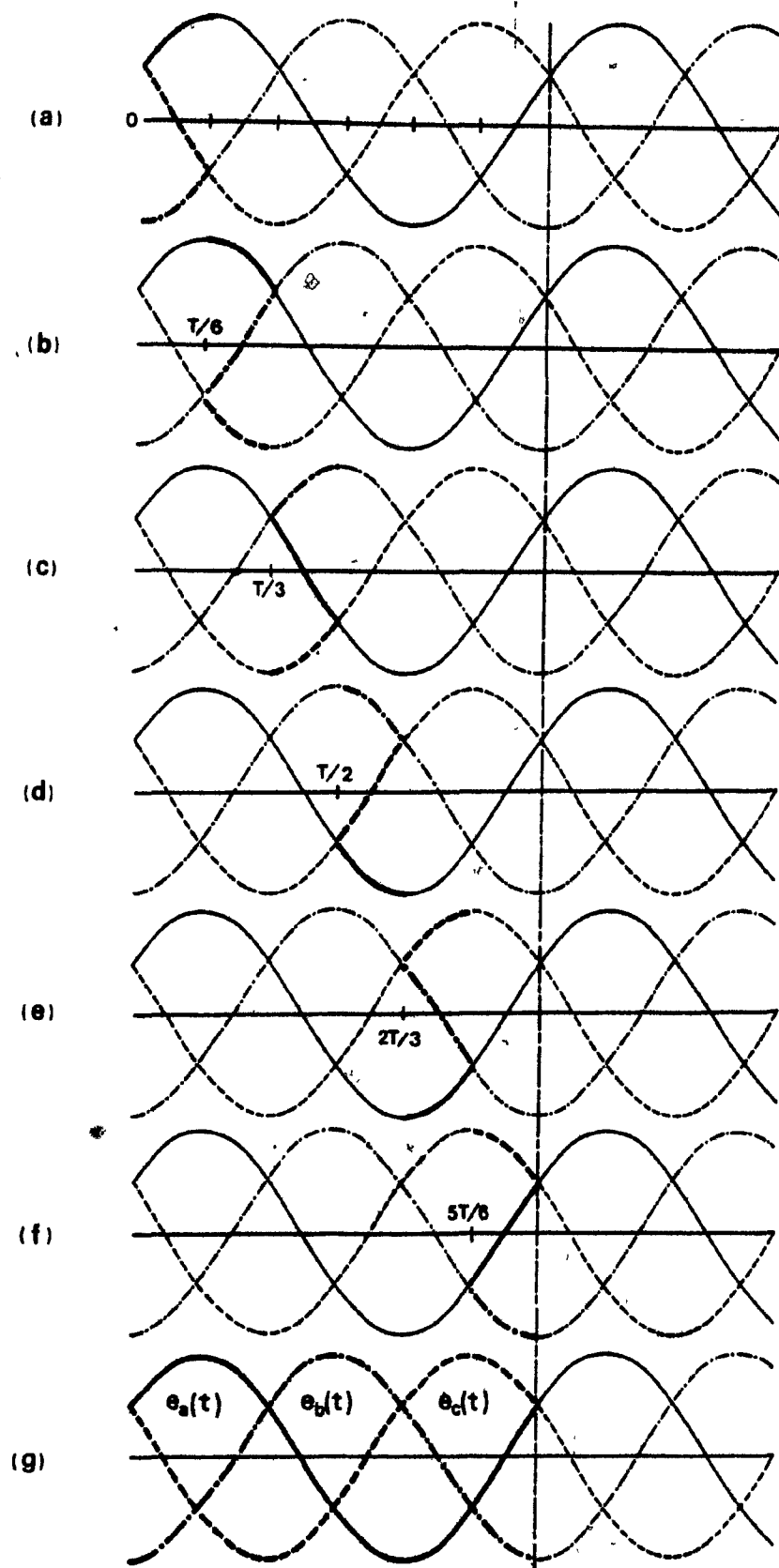


FIGURE 3.2 Example of $T/6$ periodicity property. Re-construction of full period of balanced 3-φ emfs from basic $T/6$ segment

differences exist between the defining time constants. In order to achieve numerical stability, unnecessarily small step sizes must be used in the integration algorithms.

Once the problem has been recognised as being piece-wise linear, the state description may be applied to valve networks in a variety of fashions. To describe these methods, a general switching network, consisting of N separate switching states per period is postulated. Fig. 3.3 shows the connected sequence of N sub-intervals constituting a full period of operation. The time origin has arbitrarily been chosen as $t=t_1$. The sub-network numbers 1 through N correspond to the N consecutive topologies encountered in one cycle of normal operation of the network.

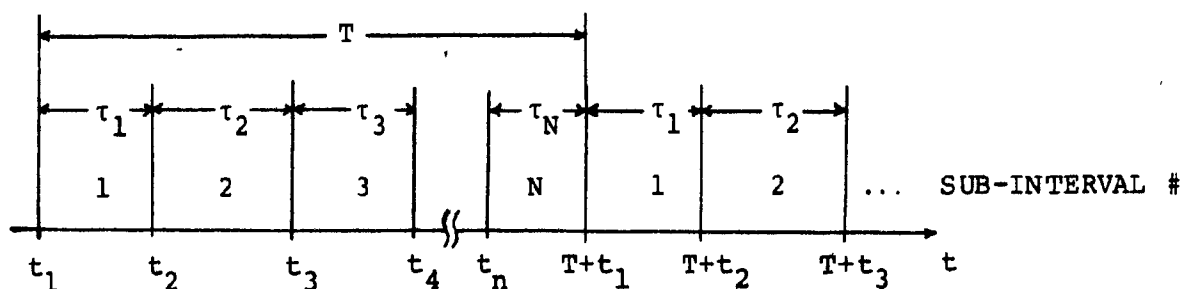


FIGURE 3.3 Sequence of sub-intervals corresponding to operation of arbitrary switching network

The state vectors describing each of the N sub-networks may contain different elements depending on the topologies. Compatibility matrices are therefore required at the N switching instants to match final and initial conditions.

$$\underline{x}_{n+1}(t_{n+1}) = [C_n] \underline{x}_n(t_{n+1}) \quad , \quad n = 1, \dots, N \quad (3.6)$$

() The N compatibility matrices are formed by applying flux and charge continuity requirements to the inductor currents and capacitor voltages respectively, at the switching instants.

3.6.1 Iterative Determination of Initial Conditions

The simplest application of linear state analysis to the problem of Fig. 3.3 involves iteratively modifying an arbitrary initial condition by applying the sub-network state solutions, boundary conditions and periodicity in T property [20].

An arbitrary initial condition $\underline{x}_1(t_1)$ is chosen and the solution advanced through a period using Eqns. 3.4 and 3.6. In each subsequent iteration $\underline{x}_1(T+t_1)$ replaces the initial condition $\underline{x}_1(t_1)$. The flow chart shown in Fig. 3.4 describes this iterative procedure.

This method eliminates the stability problem associated with the numerical integration process, however it still requires a potentially expensive iteration procedure requiring multiple calculations of the state transition matrices and solution vectors.

3.6.2 Closed-Form Solution

() A few authors have presented papers in which analytical solution techniques have been developed for handling networks containing periodically operated thyristors and switches. In 1971 Lipo [16] presented an analytical solution to the problem of a thyristor speed control for an induction

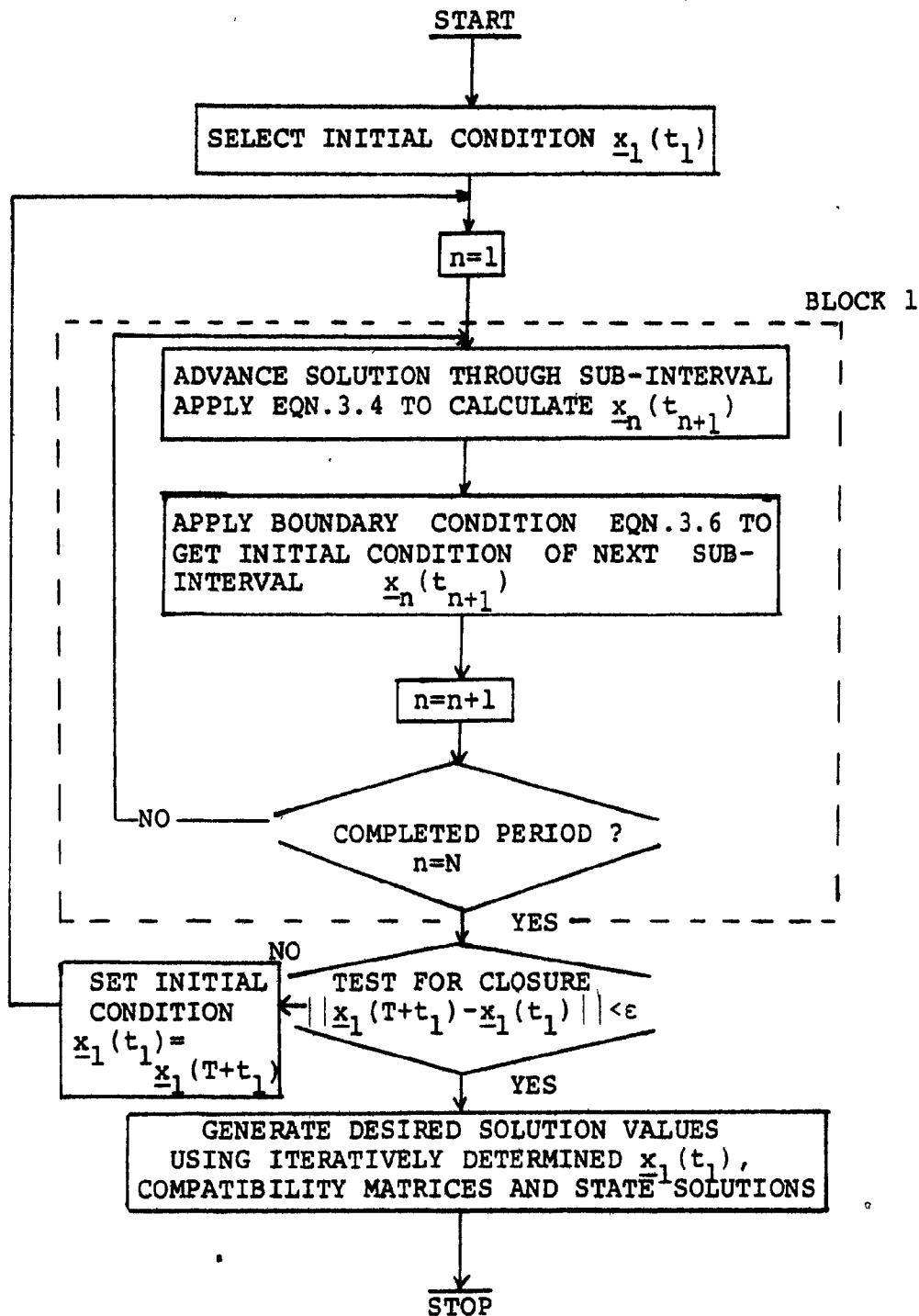


FIGURE 3.4 Flowchart for iterative determination of initial condition vector

motor, utilizing state space techniques. The following year Liou [17] presented a general solution method for handling linear circuits containing periodically operated switches. The closed-form solution presented here follows the approach of these two papers.

In this method $\underline{x}_1(t_1)$ is treated not as an iterate but rather as an unknown. Repetitive application of Eqns. 3.4 and 3.6, through the N sub-intervals, yields an equation for the final condition $\underline{x}_N(T+t_1)$ in terms of the unknown vector $\underline{x}_1(t_1)$.

$$\underline{x}_N(t_1+T) = \underline{R} + [S]\underline{x}_1(t_1) \quad (3.7)$$

In Eqn. 3.7 \underline{R} and $[S]$ consist of the first $N-1$ compatibility matrices, as well as the N state transition matrices and ZSRs evaluated at the appropriate boundary times. Since all elements of \underline{R} and $[S]$ may be calculated directly, an explicit relation may be obtained to determine the initial condition. Applying the final compatibility matrix at $t=T+t_1$,

$$\underline{x}_1(t_1+T) = \underline{x}_{N+1}(t_1+T) = [C_N]\underline{x}_N(t_1+T) \quad (3.8)$$

Substituting Eqn. 3.7 into Eqn. 3.8, applying the periodicity in T property, and re-arranging yields,

$$\underline{x}_1(t_1) = ([I] - [C_N][S])^{-1} [C_N]\underline{R} \quad (3.9)$$

The right hand side of Eqn. 3.9 may be calculated to give the initial condition and an explicit form for the entire solution. The inner loop of the flow chart of Fig. 3.4, labelled BLOCK 1, is repeated in Fig. 3.5 to describe the formulation of the explicit relation.

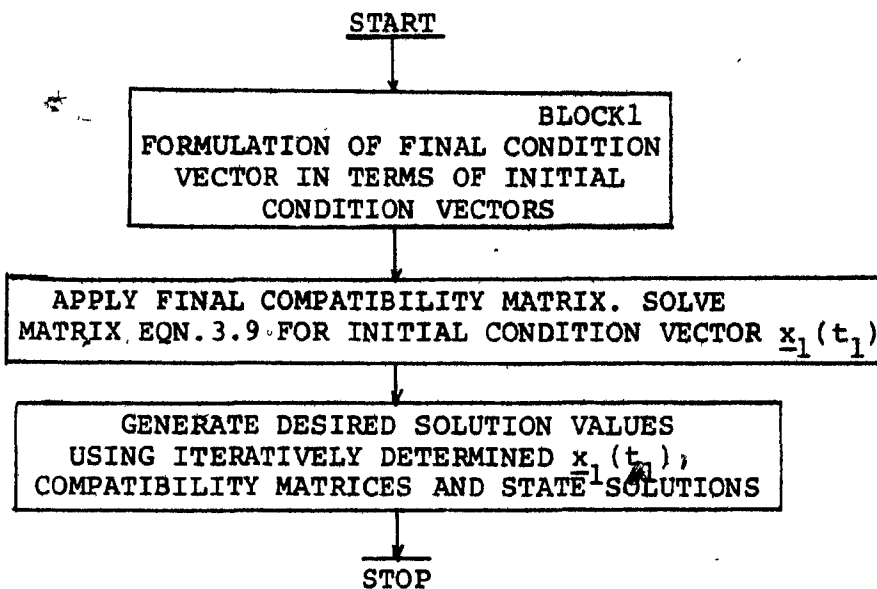


FIGURE 3.5 Flowchart for analytical determination of initial condition vector and problem solution

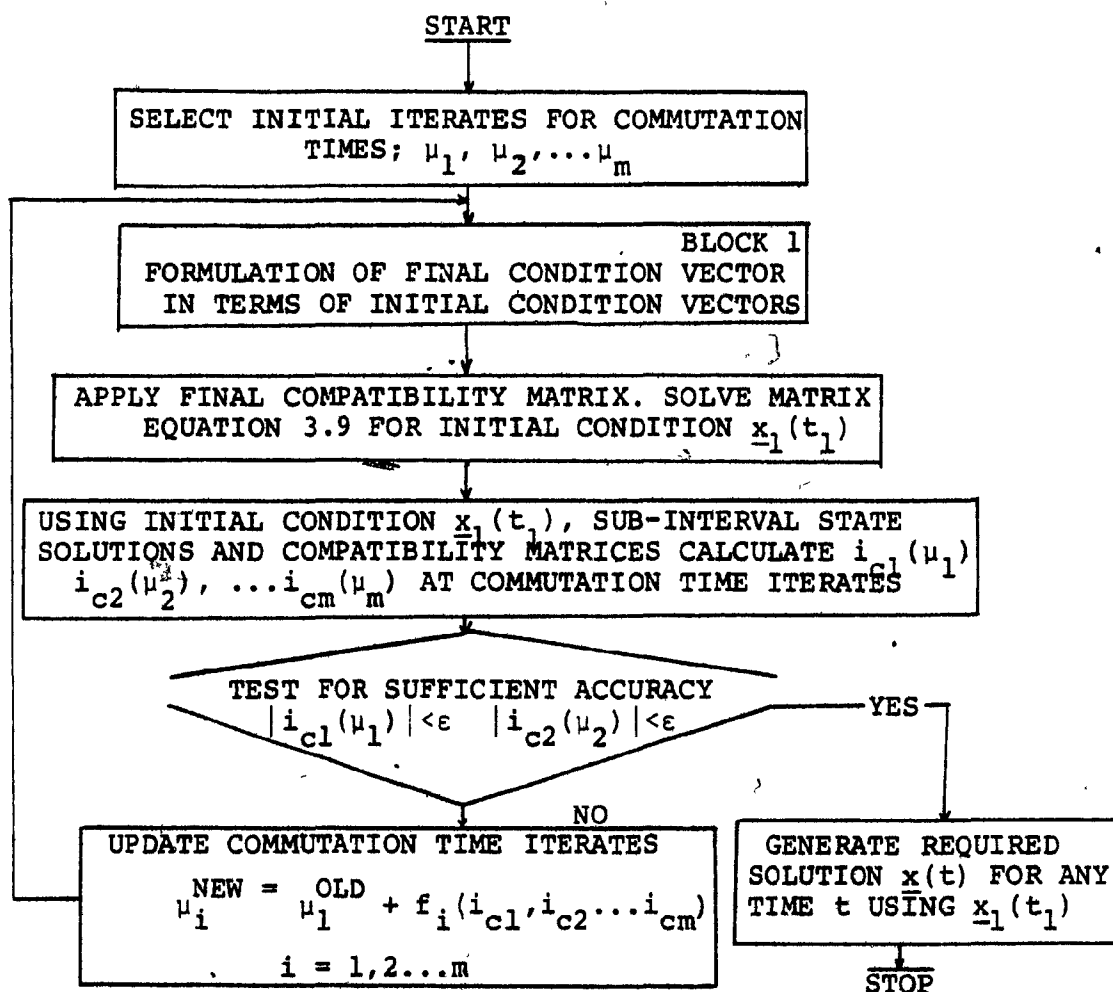


FIGURE 3.6 Flowchart for iterative determination of initial condition vector with unknown boundaries corresponding to commutation times

This method entirely removes the need for numerical iteration.

3.6.3 Unknown Boundaries in Closed-Form Solution

The analytical solution obtained for the initial condition vector in Eqn. 3.9 was obtained under the assumption that all boundary times in Fig. 3.3 were known beforehand. This of course would be the case if all the boundary times corresponded to the firing of valves at specified gating times. However, some of the changes in topology correspond to the commutation of valves, and the corresponding boundary times are therefore related to the commutation times. These commutation times are dependent on the initial conditions of the commutating sub-intervals and must therefore appear as unknowns in Eqn. 3.9. To point out this dependence, Eqn. 3.9 is rewritten as

$$\underline{x}_1(t_1) = [G(\mu_1, \mu_2, \dots, \mu_m)]^{-1} \underline{F}(\mu_1, \mu_2, \dots, \mu_m) \quad (3.10)$$

where the \underline{F} vector and $[G]$ matrix are functions of the m commutation times. The initial condition $\underline{x}_1(t_1)$ may be evaluated, using Eqn. 3.10, for commutation time iterates. Using each iterate of the initial condition vector, the solution matrices, and the compatibility matrices, the commutation currents may be evaluated at their commutation times. By numerically solving the system of equations

$$i_{cj}(\mu_j) = 0, \quad j=1, \dots, m \quad (3.11)$$

a value for each of the commutation times may be determined. The required procedure is depicted in the flowchart of

Fig. 3.6.

Such a problem was addressed by Ooi, Menemenlis and Nakra [18] in a paper discussing the particular case of a six-pulse Graetz Bridge inverter acting as a series tap. In this problem one independent variable, a single commutation time, existed. This thesis addresses the problem of the twelve-pulse converter where two independent commutation current variables exist. Chapter 4 describes a method which utilizes Eqn. 3.10 in conjunction with a minimization algorithm to numerically determine the commutation times, and overall solution.

3.7 Application of T/6 Periodicity Property

The complexity of matrix manipulations associated with the formulation of the final condition vector in terms of the initial condition vector, described by Eqn. 3.10, increase dramatically with increasing N . In the case of the twelve-pulse converter the numerous gatings and commutations constituting a full period are prohibitive when considered in terms of an analytical solution. To allow for a practical digital algorithm to handle the problem, T/6 periodicity must be applied. The number of topologies which must be considered, upon application of this property, are reduced by a factor of six.

Referring to Section 3.5.2 and Fig. 3.2

$$\begin{aligned}
 x_a(t) &= -x_c(t-5T/6) \\
 x_b(t) &= -x_a(t-5T/6) \\
 x_c(t) &= -x_b(t-5T/6) \\
 5T/6 + t_1 &\leq t \leq T + t_1
 \end{aligned} \tag{3.12}$$

where $x_a(t)$, $x_b(t)$, and $x_c(t)$ represent the a, b, and c phase components of a particular state variable. Substituting $t = T + t_1$ in Eqn. 3.12 and applying the T-periodicity property of Eqn. 3.5 yields:

$$\begin{aligned}
 x_a(t_1) &= -x_c(t_1 + T/6) \\
 x_b(t_1) &= -x_a(t_1 + T/6) \\
 x_c(t_1) &= -x_b(t_1 + T/6)
 \end{aligned} \tag{3.13}$$

Application of Eqn. 3.10 with T replaced by T/6, and using the final compatibility matrix $[C_N]$ to execute the transpositions of Eqn. 3.13 allows for a considerably simpler equation in terms of the commutation times. The expression thus formed requires considerably less matrix manipulations than if the entire period had been considered.

3.8 Summary

State space techniques allow for the full exploitation of the matrix handling capabilities of advanced digital computers in the analysis of electrical networks.

This chapter has outlined the techniques and concepts which, when applied to piece-wise linear configurations, allow for the use of state theory in their analysis. Chapter 4 describes the formation of the algorithms which

make use of these concepts in the analysis of the normal operation of the twelve-pulse converter.

CHAPTER 4

FORMATION OF SOLUTION ALGORITHMS

4.1 Introduction

The approaches used to apply linear state analysis to piece-wise linear problems were introduced in Chapter 3. This chapter applies these concepts to formulate the specific algorithms to be used in the analysis of the twelve-pulse bridge converter.

Since the commutation times are not known before the solution has been determined, the exact sub-network configurations encountered in each period are also unknown.

Because of this, separate algorithms must be prepared for different groupings of commutation lengths. The exact configuration is then determined during the solution along with the commutation variables μ_1 and μ_2 . Once the problem has been classified in terms of its commutation times, and the necessary sub-network state descriptions generated, the general method described by the flowchart of Fig. 3.6 may be applied.

4.2 Classification According to Commutation Angles

It was pointed out in Chapter 3 that through the use of the $T/6$ periodicity property, the problem was reduced to studying any given $T/6$ segment of the bridge operation. The actual topologies encountered in a given $T/6$ segment of operation are determined by the lengths of the commutation times for the valves of the two bridges. Table 4.1 lists the permutations of commutation angles which occur during bridge operation with the two commutation angles, $\omega\mu_1$ and $\omega\mu_2$, less than 60° .

CASE	$\omega\mu_1$	$\omega\mu_2$
1(i)	$< 30^\circ$	$< 30^\circ$
(ii)	$\geq 30^\circ, < 60^\circ$	$< 30^\circ$
2(i)	$< 30^\circ$	$\geq 30^\circ, < 60^\circ$
(ii)	$\geq 30^\circ, < 60^\circ$	$\geq 30^\circ, < 60^\circ$
3(i)	$\geq 30^\circ + \omega\mu_2, < 60^\circ$	$< 30^\circ$
(ii)	$< 30^\circ$	$\geq 30^\circ + \omega\mu_1, < 60^\circ$

TABLE 4.1 COMMUTATION ANGLE GROUPINGS FOR NORMAL BRIDGE OPERATION

Under normal operating conditions the two commutation angles have similar values and in the analysis that follows it will be assumed that $|\omega\mu_1 - \omega\mu_2| < 30^\circ$, thus eliminating Case 3 of Table 4.1 from consideration.

The bridge currents corresponding to bridge operation with commutation angles in the range of Case 1(i) are shown in Fig. 4.1. During the defining $T/6$ segment, $0 \leq t < T/6$, only two dynamic variables are required, one to describe each of the commutations. To simplify the notation two new

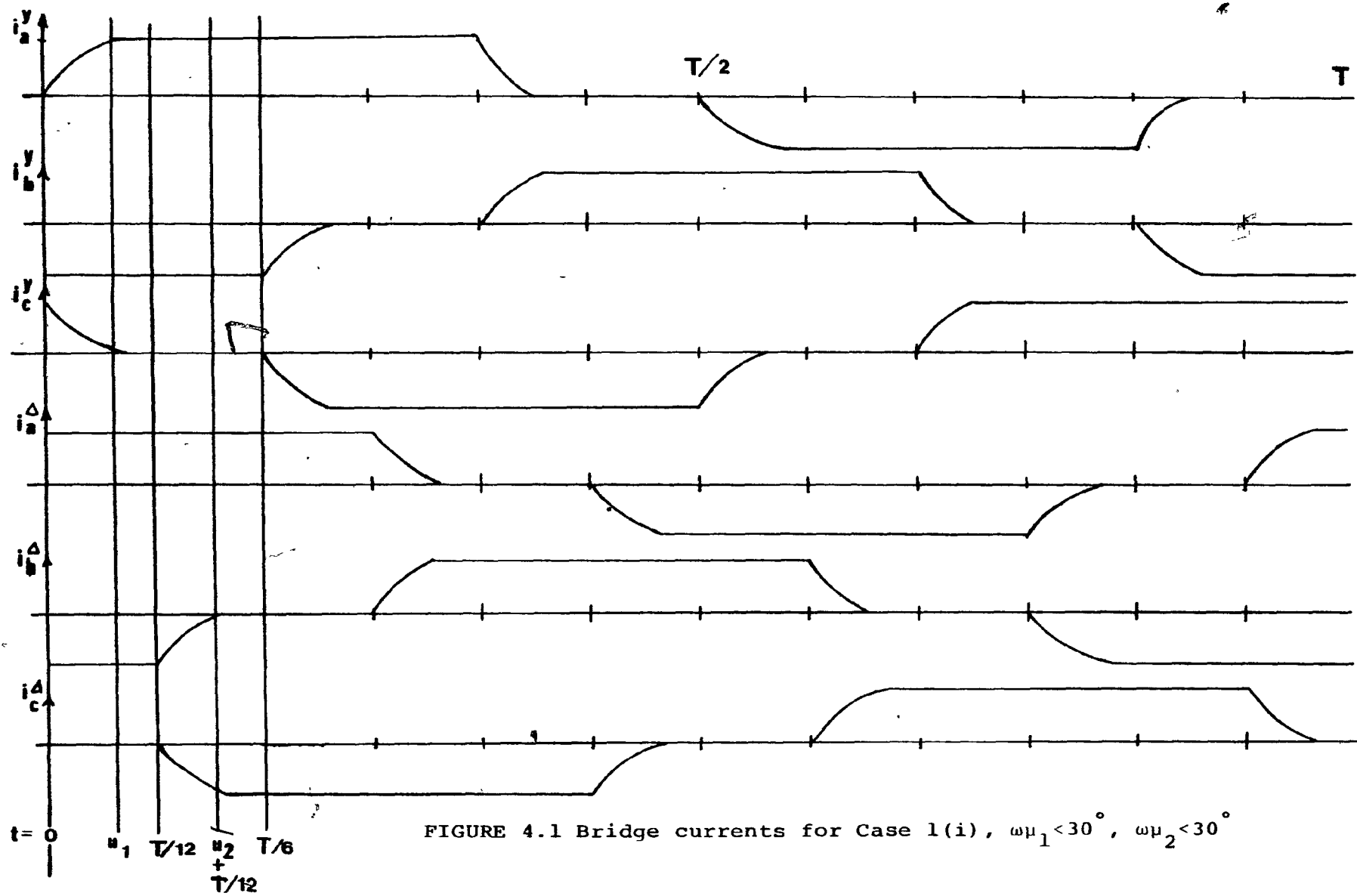


FIGURE 4.1 Bridge currents for Case 1(i), $\omega\mu_1 < 30^\circ$, $\omega\mu_2 < 30^\circ$

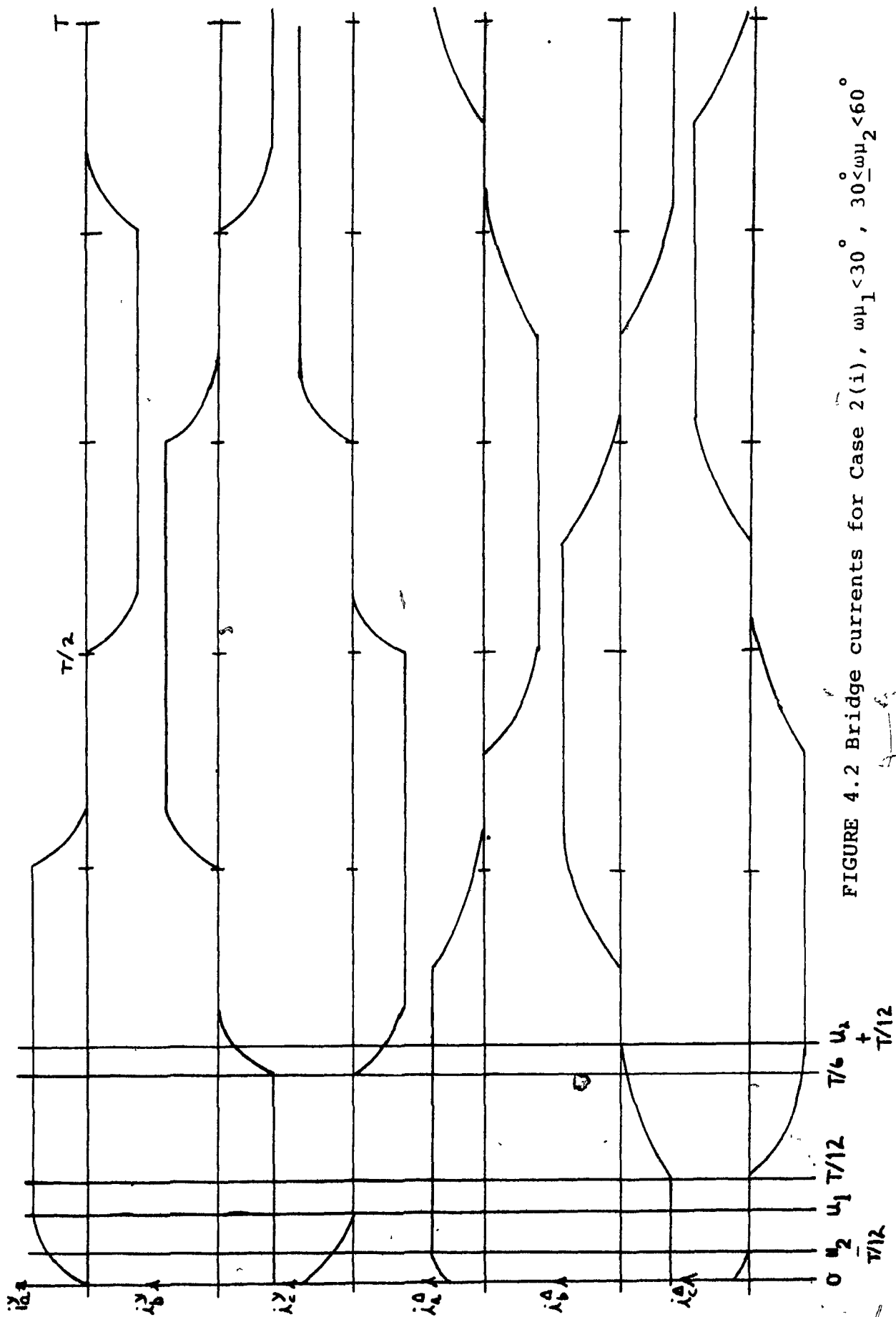


FIGURE 4.2 Bridge currents for Case 2(i), $\omega_1 < 30^\circ$, $30^\circ \leq \omega_2 < 60^\circ$

variables, $i_{cy}(=i_c^Y)$ and $i_{cd}(=-i_b^A)$, are introduced. Figs. 4.3(a) and (b) show the currents i_{cy} and i_{cd} for the first $T/6$ segment of Case 1(i) and Case 1(ii) respectively.

The bridge currents for converter operation in the range of Case 2(i) are shown in Fig. 4.2. Because of the increase in μ_2 , the commutation of VD2 by the switching of valve VD4 extends into each new period. to maintain a consistent notation, the dynamic variables used to represent the commutations remain i_{cy} and i_{cd} . Because of this selection, the commencement of the defining $T/6$ segment was chosen to coincide with the end of the VD2 commutation, $t=\mu_2-T/12$. Fig. 4.3(c) and (d) show the currents i_{cy} and i_{cd} for the $T/6$ segment, $\mu_2-T/12 \leq t < \mu_2+T/12$. The current variable i_{cy} now includes parts of two separate commutations in the defining interval. This does not lead to any real difficulty since each commutation current has the same form, due to the balanced nature of the AC circuit and the equally spaced valve triggerings. Referring to Fig. 2.3 of Chapter 2, the relation between i_{cy} evaluated at the initial and final boundary times may be written as,

$$i_{cy}(\mu_2-T/12) = I_d + i_{cy}(\mu_2+T/12) \quad (4.1)$$

This boundary condition supplies the additional information required to form the compatibility matrix used to match the boundary conditions for the defining $T/6$ segment.

Separate solution algorithms must be developed to handle the converter operation in the two $\omega\mu_2$ ranges given

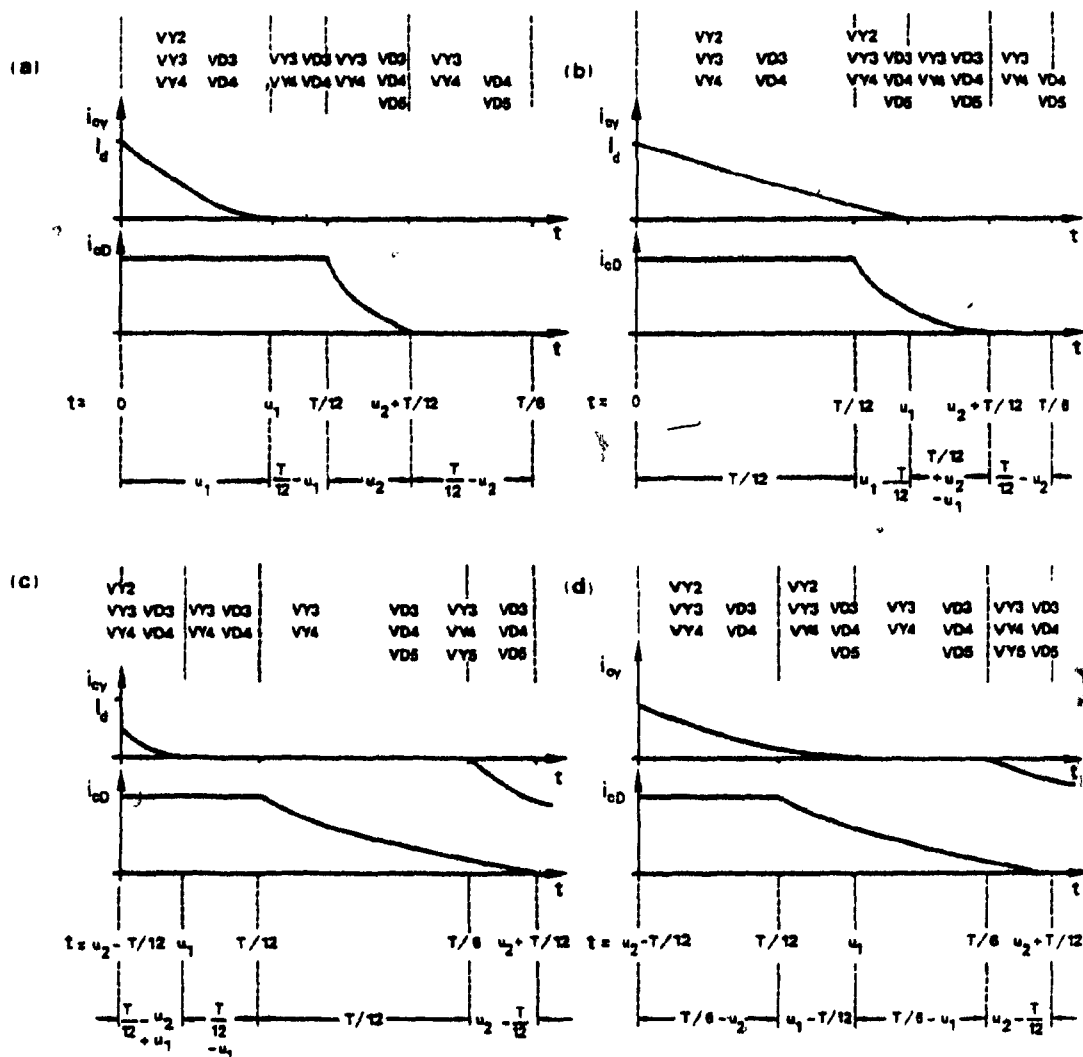


FIGURE 4.3 Wye bridge commutation current i_{cy} and delta bridge commutation current i_{cd}

(a) Case 1(i); $\omega\mu_1 < 30^\circ$, $\omega\mu_2 < 30^\circ$

(b) Case 1(ii); $30^\circ \leq \omega\mu_1 < 60^\circ$, $\omega\mu_2 < 30^\circ$

(c) Case 2(i); $\omega\mu_1 < 30^\circ$, $30^\circ \leq \omega\mu_2 < 60^\circ$

(d) Case 2(ii); $30^\circ \leq \omega\mu_1 < 60^\circ$, $30^\circ \leq \omega\mu_2 < 60^\circ$

in Table 4.1. For Case 1, Eqn. 3.10 is formulated with $t = 0$. With $\omega\mu_2 > 30^\circ$, in Case 2 operation, the initial condition vector of Eqn. 3.10 is evaluated for $t = \mu_2 - T/6$.

4.3 Selection of State Variables for Sub-Networks

The first step in formulating the solution algorithms is the determination of the state variables required to describe each sub-network constituting the basic T/6 segment. The minimum number of network variables, which allow for a complete description of the operation of each sub-network, are utilized.

4.3.1 Case 1, $\omega\mu_2 < 30$

Five separate sub-networks are required to fully describe the converter operation when the wye-delta commutation angle remains below 30° . These five sub-networks labelled 1 through 5, are shown on the following pages as Figs. 4.4(a)-(e). Open circuited branches corresponding to valves in the blocking state have been removed from the diagrams. The inductor currents and capacitor voltages labelled on each diagram indicate the state elements to be included in each state vector. The complete state vector for each sub-network is also included in the diagram.

Due to the balanced three-phase nature of all AC circuit quantities, only two state variables are necessary to fully describe each three phase inductor current or

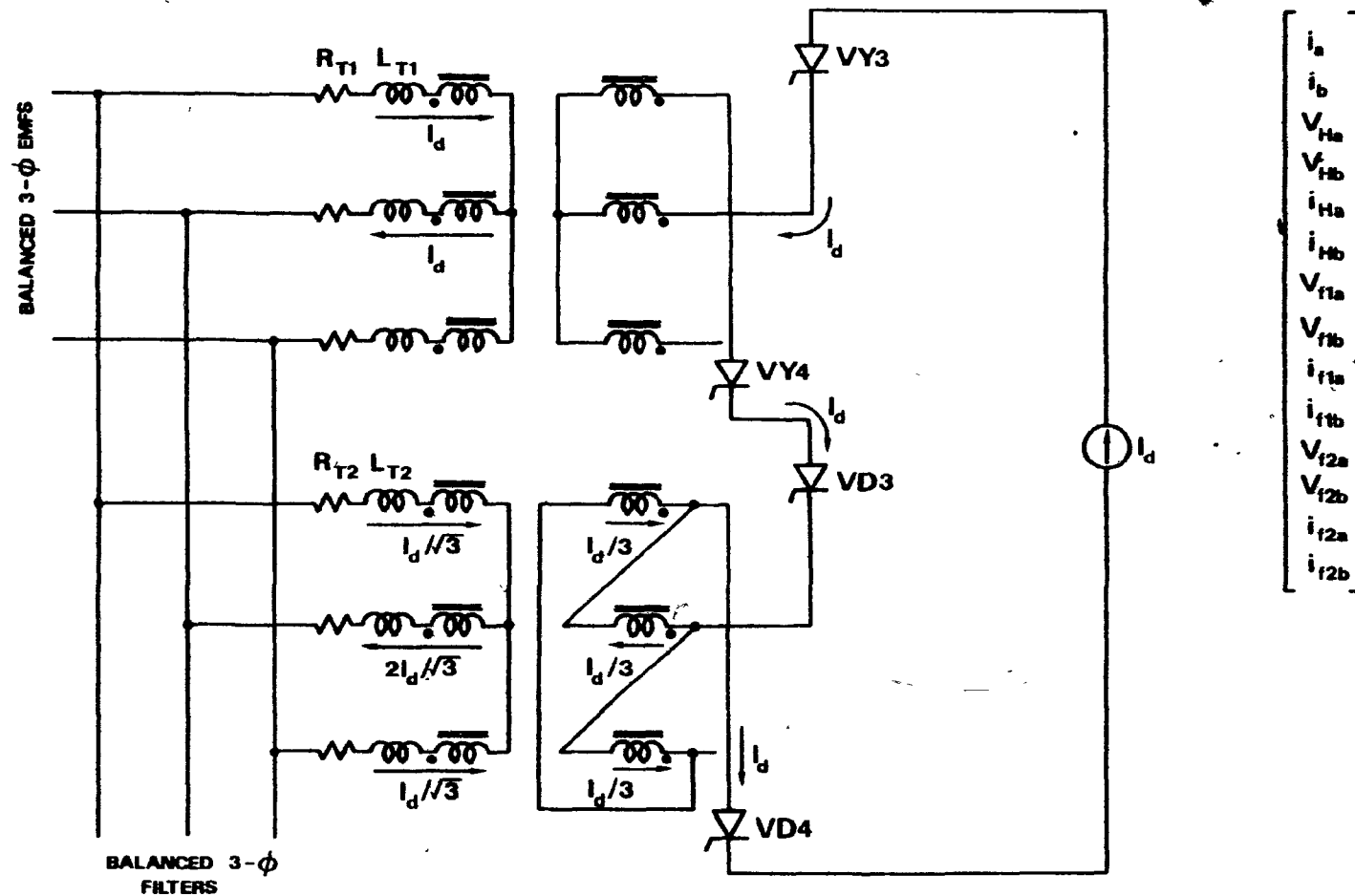


FIGURE 4.4(b) Sub-network 2, conducting valves; $VY3$, $VY4$, $VD3$, $VD4$

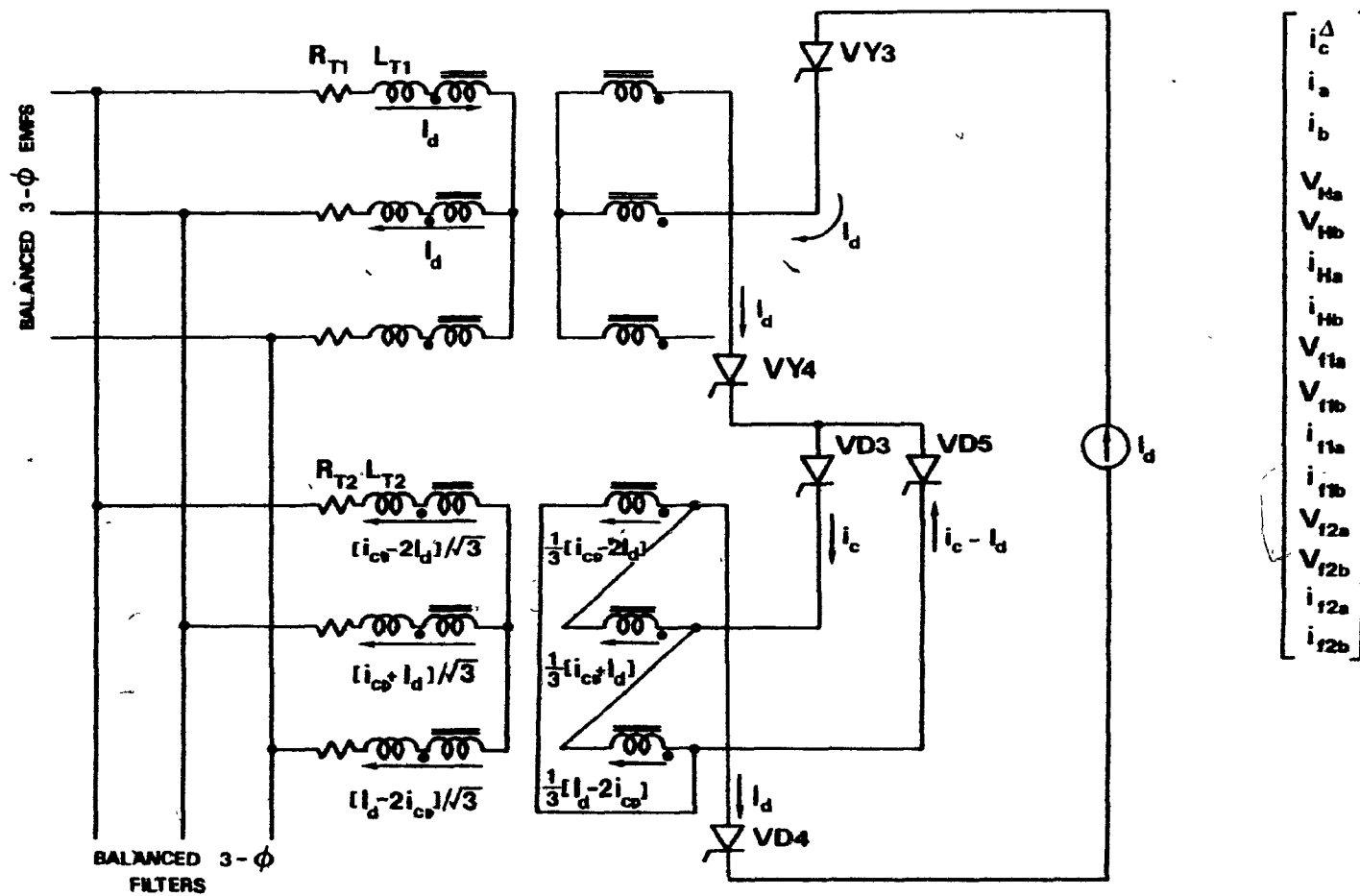


FIGURE 4.4(c) Sub-network 3, conducting valves; VY3, VY4, VD3, VD4, VD5

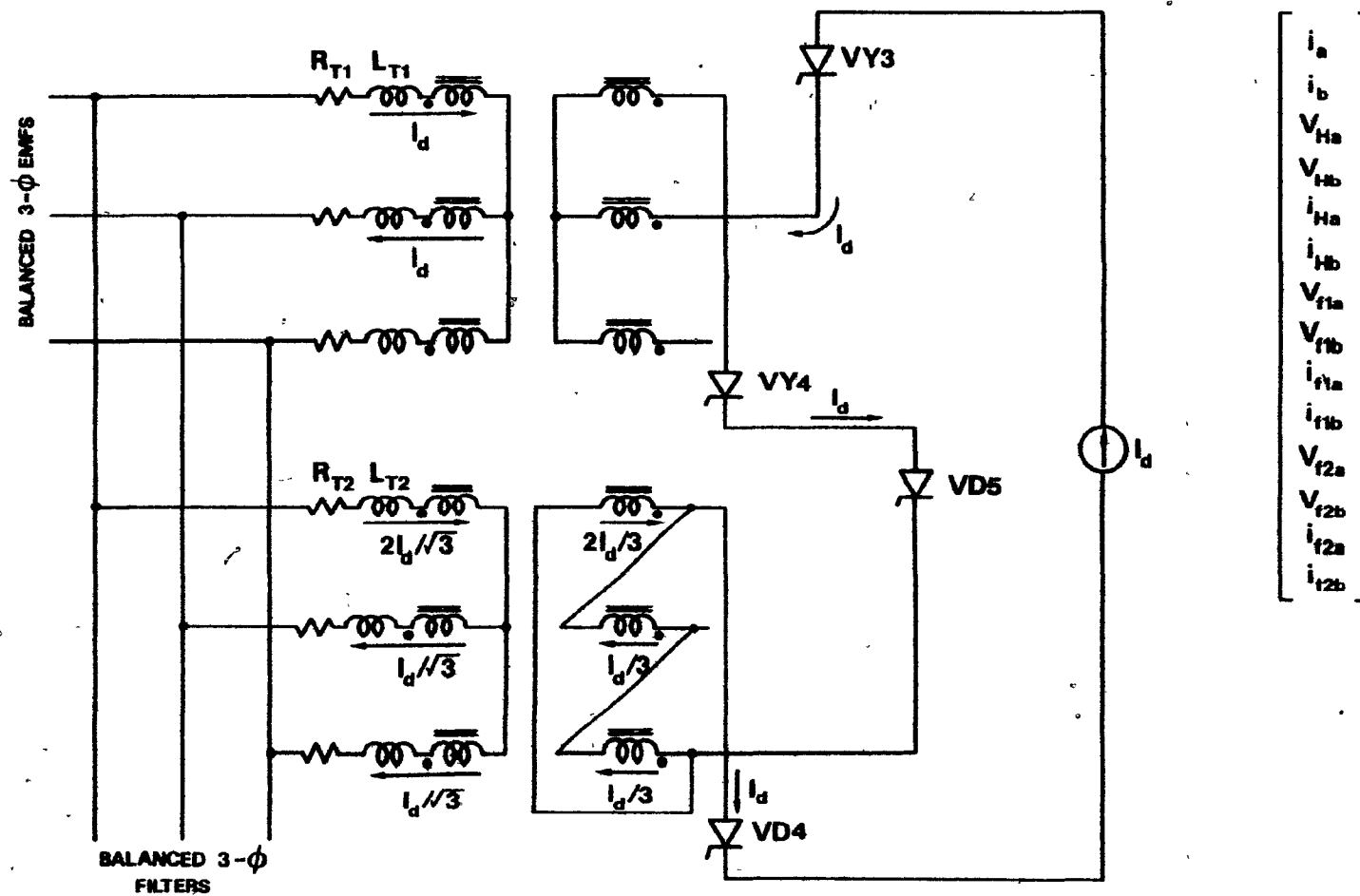


FIGURE 4.4(d) Sub-network 4, conducting valves; VY3, VY4, VD4, VD5

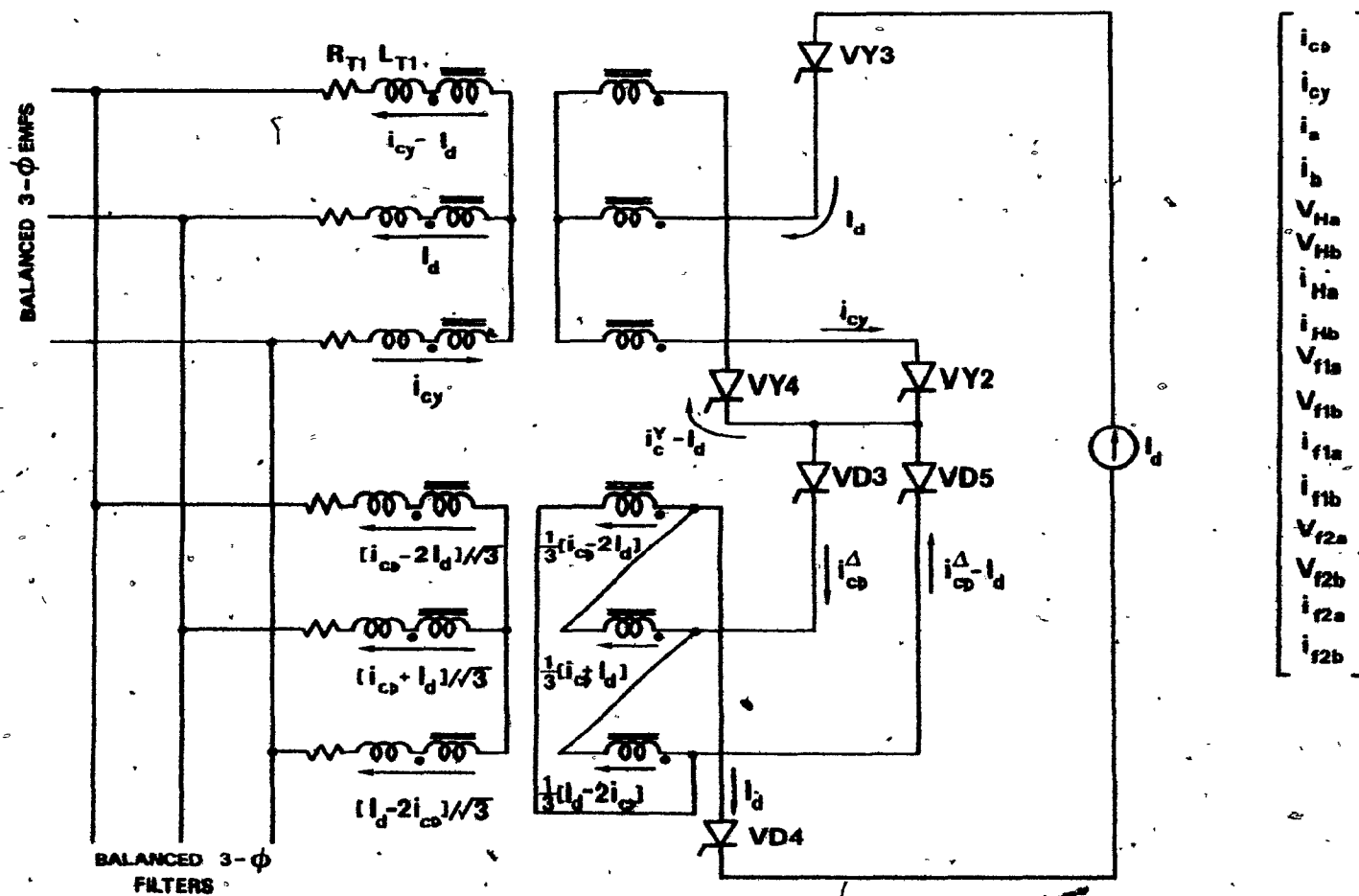


FIGURE 4.4(e) Sub-network 5, conducting valves; VY2, VY3, VY4, VD3, VD4, VD5

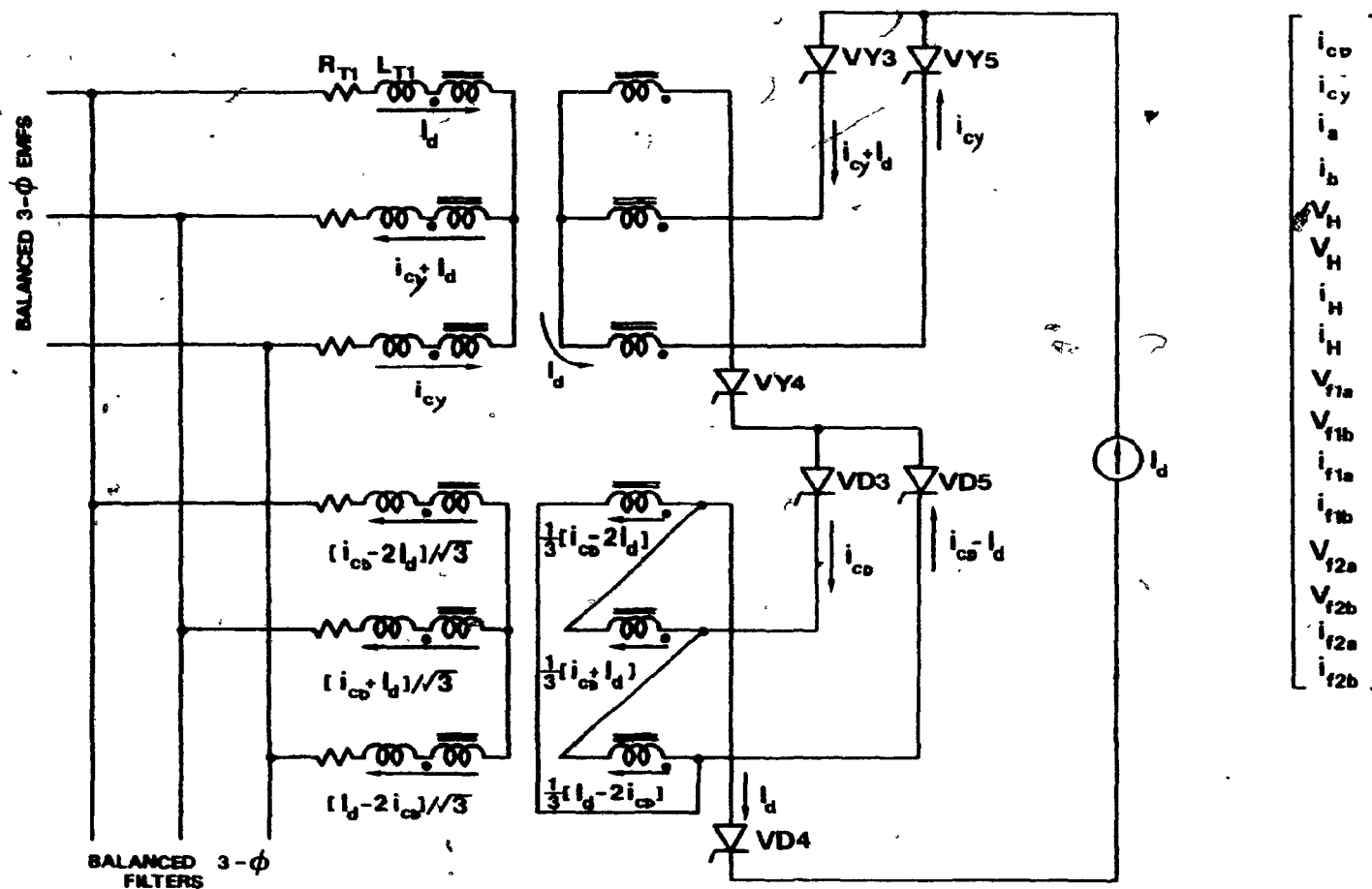


FIGURE 4.4(f) Sub-network 6, conducting valves VY3, VY4, VY5, VD3, VD4, VD5

capacitor voltage. As shown in the diagram the a and b phases have been used to define the three-phase voltage and current variables.

For the non-commutating sub-networks, numbers 2 and 4,, no other state variables are required since the wye-wye and wye-delta transformers carry only the DC line currents. The dimension of the state vector for the non-commutating sub-intervals is defined as N_2 . Clearly, for the sub-networks of Figs. 4.4(b) and (d), $N_2=14$.

Sub-networks 1, 3 and 5 represent the converter during various commutations, and the required commutation variables are included in the state vectors. Sub-networks 1 and 3 which include a single commutation each have state vectors of dimension N_2+1 . Sub-network 5 represents the network while commutations are occurring in the two bridges simultaneously. Its state vector includes the two commutation variables, i_{cy} and i_{cd} , and has a dimension equal to N_2+2 .

4.3.2 Case 2, $30^\circ < \omega\mu_2 \leq 60^\circ$

Comparison of Figs. 4.3(a), (b) with Figs. 4.3(c), (d) indicates that only one new sub-network is introduced by the $30^\circ < \omega\mu_2 \leq 60^\circ$ condition. This sub-network corresponds to a new commutation commencing in the wye-wye bridge before the wye-delta commutation is completed. Sub-network 6 is shown in Fig. 4.4(f). The state vector for sub-network 6 includes the same variables as those used to describe the fifth

sub-network and, therefore, has the same dimension, $N2+2$.

Having selected the currents and voltages to be used in describing each of the sub-networks, KVL and KCL are used to generate the required state matrices $[A]$ and $[B]$ (Appendix 1).

4.4 Solution Algorithm. Case 1

The procedure of BLOCK 1 of the flowchart of Fig. 3.4 is used in the following analysis to generate the required matrix expression for $\underline{x}_1(0)$. First the expression is derived for the $\omega\mu_1 < 30^\circ$ condition, and this result is then repeated with some modification for $30^\circ \leq \omega\mu_1 < 60^\circ$.

4.4.1 Case 1(i), $\omega\mu_1 < 30^\circ$

The notation and essential data used in this section, for the formation of a solution algorithm for Case 1(i), are collected together in Fig. 4.5.

The initial condition vector $\underline{x}_1(0)$ may be partitioned as

$$\underline{x}_1(0) = \begin{bmatrix} i_{cy}(0) \\ \underline{x}_1^*(0) \end{bmatrix} = \begin{bmatrix} I_d \\ \underline{x}_1^*(0) \end{bmatrix} \quad (4.2)$$

where the initial value I_d , of the commutation current has been substituted. The $N2$ -dimension vector $\underline{x}_1^*(t)$ contains all the AC side state variables of the $N1$ -dimension state vector $\underline{x}_1(t)$. Thus in applying the general method developed in Chapter 3 it is only necessary to solve for the vector

CONDUCTING VALVES	VY2 VY3 VY4	VD3 VD4	VY3 VY4	VD3 VD4	VY3 VY4	VD3 VD4 VD5	VY3 VY4	VD4 VD5
CIRCUIT TOPOLOGY	FIG. 4.4(a)		FIG. 4.4(b)		FIG. 4.4(c)		FIG. 4.4(d)	
STATE VECTOR	$x_1 = \begin{bmatrix} i_{cy} \\ x_1 \end{bmatrix}$		x_2		$x_3 = \begin{bmatrix} i_{cd} \\ x_3 \end{bmatrix}$		x_4	
DIMENSION	N2+1		N2		N2+1		N2	
$i_c^y =$	i_{cy}		0		0		0	
$-i_b^\Delta =$	i_d		i_d		i_{cd}		0	
COMPATIBILITY MATRIX	$[C_1]$		$[I]$		$[C_1]$		$[C_4]$	
INITIAL STATE	$\begin{bmatrix} i_d \\ [C_4] x_4(T/6) \end{bmatrix}$		$[C_1] x_1(u_1)$		$\begin{bmatrix} i_d \\ x_2(T/12) \end{bmatrix}$		$[C_1] x_3(u_2 + T/12)$	
STATE TRANSITION MATRIX	$[\Phi_1] = \begin{bmatrix} p_{11} & p_{12}^T \\ p_{21} & p_{22} \end{bmatrix}$		$[\Phi_2]$		$[\Phi_3] = \begin{bmatrix} q_{11} & q_{12}^T \\ q_{21} & q_{22} \end{bmatrix}$		$[\Phi_4]$	
$t =$	0		u_1		$T/12$		$u_2 + T/12$	
	u_1		$T/12 - u_1$		u_2		$T/12 - u_2$	
			$T/6$					

FIGURE 4.5 Case 1(i); $\omega\mu_1 < 30^\circ$, $\omega\mu_2 < 30^\circ$

Notation used in derivation of solution algorithm

$\underline{x}_1^*(0)$, in terms of the commutation times μ_1 and μ_2 .

Applying the state solution for the first sub-interval yields the expression

$$\underline{x}_1(\mu_1) = \underline{x}_1^s(\mu_1) + [\phi_1(\mu_1)] \left(\begin{bmatrix} I_d \\ \underline{x}_1^*(0) \end{bmatrix} - \underline{x}_1^s(0) \right) \quad (4.3)$$

where the superscript s is used to identify the ZSR. Referring to the state vectors shown in Figs.4.4(a),(b) the first compatibility matrix may be written as,

$$[C_1] = \begin{bmatrix} \vdots & 1 & \vdots \\ 0 & \vdots & \ddots \\ \vdots & \vdots & \vdots & 1 \end{bmatrix}_{N2} \quad (4.4)$$

The boundary condition at $t=\mu_1$ is written as

$$\underline{x}_2(\mu_1) = [C_1] \{ \underline{x}_1^s(\mu_1) - [\phi_1(\mu_1)] \underline{x}_1^s(0) \} + [C_1] [\phi_1(\mu_1)] \begin{bmatrix} I_d \\ \underline{x}_1^*(0) \end{bmatrix} \quad (4.5)$$

With the state transition matrix partitioned as

$$[\phi_1(\mu_1)] = \begin{bmatrix} P_{11}(\mu_1) & P_{12}^T(\mu_1) \\ P_{21}(\mu_1) & P_{22}(\mu_1) \end{bmatrix}_{N2} \quad (4.6)$$

Eqn. 4.5 may be re-written as

$$\underline{x}_2(\mu_1) = \underline{R}_1(\mu_1) + [P_{22}(\mu_1)] \underline{x}_1^*(0) \quad (4.7)$$

where

$$\underline{R}_1(\mu_1) = [C_1] \{ \underline{x}_1^s(\mu_1) - [\phi_1(\mu_1)] \underline{x}_1^s(0) \} + P_{21}(\mu_1) I_d \quad (4.8)$$

Eqn. 4.7 is substituted into the second sub-interval solution, evaluated at $t=T/12$, to yield,

$$\begin{aligned} \underline{x}_2(T/12) = & \underline{x}_2^s(T/12) + [\phi_2(T/12-\mu_1)] \{ \underline{R}_1(\mu_1) - \underline{x}_2^s(\mu_1) \} \\ & + [\phi_2(T/12-\mu_1)] [P_{22}(\mu_1)] \underline{x}_1^*(0) \end{aligned} \quad (4.9)$$

As was done for $\underline{x}_1(0)$, $\underline{x}_3(T/12)$ may be partitioned as

$$\underline{x}_3(T/12) = \begin{bmatrix} i_{cd}(T/12) \\ \underline{x}_3^*(T/12) \end{bmatrix} = \begin{bmatrix} I_d \\ \underline{x}_3^*(T/12) \end{bmatrix} \quad (4.10)$$

With this notation,

$$\underline{x}_3^*(T/12) = \underline{x}_2(T/12) \quad (4.11)$$

and the second compatibility matrix is simply the identity matrix.

Eqn. 4.11 is substituted into the state solution for the third sub-interval, at $t=T/12+\mu_2$ to yield,

$$\underline{x}_3(T/12+\mu_2) = \underline{x}_3^s(T/12+\mu_2) + [\Phi_3(\mu_2)] \left\{ \begin{bmatrix} I_d \\ \underline{x}_2(T/12) \end{bmatrix} - \underline{x}_3^s(T/12) \right\} \quad (4.12)$$

The same compatibility matrix may be used between the third and fourth sub-intervals as was used for the first two, and the boundary condition at $t=T/12+\mu_2$ may be written as

$$\begin{aligned} \underline{x}_4(T/12+\mu_2) = [C_1] [\Phi_3(\mu_2)] \left\{ \begin{bmatrix} I_d \\ \underline{x}_2(T/12) \end{bmatrix} - \underline{x}_3^s(T/12) \right\} \\ + [C_1] \underline{x}_3^s(T/12+\mu_2) \end{aligned} \quad (4.13)$$

Substituting Eqn. 4.9 and the partitioned state matrix,

$$[\Phi_3(\mu_2)] = \begin{bmatrix} Q_{11}(\mu_2) & Q_{12}^T(\mu_2) \\ Q_{21}(\mu_2) & [Q_{22}(\mu_2)] \end{bmatrix} \begin{matrix} 1 \\ N2 \end{matrix} \quad (4.14)$$

into Eqn. 4.13 yields

$$\underline{x}_4(T/12+\mu_2) = \underline{R}_2(\mu_1, \mu_2) + [S_2(\mu_1, \mu_2)] \underline{x}_1^*(0) \quad (4.15)$$

where

$$\begin{aligned} \underline{R}_2(\mu_1, \mu_2) = [C_1] \{ \underline{x}_3^s(T/12+\mu_2) - [\Phi_3(\mu_2)] \underline{x}_3^s(T/12) \} + Q_{21}(\mu_2) I_d \\ + [Q_{22}(\mu_2)] \{ \underline{x}_2^s(T/12) + [\Phi_2(T/12-\mu_1)] (\underline{R}_1(\mu_1) - \underline{x}_2^s(\mu_1)) \} \end{aligned} \quad (4.16)$$

and

$$[S_2(\mu_1, \mu_2)] = [Q_{22}(\mu_2)] [\Phi_2(T/12-\mu_1)] [P_{22}(\mu_1)] \quad (4.17)$$

The equation is advanced through the final sub-interval by applying the fourth state solution.

$$\underline{x}_4(T/6) = \underline{x}_4^s(T/6) + [\phi_4(T/12 - \mu_2)] \{ \underline{x}_4(T/12 + \mu_2) - \underline{x}_4^s(T/12 + \mu_2) \} \quad (4.18)$$

The final compatibility matrix applies the periodicity in $T/6$ property as well as satisfying the continuity constraints. Considering the state vectors of Figs. 4.4(a) and (d) as well as the phase transpositions of Eqn. 3.13 leads to the final boundary condition.

$$\underline{x}_1^*(0) = [C_4] \underline{x}_4(T/6) \quad (4.19)$$

where

$$[C_4] = \begin{bmatrix} 1 & 1 & 0 \\ -1 & 0 & 0 \\ 0 & 1 & 1 \\ 0 & -1 & 0 \end{bmatrix} \quad \begin{matrix} N2 \\ N2 \end{matrix} \quad (4.20)$$

Substituting Eqn. 4.15 into Eqn. 4.18 and multiplying by the compatibility matrix, as in Eqn. 4.19 gives a matrix relation for $\underline{x}_1^*(0)$ in terms of the two commutation times.

$$\begin{aligned} \underline{x}_1^*(0) = [C_4] \{ \underline{x}_4^s(T/6) + [\phi_4(T/12 - \mu_2)] (\underline{R}_2(\mu_1, \mu_2) - \underline{x}_4^s(T/12 + \mu_2)) \} \\ + [C_4] [\phi_4(T/12 - \mu_2)] [S_2(\mu_1, \mu_2)] \underline{x}_1^*(0) \end{aligned} \quad (4.21)$$

Combining the $\underline{x}_1^*(0)$ terms and inverting leads to the final equation,

$$\underline{x}_1^*(0) = [G_1(\mu_1, \mu_2)]^{-1} \underline{F}_1(\mu_1, \mu_2) \quad (4.22)$$

where

$$[G_1(\mu_1, \mu_2)] = [I] - [C_4] [\phi_4(T/12 - \mu_2)] [S_2(\mu_1, \mu_2)]$$

$$\underline{F}_1(\mu_1, \mu_2) = [C_4] \{ \underline{x}_4^s(T/6)$$

$$+ [\phi_4(T/12 - \mu_2)] (\underline{R}_2(\mu_1, \mu_2) - \underline{x}_4^s(T/12 + \mu_2)) \} \quad (4.23)$$

The right hand side of Eqn. 4.22 may be calculated

(-) straightforwardly for given iterates of the commutation times μ_1 and μ_2 . The determination of the commutation times leading to a final solution of Eqn. 4.22 is described in Section 4.6.


CONDUCTING VALVES	VY2 VY3 VY4	VD3 VD4	VY2 VY3 VY4	VD3 VD4 VD5	VY3 VY4	VD3 VD4 VD5	VY3 VY4	VD4 VD5
CIRCUIT TOPOLOGY	FIG.4.4(a)		FIG.4.4(e)		FIG.4.4(c)		FIG.4.4(d)	
STATE VECTOR	$\underline{x}_1 = \begin{bmatrix} i_{cy} \\ \underline{x}_1^* \end{bmatrix}$		$\underline{x}_5 = \begin{bmatrix} i_{cd} \\ i_{cy} \\ \underline{x}_5^* \end{bmatrix}$		$\underline{x}_3 = \begin{bmatrix} i_{cd} \\ \underline{x}_3^* \end{bmatrix}$		\underline{x}_4	
DIMENSION	N2+1		N2+2		N2+1		N2	
$i_c^y =$	i_{cy}		i_{cy}		0		0	
$-i_b^\Delta =$	i_d		i_{cd}		i_{cd}		0	
COMPATIBILITY MATRIX	[I]		[C ₂]		[C ₁]		[C ₄]	
INITIAL STATE	$\begin{bmatrix} i_d \\ [C_4] \underline{x}_4(T/6) \end{bmatrix}$		$\begin{bmatrix} i_d \\ \underline{x}_1(T/12) \end{bmatrix}$		$[C_2] \underline{x}_5(u_1)$		$[C_1] \underline{x}_3(u_2 + T/12)$	
STATE TRANSITION MATRIX	$[\Phi_1] = \begin{bmatrix} P_{11} & P_{12}^T \\ P_{21} & P_{22} \end{bmatrix}$		$[\Phi_5] = \begin{bmatrix} M_{11} & M_{12}^T \\ M_{21} & M_{22} \end{bmatrix}$		$[\Phi_3]$		$[\Phi_4]$	
t =	0	T/12	u_1	T/12+ u_2	T/6			
	T/12		$u_1 - T/12$		T/12+ $u_2 - u_1$		T/12- u_2	
			T/6					

FIGURE 4.6 Case 1(ii); $30^\circ \leq \omega\mu_1 < 60^\circ$, $\omega\mu_2 < 30^\circ$

Notation used in derivation of solution algorithm

4.4.2 Case 1(ii), $30^\circ \leq \omega\mu_1 < 60^\circ$

The notation and a summary of the essential data used for Case 1(ii) is shown in Fig. 4.6. The procedure of Section 4.4.1 may be repeated, with some modifications, to generate the required matrix relation for $\underline{x}_1^*(0)$ when the commutation angle is in the range, $30^\circ \leq \omega\mu_1 < 60^\circ$.

Rather than repeating the matrix formulation, the required state solutions and boundary conditions are listed. The four state solutions evaluated at each sub-intervals final time are:

$$1) \quad \underline{x}_1(T/12) = \underline{x}_1^s(T/12) + [\phi_1(T/12)] \{ \underline{x}_1(0) - \underline{x}_1^s(0) \} \quad (4.24)$$

$$2) \quad \underline{x}_5(\mu_1) = \underline{x}_5^s(\mu_1) + [\phi_5(\mu_1 - T/12)] \{ \underline{x}_5(T/12) - \underline{x}_5^s(T/12) \} \quad (4.25)$$

$$3) \quad \underline{x}_3(T/12 + \mu_2) = \underline{x}_3^s(T/12 + \mu_2) + [\phi_3(T/12 + \mu_2 - \mu_1)] \{ \underline{x}_3(\mu_1) - \underline{x}_3^s(\mu_1) \} \quad (4.26)$$

$$4) \quad \underline{x}_4(T/6) = \underline{x}_4^s(T/6) + [\phi_4(T/12 - \mu_2)] \{ \underline{x}_4(T/12 + \mu_2) - \underline{x}_4^s(T/12 + \mu_2) \} \quad (4.27)$$

The four boundary conditions required to connect the solution are given by:

$$1) \quad \underline{x}_5(T/12) = \begin{bmatrix} I_d \\ iY(T/12) \\ \underline{x}_5^*(T/12) \end{bmatrix} = \begin{bmatrix} I_d \\ \underline{x}_1(T/12) \end{bmatrix} \quad (4.28)$$

$$2) \quad \underline{x}_3(\mu_1) = [C_2] \underline{x}_5(\mu_1)$$

where

$$[C_2] = \begin{bmatrix} 1 & \cdots & 0 \\ \vdots & \ddots & \vdots \\ 0 & \cdots & 1 \\ \vdots & \ddots & \vdots \\ 0 & \cdots & 0 \end{bmatrix} \begin{matrix} 1 \\ \vdots \\ N2 \\ \vdots \\ 1 \end{matrix} \quad (4.29)$$

$$3) \underline{x}_4(T/12+\mu_2) = [C_1] \underline{x}_3(T/12+\mu_2) \quad (4.30)$$

where $[C_1]$ was defined by Eqn. 4.4.

4) The final boundary condition remains Eqn. 4.19.

If the state transition matrices are partitioned as,

$$[\Phi_1(T/12)] = \begin{bmatrix} P_{11}(T/12) & P_{12}^T(T/12) \\ P_{21}(T/12) & [P_{22}(T/12)] \end{bmatrix} \begin{matrix} 1 \\ N2 \end{matrix} \quad (4.31)$$

$$[\Phi_5(\mu_1-T/12)] = \begin{bmatrix} M_{11}(\mu_1-T/12) & M_{12}^T(\mu_1-T/12) \\ M_{21}(\mu_1-T/12) & [M_{22}(\mu_1-T/12)] \end{bmatrix} \begin{matrix} 1 \\ N2+1 \end{matrix} \quad (4.32)$$

the final equation may be written as

$$\underline{x}_1^*(0) = [G_2(\mu_1, \mu_2)]^{-1} \underline{F}_2(\mu_1, \mu_2) \quad (4.33)$$

where

$$[G_2(\mu_1, \mu_2)] = [I] - [C_4][\Phi_4(T/12-\mu_2)][S_4(\mu_1, \mu_2)] \quad (4.34)$$

$$\underline{F}_2(\mu_1, \mu_2) = [C_4]\{\underline{x}_4^s(T/6) + [\Phi_4(T/12-\mu_2)] \times \\ (\underline{R}_4(\mu_1, \mu_2) - \underline{x}_4^s(T/12+\mu_2))\} \quad (4.35)$$

$$[S_4(\mu_1, \mu_2)] = [C_1][\Phi_3(T/12+\mu_2-\mu_1)][C_2][S_3(\mu_1)] \quad (4.36)$$

$$\underline{R}_4(\mu_1, \mu_2) = [C_1]\{\underline{x}_3^s(T/12+\mu_2) + [\Phi_3(T/12+\mu_2-\mu_1)] \times \\ ([C_2]\underline{R}_3(\mu_1) - \underline{x}_3^s(\mu_1))\} \quad (4.37)$$

$$[S_3(\mu_1)] = \begin{bmatrix} M_{12}^T(\mu_1-T/12) \\ [M_{22}(\mu_1-T/12)] \end{bmatrix} \begin{bmatrix} P_{12}^T(T/12) \\ [P_{22}(T/12)] \end{bmatrix} \quad (4.38)$$

$$\underline{R}_3(\mu_1) = \underline{x}_5^s(\mu_1) - [\Phi_5(\mu_1-T/12)] \underline{x}_5^s(T/12) + \begin{bmatrix} M_{11}(\mu_1-T/12) \\ M_{21}(\mu_1-T/12) \end{bmatrix} I_d \\ + \begin{bmatrix} M_{12}^T(\mu_1-T/12) \\ [M_{22}(\mu_1-T/12)] \end{bmatrix} \quad (4.39)$$

$$\times \{\underline{x}_1^s(T/12) + \begin{bmatrix} P_{11}(T/12) \\ P_{21}(T/12) \end{bmatrix} I_d - [\Phi_1(T/12)] \underline{x}_1^s(0)\}$$







CONDUCTING VALVES	VY2 VY3 VY4	VD3 VD4	VY3 VY4	VD3 VD4	VY3 VY4	VD3 VD4 *VD5	VY3 VY4 VY5	VD3 VD4 VD5
CIRCUIT TOPOLOGY	FIG. 4.4(a)		FIG. 4.4(b)		FIG. 4.4(c)		FIG. 4.4(f)	
STATE VECTOR	$\mathbf{x}_1 = \begin{bmatrix} i_{cy} \\ \mathbf{x}_1^T \end{bmatrix}$		\mathbf{x}_2		$\mathbf{x}_3 = \begin{bmatrix} i_{cd} \\ \mathbf{x}_3^T \end{bmatrix}$		$\mathbf{x}_6 = \begin{bmatrix} i_{cd} \\ i_{cy} \\ \mathbf{x}_6^T \end{bmatrix}$	
DIMENSION	N2+1		N2		N2+1		N2+2	
$i_c^y =$			0		0			
$-i_b^a =$								
COMPATIBILITY MATRIX	$[C_1]$		$[I]$		$[C_3]$		$[C_5]$	
INITIAL STATE	$[C_5] \mathbf{x}_6(u_2 + T/12)$		$[C_1] \mathbf{x}_1(u_1)$		$\begin{bmatrix} I_d \\ \mathbf{x}_2(T/12) \end{bmatrix}$		$[C_3] \mathbf{x}_3(T/6)$	
STATE TRANSITION MATRIX	$[\Phi_1]$		$[\Phi_2]$		$[\Phi_3] = \begin{bmatrix} Q_{11} & Q_{12}^T \\ Q_{21} & Q_{22} \end{bmatrix}$		$[\Phi_6]$	
$t =$	$u_2 - T/12$		u_1		$T/12$		$T/6$	
	$u_1 - u_2 + T/12$		$T/12 - u_1$		$T/12$		$u_2 - T/12$	
			$T/6$					

FIGURE 4.7 Case 2(i); $\omega\mu_1 < 30^\circ$, $30^\circ \leq \omega\mu_2 < 60^\circ$

Notation used in derivation of solution algorithm

4.5 Solution Algorithm. Case 2

Once again the procedure depicted in Fig. 3.6 is applied, however in this case it is utilized to generate the initial conditions at $t = \mu_2 - T/12$. It is noteworthy, that in Figs. 4.3(c) and (d) at each boundary point there is at least one commutation occurring. Because of this it is necessary to include a commutation current variable in the initial state vector no matter where the time origin is selected.

4.5.1 Case 2(i), $\omega\mu_1 < 30^\circ$

Following the precedent of the previous section, the collected notation of this section is shown in Fig. 4.7.

At the initial boundary time, $t = \mu_2 - T/12$ the commutation current must be included with the other unknown state variables. The initial condition vector is advanced to $t = \mu_1$ using the first state solution.

$$\underline{x}_1(\mu_1) = \underline{x}_1^s(\mu_1) + [\Phi_1(\mu_1 - \mu_2 + T/12)] \{ \underline{x}_1(\mu_2 - T/12) - \underline{x}_1^s(\mu_2 - T/12) \} \quad (4.40)$$

The first compatibility matrix $[C_1]$ is once again defined by Eqn. 4.4. Applying the boundary condition at $t = \mu_1$ and the state solution for the second sub-interval leads to the expression,

$$\underline{x}_2(T/12) = \underline{R}_5(\mu_1, \mu_2) + [S_5(\mu_1, \mu_2)] \underline{x}_1(\mu_2 - T/12) \quad (4.41)$$

where

$$[S_5(\mu_1, \mu_2)] = [\Phi_2(T/12 - \mu_1)] [C_1] [\Phi_1(\mu_1 - \mu_2 + T/12)] \quad (4.42)$$

$$\begin{aligned} \underline{R}_5(\mu_1, \mu_2) = & \underline{x}_2^s(T/12) + [\Phi_2(T/12 - \mu_1)] \times \\ & \{ [C_1] (\underline{x}_1^s(\mu_1) - [\Phi_1(\mu_1 - \mu_2 + T/12)] \underline{x}_1^s(\mu_2 - T/12)) - \underline{x}_2^s(\mu_1) \} \end{aligned} \quad (4.43)$$

The boundary condition at $t=T/12$ has the form of Eqn. 4.11. Combining this boundary condition with the state solution for the third sub-interval evaluated at $t=T/6$ yields,

$$\underline{x}_3(T/6) = \underline{x}_3^s(T/6) + [\phi_3(T/12)] \left\{ \begin{bmatrix} I_d \\ \underline{x}_2(T/12) \end{bmatrix} - \underline{x}_3^s(T/12) \right\} \quad (4.44)$$

Comparing the state vectors shown in Figs. 4.4(c) and (f) leads to the boundary condition,

$$\underline{x}_6(T/6) = \begin{bmatrix} i_{cd}(T/6) \\ 0 \\ \underline{x}_6^*(T/6) \end{bmatrix} = [C_3] \underline{x}_3(T/6) \quad (4.45)$$

where

$$[C_3] = \begin{bmatrix} 1 & & 0 \\ 0 & 1 & 0 \\ 0 & 0 & 1 \end{bmatrix} \begin{matrix} 2 \\ N2 \\ 1 \end{matrix} \quad (4.46)$$

Substituting the partitioned state transition matrix,

$$[\phi_3(T/12)] = \begin{bmatrix} Q_{11}(T/12) & Q_{12}^T(T/12) \\ Q_{21}(T/12) & Q_{22}(T/12) \end{bmatrix} \begin{matrix} 1 \\ N2 \end{matrix} \quad (4.47)$$

Plugging Eqn. 4.41 into Eqn. 4.44 and substituting the result into the boundary condition of Eqn. 4.45 yields

$$\underline{x}_6(T/6) = \underline{R}_6(\mu_1, \mu_2) + [S_6(\mu_1, \mu_2)] \underline{x}_1(\mu_2 - T/12) \quad (4.48)$$

where

$$\underline{R}_6(\mu_1, \mu_2) = [C_3] \{ \underline{x}_3^s(T/6) + \begin{bmatrix} Q_{11}(T/12) \\ Q_{21}(T/12) \end{bmatrix} I_d + \begin{bmatrix} Q_{12}^T(T/12) \\ Q_{22}(T/12) \end{bmatrix} \underline{R}_5(\mu_1, \mu_2) - [\Phi_3(T/12)] \underline{x}_3^s(T/12) \} \quad (4.49)$$

$$[S_6(\mu_1, \mu_2)] = [C_3] \begin{bmatrix} Q_{12}(T/12) \\ Q_{22}(T/12) \end{bmatrix} [S_5(\mu_1, \mu_2)] \quad (4.50)$$

Eqn. 4.48 is substituted into the state solution for the sixth sub-network, evaluated at $t = \mu_2 + T/12$, resulting in the expression,

$$\underline{x}_6(\mu_2 + T/12) = \underline{x}_6^s(\mu_2 + T/12) + [\Phi_6(\mu_2 - T/12)] \{ \underline{R}_6(\mu_1, \mu_2) - \underline{x}_6^s(T/6) \} + [\Phi_6(\mu_2 - T/12)] [S_6(\mu_1, \mu_2)] \underline{x}_1(\mu_2 - T/12) \quad (4.51)$$

As in the Case 1 analysis, the final compatibility matrix applies the $T/6$ periodicity property along with the continuity constraints. In Section 4.2 it was mentioned that particular attention was required in applying the final boundary conditions to the wye-bridge commutation currents for Case 2 analysis. Upon consideration of Figs. 4.3(c) and (d) as well as the sketch of Fig. 2.3(b), Eqn. 4.1 was derived. The remainder of the terms are matched by the equation

$$\underline{x}_1^*(\mu_2 - T/12) = [C_4] \underline{x}_6^*(\mu_2 + T/12) \quad (4.52)$$

where $[C_4]$ was previously defined in Eqn. 4.20.

Eqns. 4.1 and 4.52 may be combined to form an overall compatibility relation between $\underline{x}_1(\mu_2 - T/12)$ and $\underline{x}_6(\mu_2 + T/12)$.

$$\underline{x}_1(\mu_2 - T/12) = \underline{K}_1 + [C_5] \underline{x}_6(\mu_2 + T/12) \quad (4.53)$$

where

$$\underline{K}_1 = \begin{bmatrix} I \\ 0^d \\ \vdots \\ Q \end{bmatrix} \begin{matrix} 1 \\ N2 \end{matrix} \quad [C_5] = \begin{bmatrix} 0 & 1 & 0 \\ 0 & \vdots & [C_4] \end{bmatrix} \begin{matrix} 1 \\ N2 \end{matrix} \quad (4.54)$$

2 N2

Upon substitution of Eqn. 4.51 into Eqn. 4.53 the final matrix relation for the initial condition $\underline{x}_1(\mu_2 - T/12)$ in terms of the commutation times is written,

$$\underline{x}_1(\mu_2 - T/12) = [G_3(\mu_1, \mu_2)]^{-1} \underline{F}_3(\mu_1, \mu_2) \quad (4.55)$$

where

$$[G_3(\mu_1, \mu_2)] = [I] - [C_5] [\Phi_6(\mu_2 - T/12)] [S_6(\mu_1, \mu_2)] \quad (4.56)$$

$$\underline{F}_3(\mu_1, \mu_2) = \underline{K}_1 + [C_5] \underline{x}_6^s(\mu_2 + T/12) + [\Phi_6(\mu_2 - T/12)] (\underline{R}_6(\mu_1, \mu_2) - \underline{x}_6^s(T/6)) \quad (4.57)$$

CONDUCTING VALVES	VY2 VY3 VD3 VY4 VD4	VY2 VD3 VY3 VD4 VY4 VD5	VY3 VD3 VY4 VD5	VY3 VD3 VY4 VD5 VY5 VD5
CIRCUIT TOPOLOGY	FIG.4.4(a)	FIG.4.4(e)	FIG.4.4(g)	FIG.4.4(i)
STATE VECTOR	$\underline{x}_1 = \begin{bmatrix} i_{cy} \\ x_1 \end{bmatrix}$	$\underline{x}_5 = \begin{bmatrix} i_{cd} \\ i_{cy} \\ x_5 \end{bmatrix}$	$\underline{x}_3 = \begin{bmatrix} i_{cd} \\ x_3 \end{bmatrix}$	$\underline{x}_6 = \begin{bmatrix} i_{cd} \\ i_{cy} \\ x_6 \end{bmatrix}$
DIMENSION	$N2+1$	$N2+2$	$N2+1$	$N2+2$
i_c^y	i_{cy}	i_{cy}		i_{cy}
$-i_b^A$	i_d	i_{cd}	i_{cd}	i_{cd}
COMPATIBILITY MATRIX		$[1]$	$[C_2]$	$[C_3]$
INITIAL STATE	$[C_5] \underline{x}_6(u_2 + T/12)$	$\begin{bmatrix} i_d \\ x_1(T/12) \end{bmatrix}$	$[C_2] \underline{x}_5(u_1)$	$[C_3] \underline{x}_3(T/6)$
STATE TRANSITION MATRIX	$[\Phi_1]$	$[\Phi_5] = \begin{bmatrix} M_{11} & M_{12}^T \\ M_{21} & M_{22} \end{bmatrix}$	$[\Phi_3]$	$[\Phi_6]$
$t =$	$u_2 - T/12$	$T/12$	u_1	$T/6$
	$T/6 - u_2$	$u_1 - T/12$	$T/6 - u_1$	$u_2 - T/12$
			$T/6$	

FIGURE 4.8 Case 2(ii); $30^\circ \leq \omega\mu_1 < 60^\circ$, $30^\circ \leq \omega\mu_2 < 60^\circ$

Notation used in derivation of solution algorithm

4.5.2 Case 2(ii), $30^\circ \leq \omega\mu_1 < 60^\circ$

As was done for Section 4.4.2, the four sub-interval solutions and boundary conditions are listed, and the initial condition relation derived by comparison with the $\omega\mu_1 < 30^\circ$ result.

$$1) \underline{x}_1(T/12) = \underline{x}_1^S(T/12) + [\phi_1(T/6 - \mu_2)] \{ \underline{x}_1(\mu_2 - T/12) - \underline{x}_1^S(\mu_2 - T/12) \} \quad (4.58)$$

$$2) \text{ Eqn. 4.25}$$

$$3) \underline{x}_3(T/6) = \underline{x}_3^S(T/6) + [\phi_3(T/6 - \mu_1)] \{ \underline{x}_3(\mu_1) - \underline{x}_3^S(\mu_1) \} \quad (4.59)$$

$$4) \underline{x}_6(\mu_2 + T/12) = \underline{x}_6^S(\mu_2 + T/12) + [\phi_6(\mu_2 - T/12)] \{ \underline{x}_6(T/6) - \underline{x}_6^S(T/6) \} \quad (4.60)$$

The boundary conditions required to formulate the solution have already been presented as Eqn. 4.28, Eqn. 4.29, Eqn. 4.45 and Eqn. 4.53. With the state transition matrix for the fifth sub-network partitioned as in Eqn. 4.32, the final equation is written as

$$\underline{x}_1(\mu_2 - T/12) = [G_4(\mu_1, \mu_2)]^{-1} \underline{F}_4(\mu_1, \mu_2) \quad (4.61)$$

where

$$[G_4(\mu_1, \mu_2)] = [I] - [C_5] [\phi_6(\mu_2 - T/12)] [S_8(\mu_1, \mu_2)] \quad (4.62)$$

$$\underline{F}_4(\mu_1, \mu_2) = [C_5] \{ \underline{x}_6^S(\mu_2 + T/12) + [\phi_6(\mu_2 - T/12)] (\underline{R}_8(\mu_1, \mu_2) - \underline{x}_6^S(T/6)) \} \quad (4.63)$$

$$[S_8(\mu_1, \mu_2)] = [C_3] [\phi_3(T/6 - \mu_1)] [C_2] [S_7(\mu_1, \mu_2)] \quad (4.64)$$

$$\underline{R}_8(\mu_1, \mu_2) = [C_3] \{ \underline{x}_3^S(T/6) + [\phi_3(T/6 - \mu_1)] ([C_2] \underline{R}_7(\mu_1, \mu_2) - \underline{x}_3^S(\mu_1)) \} \quad (4.65)$$

$$[S_7(\mu_1, \mu_2)] = \begin{bmatrix} \underline{M}_{12}^T(\mu_1 - T/12) \\ [\underline{M}_{22}(\mu_1 - T/12)] \end{bmatrix} [\phi_1(T/6 - \mu_2)] \quad (4.66)$$

$$\underline{R}_7(\mu_1, \mu_2) = \underline{x}_5^S(\mu_1) + \begin{bmatrix} \underline{M}_{11}(\mu_1 - T/12) \\ \underline{M}_{21}(\mu_1 - T/12) \end{bmatrix} \underline{I}_d - [\phi_5(\mu_1 - T/12)] \underline{x}_5^S(T/12)$$

$$\begin{bmatrix} \underline{M}_{12}^T(\mu_1 - T/12) \\ [\underline{M}_{22}(\mu_1 - T/12)] \end{bmatrix} \{ \underline{x}_1^S(T/12) - [\phi_1(T/6 - \mu_2)] \underline{x}_1^S(\mu_2 - T/12) \} \quad (4.67)$$

4.6 Determination of Commutation Times

The four vector equations developed in Sections 4.41, 4.42, 4.51 and 4.52 give initial conditions in terms of commutation times for the converter operating anywhere within the range $0^\circ \leq \omega\mu_1 < 60^\circ$ and $0^\circ \leq \omega\mu_2 < 60^\circ$. Since the commutation times are not known beforehand, the selection of the initial condition equation must be made to match the commutation iterates. The flowchart of Fig. 3.6 could be modified to include this step by inserting a selection block within the inner loop, before BLOCK 1. Each time the commutation time iterates are updated the routine branches to the appropriate evaluation of one of Eqns. 4.22, 4.33, 4.55 or 4.61.

Once an initial condition has been formed, either at $t=0$ or $t=\mu_2-T/12$, the solution is advanced, using the appropriate state solutions and compatibility matrices, to $t=T/6$ or $t=\mu_1+T/12$. If the commutation currents are sufficiently small at these points, $|i_{cy}(\mu_1)|$ and $|i_{cd}(\mu_2+T/12)|$, the initial condition may be used to generate values for the network variables for an entire period. If sufficient accuracy has not been attained, the two currents are treated as the general functions,

$$f_1(\mu_1, \mu_2) = i_{cy}(\mu_1) \quad (4.68)$$

$$f_2(\mu_1, \mu_2) = i_{cd}(\mu_2+T/12) \quad (4.69)$$

The roots of

$$f_1(\mu_1, \mu_2) = 0$$

$$f_2(\mu_1, \mu_2) = 0 \quad (4.70)$$

are determined using a second order Newton method. If k is the iterate number, the equations for the new iterates are written as

$$\mu_1^{k+1} = \mu_1^k + \begin{vmatrix} -f_1(\mu_1^k, \mu_2^k) & df_1(\mu_1^k, \mu_2^k)/d\mu_2 \\ -f_2(\mu_1^k, \mu_2^k) & df_2(\mu_1^k, \mu_2^k)/d\mu_2 \end{vmatrix} / \text{DET} \quad (4.71)$$

$$\mu_2^{k+1} = \mu_2^k + \begin{vmatrix} df_1(\mu_1^k, \mu_2^k)/d\mu_1 & -f_1(\mu_1^k, \mu_2^k) \\ df_2(\mu_1^k, \mu_2^k)/d\mu_1 & -f_2(\mu_1^k, \mu_2^k) \end{vmatrix} / \text{DET} \quad (4.72)$$

where

$$\text{DET} = \begin{vmatrix} df_1(\mu_1^k, \mu_2^k)/d\mu_1 & df_1(\mu_1^k, \mu_2^k)/d\mu_2 \\ df_2(\mu_1^k, \mu_2^k)/d\mu_1 & df_2(\mu_1^k, \mu_2^k)/d\mu_2 \end{vmatrix} \quad (4.73)$$

The partial derivatives are approximated numerically.

For example

$$df_1(\mu_1^k, \mu_2^k)/d\mu_2 = [f_1(\mu_1^k, \mu_2^k + \Delta) - f_1(\mu_1^k, \mu_2^k)] / \Delta$$

where Δ is an arbitrary step size.

Although other methods may be used to solve Eqn. 4.70, practical experience indicates that the Newton method used converges rapidly for this application.

4.7 Summary

Algorithms have been formulated which allow for simulation of the twelve-pulse converter operating with commutation angles less than 60° . Separate formulations of the initial conditions were made dependent on the value of the commutation angle iterates specified.

The results of this chapter allow for a determination

of the commutation times and the initial condition vector. For these results to be useful in design and analysis various forms of output are required. The next chapter deals with the development of output programs.

CHAPTER 5

OUTPUT IN TIME AND FREQUENCY DOMAIN

5.1 Introduction

The algorithms developed in Chapter 4 allow for the numerical determination of the commutation times and the initial condition vector. For the purpose of analysis, it is necessary to present the results of converter simulations in a more accessible form. First, in the time domain, plots of the various network currents and voltages are produced. These plots aid in understanding the converter operation and may be used to compare the conversion process under various operating conditions. The second basic category of output used in this thesis is presented in the frequency domain. Frequency decompositions of the network currents allow for an evaluation of the effect of particular circuit elements on the characteristic harmonics. The frequency analysis is particularly useful in the selection of filters and other network components designed to reduce harmonics in the AC network.

This chapter describes the methods by which the program time and frequency domain outputs are produced. Equations are derived which may be used to calculate the Fourier coefficients for any general piece-wise linear problem.

5.2 Time Domain Output

To produce plots of the state variables and other network voltages and currents through a full period requires the use of the initial condition vector, commutation times, sub-interval state solutions, compatibility matrices and transposition properties. Starting from the appropriate initial condition vector, the first sub-interval state solution may be used to generate values at any time t within the sub-interval. At the boundary time, the compatibility matrix may be used to formulate the initial conditions for the following sub-interval. This process is continued until plot points are generated for the entire defining $T/6$ segment.

Having generated the required solution values for the first 60° segment no further calculation of state variables is required. The current and voltage values for the remainder of the period may be formed using the $T/6$ transposition property described in Section 3.4.2.

This method may be applied straight-forwardly when the network solution yields a wye-delta commutation angle in the range, $\omega\mu_2 < 30^\circ$. For network configurations in which $\omega\mu_2$ exceeds 30° the defining $T/6$ segment was chosen to commence at $t = \mu_2 - T/12$. Therefore, to allow for meaningful comparisons, the first step in generating Case 2 plots is to use the transposition property immediately to generate values between $0 \leq t < \mu_2 - T/12$. Applying the transpositions of Eqn. 3.13 to the state equations associated with the sixth

sub-network and using the notation of Fig. 4.2 allows for a complete re-construction of the period commencing at $t=0$.

A number of the network currents and voltages are not included in the state vectors. To obtain values for these variables throughout a period, KCL and KVL are used to form algebraic expressions in terms of the state variables.

These methods were utilized to produce the plots shown in Chapter 6.

5.3 Frequency Domain Output

Output in the frequency domain is not directly available from the results of the solution algorithms. Instead, the Fourier coefficients of the various current and voltage variables must be calculated from the available time domain information. Rather than relying on numerical analysis programs, which calculate approximations to the coefficients, the piece-wise linear description of the converter variables is exploited to achieve analytical forms for the coefficients.

The first step in the analysis, involves writing equations for the coefficients in each sub-interval. Next, $T/6$ periodicity is applied to generate values for the Fourier coefficients for a full period.

5.3.1 Calculation of Fourier Coefficients in Piece-wise Linear Problem

Each state variable contained in the solution vectors of Chapter 4 may be represented by a Fourier series,

$$x(t) = a_0 + \sum_{k=1}^{\infty} (a_k \cos k\omega t + b_k \sin k\omega t) \quad (5.1)$$

where $\omega = 2\pi/T$, and T is both the source and switching period for the converter.

The Fourier coefficients of Eqn. 5.1 may be written,

$$a_0 = (1/T) \int_{t_1}^{T+t_1} x(t) dt \quad (5.2)$$

$$a_k = (2/T) \int_{t_1}^{T+t_1} x(t) \cos k\omega t dt \quad (5.3)$$

$$b_k = (2/T) \int_{t_1}^{T+t_1} x(t) \sin k\omega t dt \quad (5.4)$$

For the general piece-wise linear problem discussed in Chapter 5 each state element may be separated into components corresponding to the N sub-intervals per period,

$$x(t) = x_n(t), \quad t_n \leq t < t_{n+1} \quad (5.5)$$

where n ranges from 1 to N .

Using the definition of Eqn. 5.5 the integrals of Eqns. 5.2 to 5.4 may be re-written,

$$a_0 = (1/T) \sum_{n=1}^N \int_{t_n}^{t_{n+1}} x_n(t) dt = (1/T) \sum_{n=1}^N a_{0n} \quad (5.6)$$

$$a_k = (2/T) \sum_{n=1}^N \int_{t_n}^{t_{n+1}} x_n(t) \cos k\omega t dt = (2/T) \sum_{n=1}^N a_{kn} \quad (5.7)$$

$$b_k = (2/T) \sum_{n=1}^N \int_{t_n}^{t_{n+1}} x_n(t) \sin k\omega t dt = (2/T) \sum_{n=1}^N b_{kn} \quad (5.8)$$

Each term of Eqns. 5.6 through 5.8 may be calculated analytically since in each sub-interval the state variable

solution may be written (Appendix 1),

$$x_n(t) = d_n + g_n \cos \omega t + h_n \sin \omega t + \sum_{\ell=1}^L C_{\ell n} e^{\lambda_{\ell n} (t-t_n)} \quad (5.9)$$

where L is the dimension of the n -th sub-interval state vector, and $C_{\ell n}$ and $\lambda_{\ell n}$ are complex coefficients.

The integrations of Eqn. 5.6 are straightforward and only the results for the sin and cos terms will be reproduced here for reference.

The n -th term of Eqn. 5.7 may be re-written, upon substitution of Eqn. 5.9, as

$$a_{kn} = \int_{t_n}^{t_{n+1}} (d_n + g_n \cos \omega t + h_n \sin \omega t + \sum_{\ell=1}^L C_{\ell n} e^{\lambda_{\ell n} (t-t_n)}) \cos k \omega t \, dt \quad (5.10)$$

Each term of Eqn. 5.10 may be integrated separately, and the overall result written as

$$a_{kn} = (d_n/k\omega) \times (\sin k \omega t_{n+1} - \sin k \omega t_n) + C_{\ell n} \times \{ e^{\lambda_{\ell n} (t_{n+1}-t_n)} (\lambda_{\ell n} \cos k \omega t_{n+1} + k \omega \sin k \omega t_{n+1} - \lambda_{\ell n} \cos k \omega t_n - k \omega \sin k \omega t_n) / (\lambda_{\ell n}^2 + k^2 \omega^2) \}$$

$$+ \left(\begin{array}{l} g_n \times \{ (t_{n+1}-t_n)/2 + (\sin 2 \omega t_{n+1} - \sin 2 \omega t_n)/4 \omega \} \\ + h_n (\sin^2 \omega t_{n+1} - \sin^2 \omega t_n) \end{array} \right) \quad k=1$$

OR

$$+ \left(\begin{array}{l} g_n \{ (\sin(k-1) \omega t_{n+1} - \sin(k-1) \omega t_n)/2(k-1)\omega \\ + (\sin(k+1) \omega t_{n+1} - \sin(k+1) \omega t_n)/2(k+1)\omega \} \\ + h_n \{ (\cos(k-1) \omega t_{n+1} - \cos(k-1) \omega t_n)/2(k-1)\omega \\ + (\cos(k+1) \omega t_{n+1} - \cos(k+1) \omega t_n)/2(k+1)\omega \} \end{array} \right) \quad k \neq 1$$

$$(5.11)$$

An analogous derivation for the sin term yields,

$$\begin{aligned}
 b_{kn} &= (d_n/k\omega) \times (\cos k\omega t_n - \cos k\omega t_{n+1}) \\
 &+ C_{\ell n} \times \{ e^{\lambda_{\ell n}(t_{n+1}-t_n)} (\lambda_{\ell n} \sin k\omega t_{n+1} - k\omega \cos k\omega t_{n+1}) \\
 &\quad - \lambda_{\ell n} \sin k\omega t_n + k\omega \cos k\omega t_n \} / (\lambda_{\ell n}^2 + k^2 \omega^2) \\
 &+ \left(\begin{aligned} &g_n (\sin^2 \omega t_{n+1} - \sin^2 \omega t_n) / 2\omega \\ &+ h_n \{ (t_{n+1} - t_n) + (\sin 2\omega t_n - \sin 2\omega t_{n+1}) / 4\omega \} \end{aligned} \right) \quad k=1 \\
 &+ \left(\begin{aligned} &\text{OR} \\ &g_n \{ (\cos(k-1)\omega t_n - \cos(k-1)\omega t_{n+1}) / 2(k-1)\omega \\ &\quad + (\cos(k+1)\omega t_n - \cos(k+1)\omega t_{n+1}) / 2(k+1)\omega \} \\ &+ h_n \{ (\sin(k-1)\omega t_n - \sin(k-1)\omega t_{n+1}) / 2(k-1)\omega \\ &\quad + (\sin(k+1)\omega t_n - \sin(k+1)\omega t_{n+1}) / 2(k+1)\omega \} \end{aligned} \right) \quad k \neq 1
 \end{aligned}$$

(5.12)

Eqns. 5.11, 5.12 and 5.2 allow for the evaluation of each component of the Fourier coefficients. Summing the contributions of each sub-interval allows for a determination of the overall coefficients.

5.3.2 Application of T/6 Periodicity

To avoid the calculation of the coefficients of Section 5.3.1 for the 24 sub-intervals which constitute a full period of converter operation, T/6 periodicity is exploited. To illustrate the application of this property, the a_k coefficients of the stator phase current i_a will be considered.

To simplify the notation used in the analysis, the coefficient components of the first two T/6 segments are grouped as,

$$a_{k(T/6)}^a = a_{k1}^a + a_{k2}^a + a_{k3}^a + a_{k4}^a \quad (5.13)$$

and

$$a_{k(T/3)}^a = a_{k5}^a + a_{k6}^a + a_{k7}^a + a_{k8}^a \quad (5.14)$$

where the superscript a refers to the current i_a .

With this notation, the first four terms of Eqn. 5.7 may be written,

$$a_{k(T/6)}^a = (2/T) \int_{t_1}^{T/6+t_1} i_a \cos \omega t \, dt \quad (5.13)$$

The next four terms of Eqn. 5.7 are written,

$$a_{k(T/3)}^a = (2/T) \int_{T/6+t_1}^{T/3+t_1} i_a \cos \omega t \, dt \quad (5.16)$$

The computations involved in evaluating the overall coefficients are greatly reduced by applying $T/6$ periodicity. Applying the periodicity properties allows for Eqn. 5.16 to be evaluated by modifying the results achieved in the first $T/6$ segment. To achieve this, $\tau = t - T/6$ is substituted into Eqn. 5.16.

$$a_{k(T/3)}^a = (2/T) \int_{t_1}^{T/6+t_1} i_a(\tau + T/6) \cos \omega(\tau + T/6) \, d\tau \quad (5.17)$$

Using the trigonometric identity

$$\cos \omega(\tau + T/6) = \cos \omega \tau \cos \omega T/6 - \sin \omega \tau \sin \omega T/6 \quad (5.18)$$

Eqn. 5.17 may be re-written as

$$a_{k(T/3)}^a = (2/T) \times \left\{ \cos \omega T/6 \int_{t_1}^{T/6+t_1} i_a(\tau + T/6) \cos \omega \tau \, d\tau - \sin \omega T/6 \int_{t_1}^{T/6+t_1} i_a(\tau + T/6) \sin \omega \tau \, d\tau \right\} \quad (5.19)$$

Applying the $T/6$ periodicity property,

$$i_a(\tau + T/6) = -i_b(\tau) \quad (5.20)$$

and using a notation consistent with Eqns. 5.13 and 5.14,

Eqn. 5.19 may be re-written,

$$a_{k(T/3)}^a = (2/T) \times \left\{ -a_{k(T/6)}^b \cos \omega T/6 + b_{k(T/6)}^b \sin \omega T/6 \right\} \quad (5.21)$$

Clearly this method may be applied to the coefficient components for the remainder of the period, to obtain an

expression for the overall coefficients, Eqns. 5.6, 5.7 and 5.8, in terms of the three-phase components in the defining $T/6$ segment. In actual fact only two phase components of the coefficients are required since the following equations are satisfied.

$$a_k^a + a_k^b + a_k^c = 0 \quad (5.22)$$

and

$$b_k^a + b_k^b + b_k^c = 0 \quad (5.23)$$

Applying the procedure described by Eqns. 5.17 through 5.20, along with the phase transpositions described in Section 3.5.2, for the entire period yields the overall coefficient solutions.

$$\begin{aligned} a_k = & a_{k(T/6)}^a \times \{1 - \cos \omega T/3 - \cos \omega T/2 + \cos \omega 5T/6\} \\ & + a_{k(T/6)}^b \times \{-\cos \omega T/6 - \cos \omega T/3 + \cos \omega 2T/3 + \cos \omega 5T/6\} \\ & + b_{k(T/6)}^a \times \{\sin \omega T/3 + \sin \omega T/2 - \sin \omega 5T/6\} \\ & + b_{k(T/6)}^b \times \{\sin \omega T/6 + \sin \omega T/3 - \sin \omega 2T/3 - \sin \omega 5T/6\} \end{aligned} \quad (5.24)$$

$$\begin{aligned} b_k = & a_{k(T/6)}^a \times \{-\sin \omega T/3 - \sin \omega T/2 + \sin \omega 5T/6\} \\ & + a_{k(T/6)}^b \times \{-\sin \omega T/6 - \sin \omega T/3 + \sin \omega 2T/3 + \sin \omega 5T/6\} \\ & + b_{k(T/6)}^a \times \{1 - \cos \omega T/3 - \cos \omega T/2 + \cos \omega 5T/6\} \\ & + b_{k(T/6)}^b \times \{-\cos \omega T/6 - \cos \omega T/3 + \cos \omega 2T/3 + \cos \omega 5T/6\} \end{aligned} \quad (5.25)$$

5.4 Summary

As was the case in developing the solution algorithms of Chapter 4, $T/6$ periodicity plays a pivotal role in the presentation of results in both the time and frequency domain. Time plots and Fourier coefficients are derived, based on the defining state solutions of the first $T/6$ segment. The results of this chapter are used to generate the output for the simulations of Chapter 6.

CHAPTER 6

SIMULATION EXAMPLES

6.1 Introduction

For the solution algorithms of Chapter 4 to be useful in an engineering environment, post-processing of the results is required. Chapter 5 described the methods which exploited the piece-wise linear state description and periodicity properties to generate time and frequency domain results.

This chapter demonstrates the use of these programs in the analysis of the twelve-pulse converter. Results are presented for two different AC network shunt configurations and for varying operating conditions.

The final section is devoted to a brief description of some of the numerical aspects of the program operation.

6.2 Time Domain Results

The piece-wise linear description of the converter allows for considerable flexibility in the formation of output results in the time domain. Through this description an exact formulation for the network variables solutions in terms of the initial conditions are available for any point in time. This allows for the production of relatively

inexpensive plots of unlimited resolution.

6.2.1 Converter with Shunt AC Filters

The first converter configuration to be considered is the connection of Fig. 3.1 in which 11-th, 13-th and HP filters are attached to the AC network. The component values used in the simulation are:

1) Source Values;

$$\begin{aligned} E_m &= 81.65V & L_s &= 60\text{mH} \\ I_d &= .5A & R_s &= .1 \times 10^{-2} \Omega \\ f_s &= 60\text{Hz} \\ \theta &= 120^\circ \end{aligned}$$

2) Transformer Impedances;

$$\begin{aligned} L_{T1} &= L_{T2} = 50\text{mH} \\ R_{T1} &= R_{T2} = .5 \times 10^{-2} \Omega \end{aligned}$$

3) Filter Impedances;

$$\begin{aligned} L_{11} &= 46.48\text{mH} \\ C_{11} &= 1.1394 \mu\text{F} \\ R_{11} &= .01184 \Omega \\ L_{13} &= 46.48\text{mH} \\ C_{13} &= .8958 \mu\text{F} \\ R_{13} &= 2.272 \Omega \\ L_{HP} &= 4.46\text{mH} \\ C_{HP} &= 3.583 \mu\text{F} \\ R_{HP} &= 64.45 \Omega \end{aligned}$$

These values are used to approximate the components used in HVDC analog simulators and network analysers. The selection of filter resonant frequencies and quality factors will be discussed in Section 6.3 in which frequency domain results are presented for this system.

With the tolerance ϵ set to 10^{-6} , as specified by Eqns. 6.1 and 6.2, the program converged to the steady-state solution in two steps.

$$|i_{cy}(\mu_1)| < \epsilon \quad (6.1)$$

$$|i_{cd}(\mu_2 + T/12)| < \epsilon \quad (6.2)$$

The two bridges have identical bank transformer ratios and since the transformer impedances are equal in this simulation the two commutation angles are identical, $\omega\mu = 14.7^\circ$.

The following pages contain plots of the various network variables. Fig. 6.1 shows the total c-phase bridge currents, the algebraic sum of i_c^y and $i_z/\sqrt{3}$, as defined in Fig. 3.1, along with the c-phase stator current i_c for a full period. This plot dramatically indicates the degree to which harmonics are removed from the AC system by the shunt filters.

The two subsequent plots, Figs. 6.2 and 6.3 show the currents in the 11-th and 13-th harmonic filters respectively. The magnitude of the high frequency alternating components of the two currents are between 5 and 8 percent of the peak value of the fundamental carried by the stator phase. As expected these results are below the

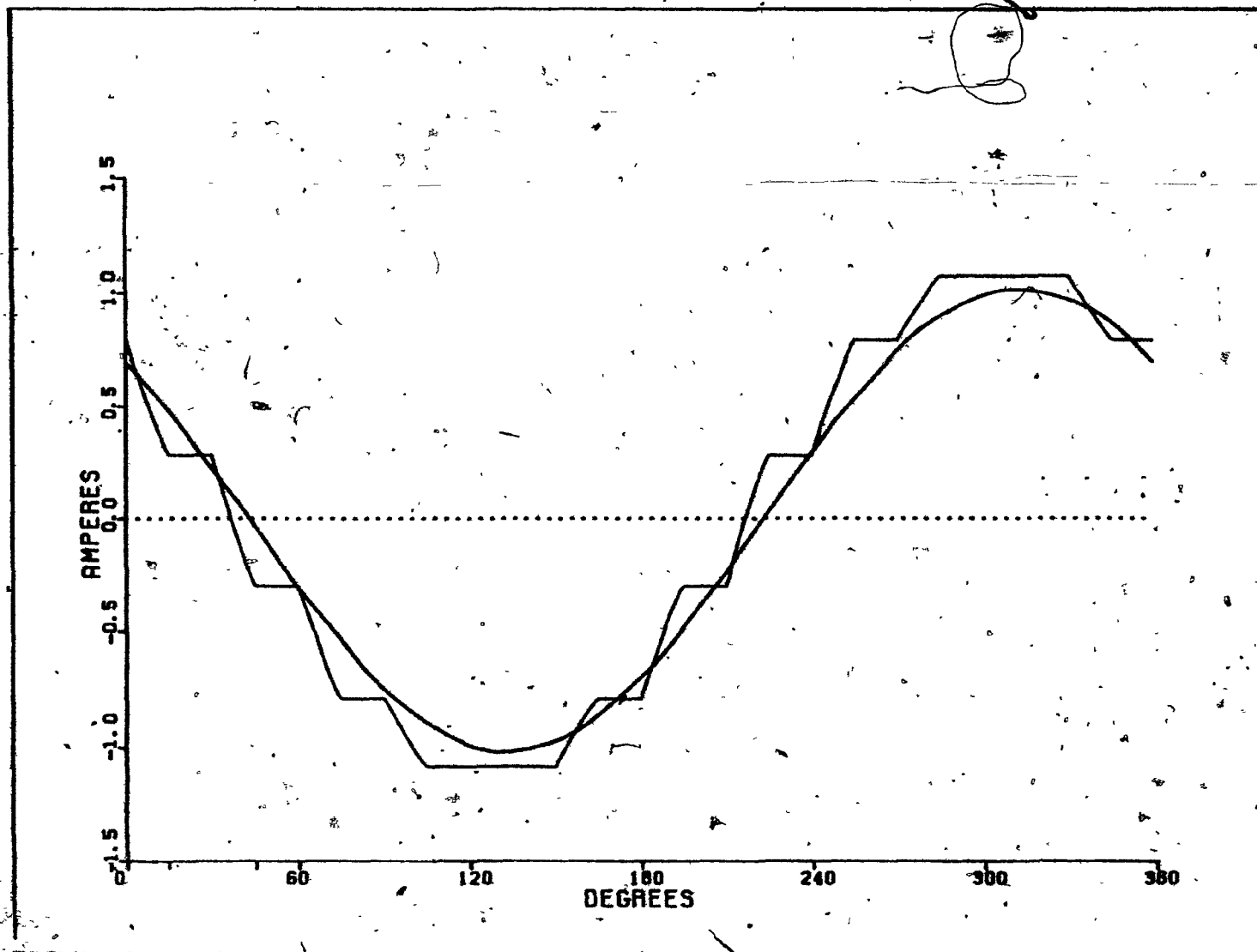


FIGURE 6.1 Bridge operating with HP, 11-th and 13-th filter. Sum of bridge currents along with stator phase current i_c

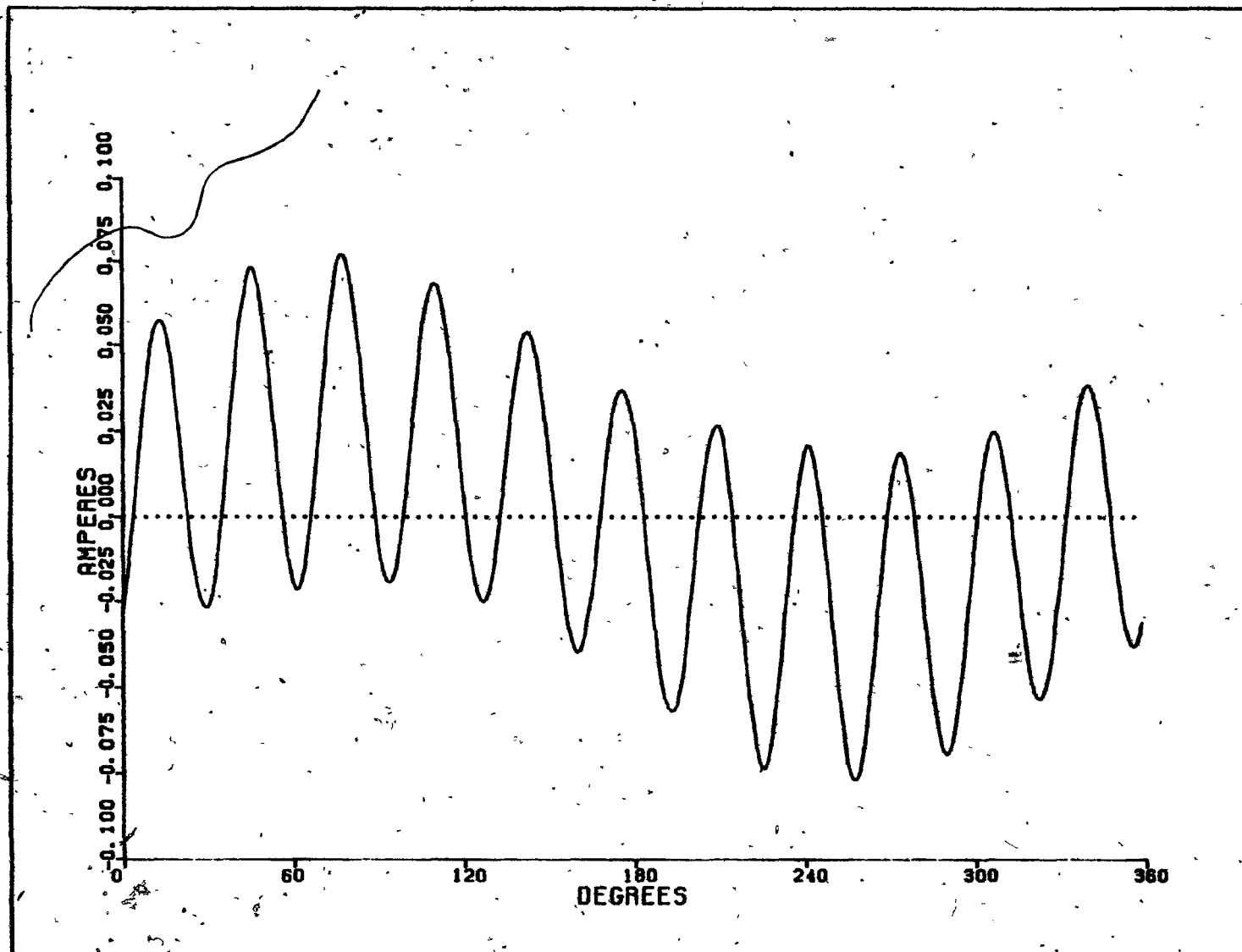


FIGURE 6.2 Bridge operating with HP, 11-th, and 13-th filters. Current i_{fla} through 11-th harmonic filter

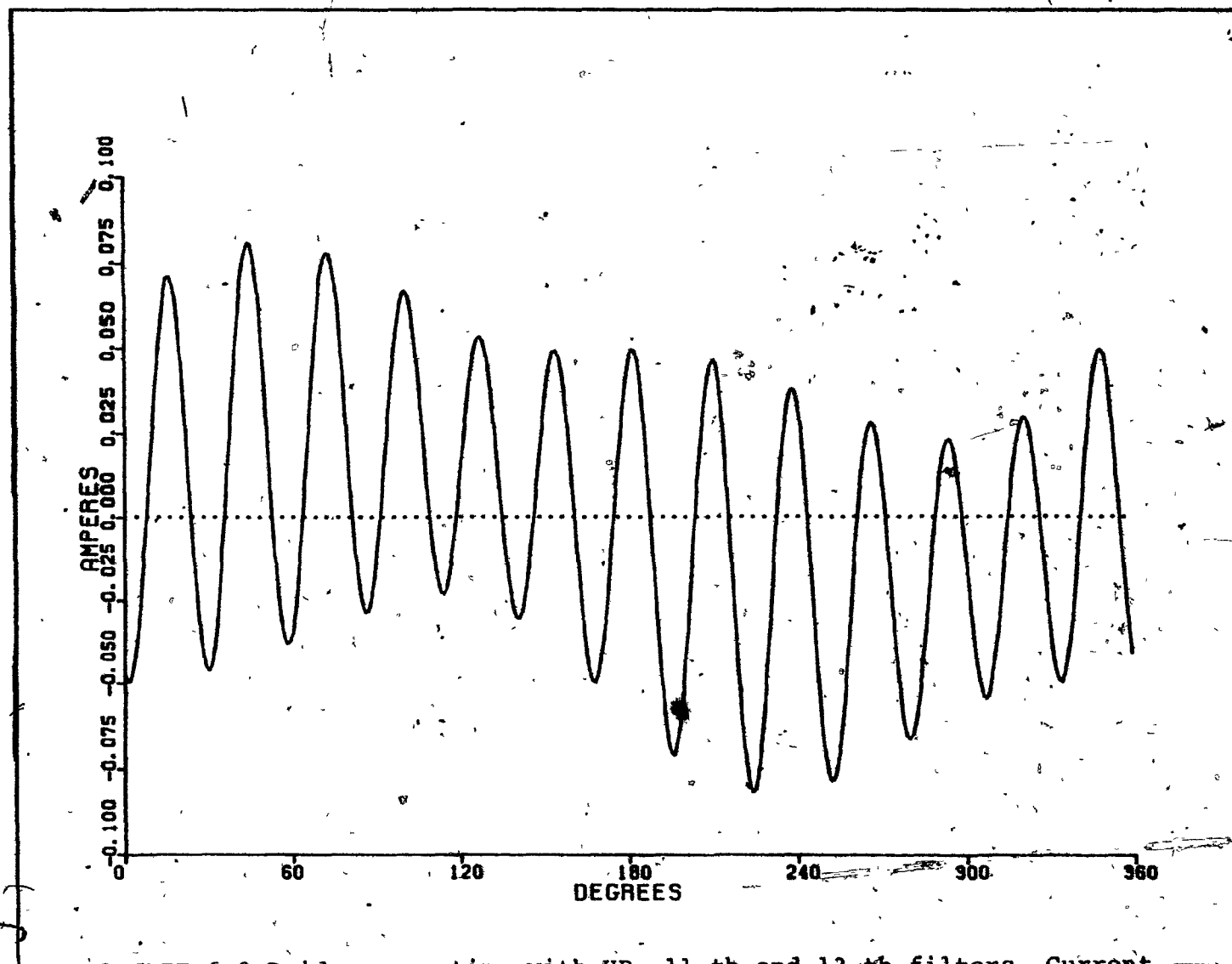


FIGURE 6.3 Bridge operating with HP, 11-th and 13-th filters. Current i_{f2a} through 13-th harmonic filter

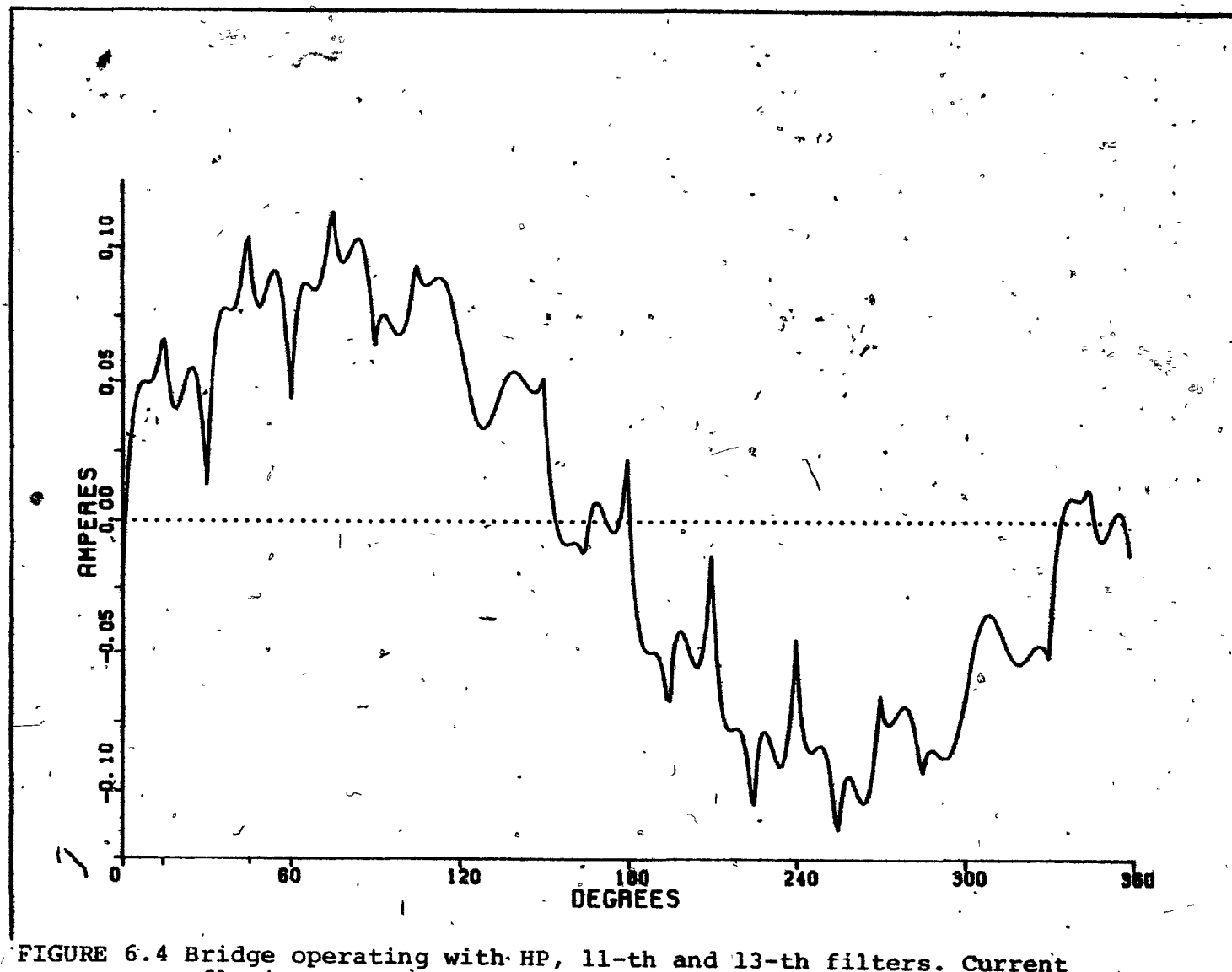


FIGURE 6.4 Bridge operating with HP, 11-th and 13-th filters. Current flowing through high-pass filter capacitor

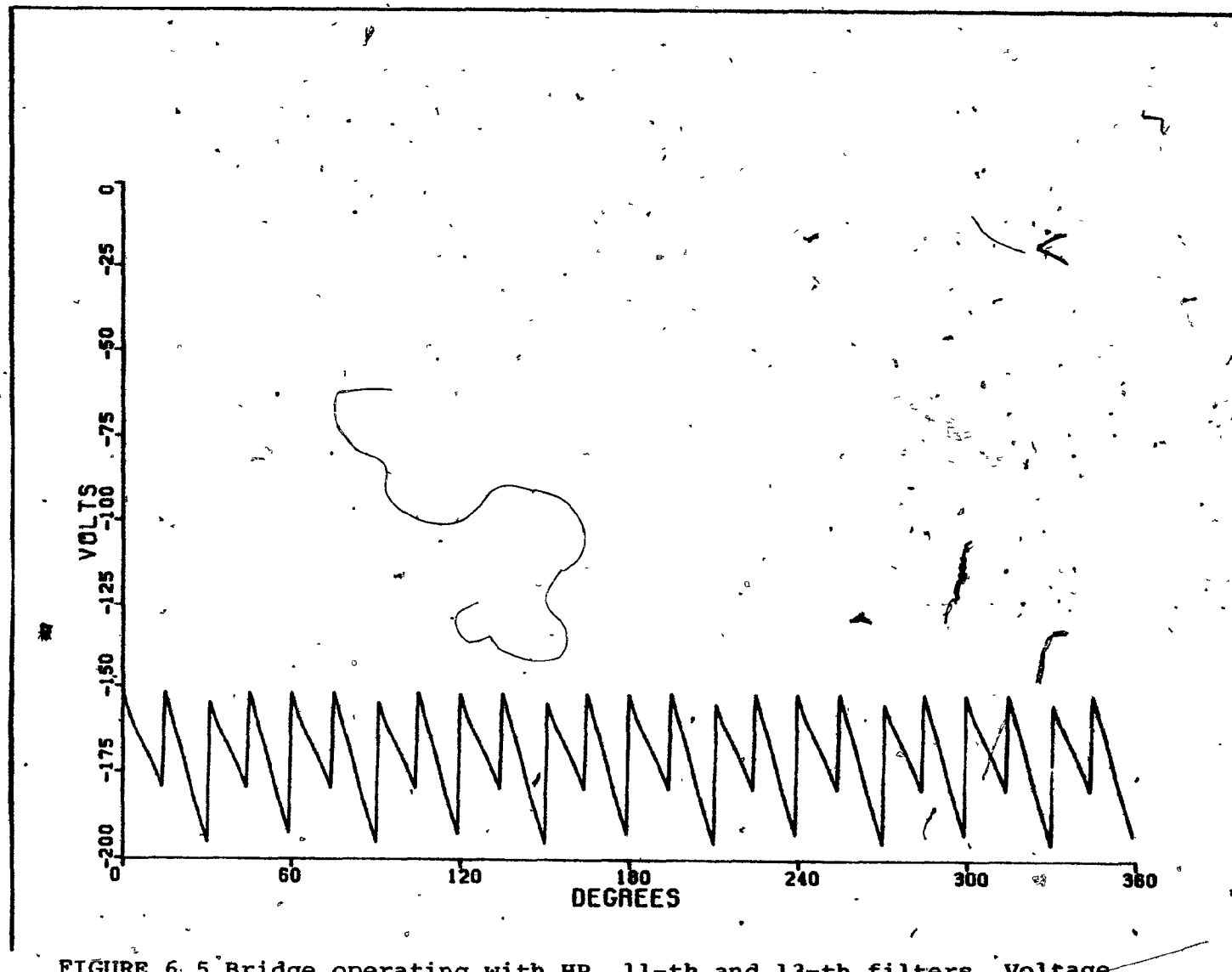


FIGURE 6.5 Bridge operating with HP, 11-th and 13-th filters. Voltage v_d across DC line

values of 9.1% and 7.7% for the 11-th and 13-th harmonic components of the bridge currents at zero commutation.

Fig. 6.4 shows the current flowing through the capacitor C_{HP} of the HP filter. The spikes in the waveform occur at the instants of topology changes caused by valve firing or commutation.

All three shunt currents contain small fundamental components due to the three-phase generators. The final plot for these system values is of the DC voltage v_d shown in Fig. 6.5.

6.2.2 Converter with HP AC Filter

The next converter configuration to be analysed consists of the connection of Section 6.2.1 without the AC tuned filters. The HP filter is tuned to remove all characteristic harmonics including the 11-th and 13-th. The system values used are:

1) Source Values;

$$\begin{aligned}
 E_M &= 81.65V & L_S &= 60\text{mH} \\
 I_d &= .5A & R_S &= .1 \times 10^{-2} \Omega \\
 f_S &= 60\text{Hz} \\
 \theta &= 130^\circ
 \end{aligned}$$

2) Transformer Impedances;

$$\begin{aligned}
 L_{T1} &= L_{T2} = 50\text{mH} \\
 R_{T1} &= R_{T2} = .5 \times 10^{-3} \Omega
 \end{aligned}$$

3) Filter Impedance;

$$\begin{aligned}
 L_{HP} &= 46.48\text{mH} \\
 C_{HP} &= 1.251\mu\text{F} \\
 R_{HP} &= 35 \Omega
 \end{aligned}$$

The lower resistance reduces the Q factor in the second order HP filter thus allowing for effective operation over a wider range of frequencies. The program converged to the final commutation angle values of $\omega\mu = 27.9^\circ$ in three steps. The increased commutation angles reduce the level of characteristic harmonics injected into the AC system.

The stator phase current, i_c , is shown in Fig. 6.6 for the operating conditions of this section. Comparison with Fig. 6.1 clearly indicates the superiority of the first filtering scheme. Fig. 6.7 shows the current through the HP filter.

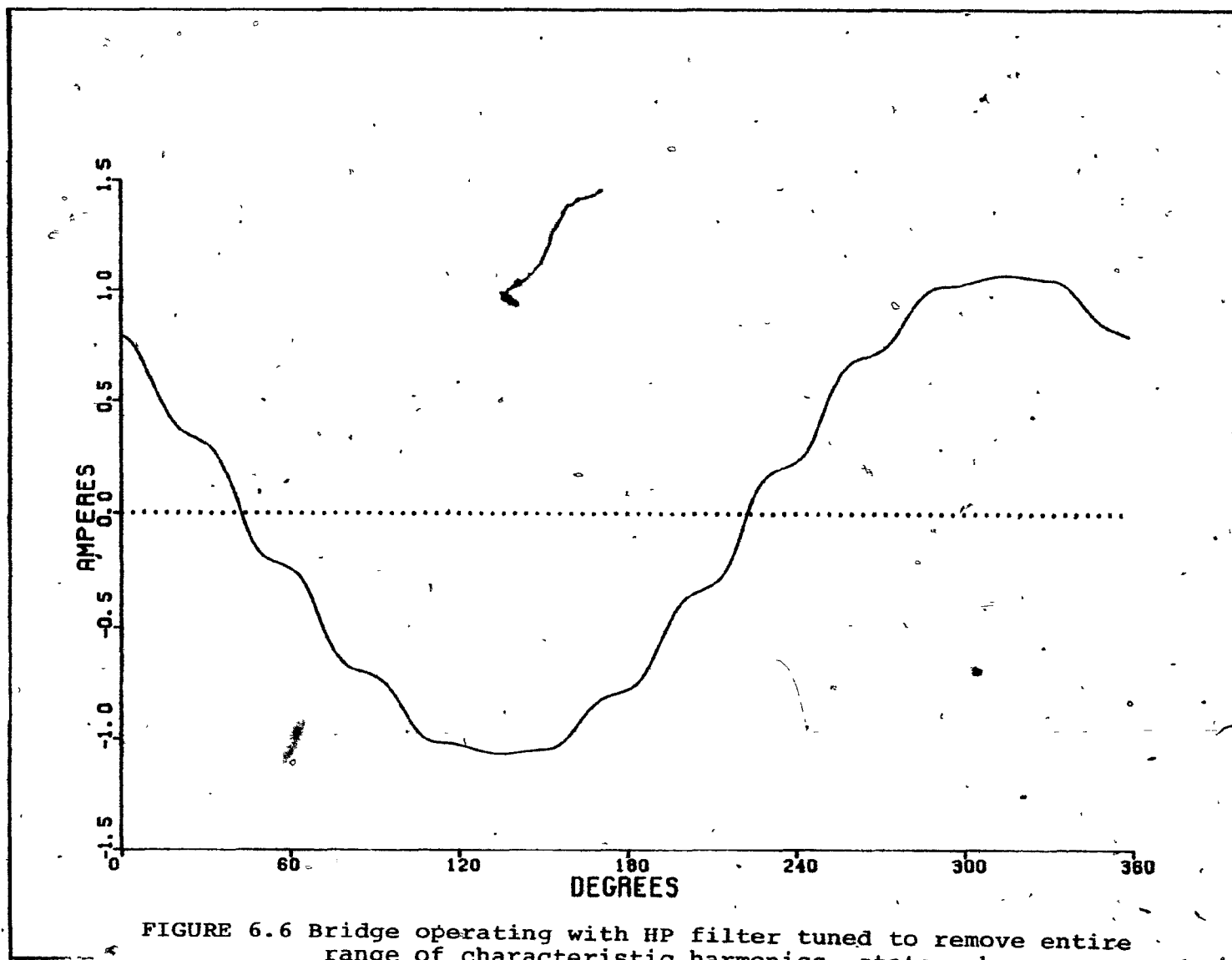


FIGURE 6.6 Bridge operating with HP filter tuned to remove entire range of characteristic harmonics. stator phase current i_c

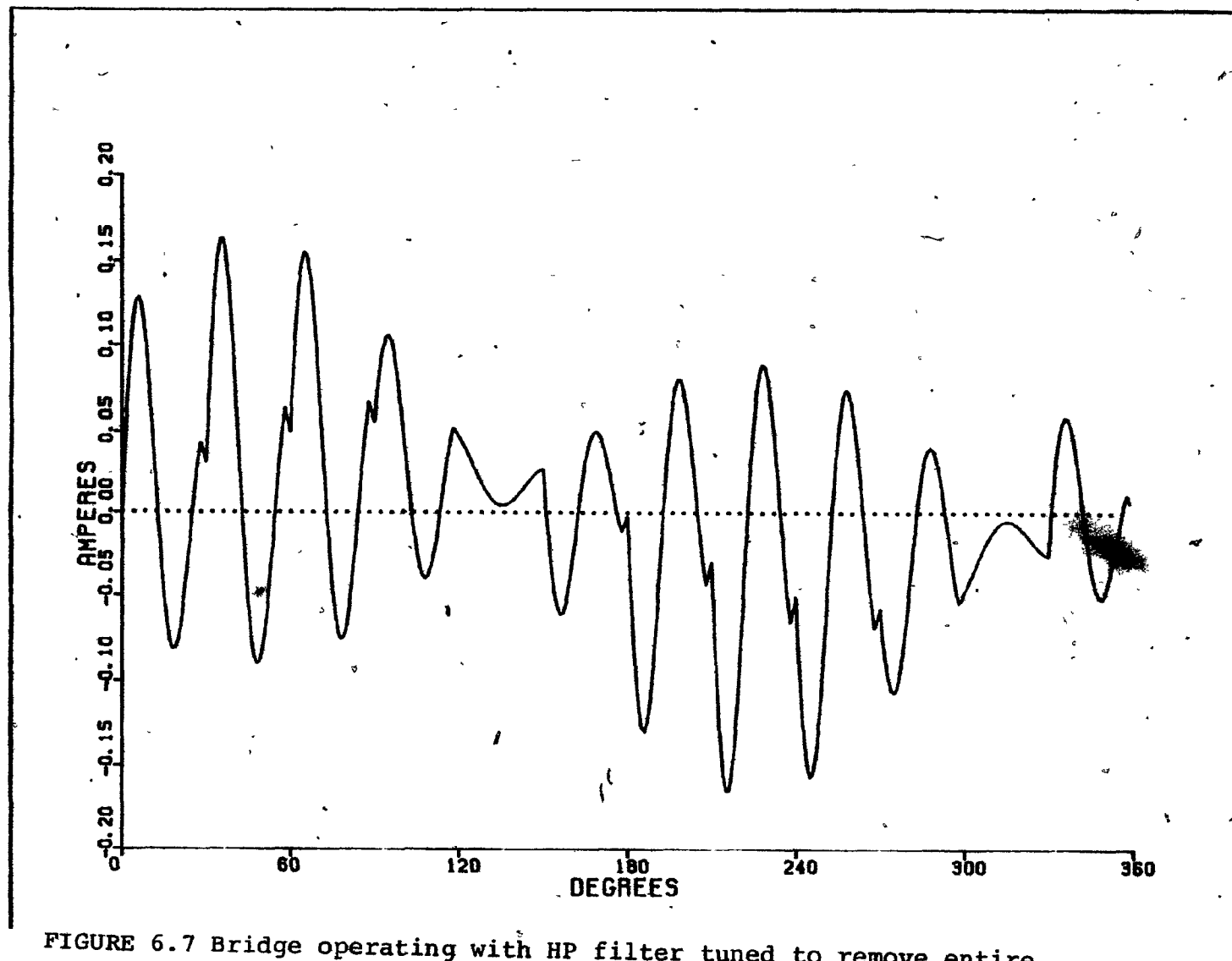


FIGURE 6.7 Bridge operating with HP filter tuned to remove entire range of characteristic harmonics. Current through capacitor of high-pass filter

6.3 Frequency Decomposition of Full Filtering Scheme

The frequency domain output algorithms described in Section 5.3 were used to study the effect of the commutation angles on the harmonic content of the stator phase current. The system of Section 6.2.1, which was used for this purpose, has the following filter characteristics:

1) 11-th Harmonic Tuned Filter

$$\omega_r = 11.526 \times \omega_s \quad \text{rad./sec.}$$

$$Q = 9.063$$

2) 13-th Harmonic Tuned Filter

$$\omega_r = 13.0 \times \omega_s \quad \text{rad./sec.}$$

$$Q = 7.7138$$

3) HP Filter

$$\omega_r = 20.99 \times \omega_s \quad \text{rad./sec.}$$

$$Q = 38.33$$

where the standard definitions for the resonant frequencies and quality factors have been used.

$$\omega_r = 1/\sqrt{LC} \quad (6.3)$$

$$Q = \begin{cases} \omega_s L/R & \text{tuned filter} \\ R/\omega_s L & \text{high-pass filter} \end{cases} \quad (6.4)$$

Figs. 6.8 and 6.9 plot the variation of harmonic current as a percentage of the fundamental component versus the commutation angle $\omega\mu$.

From Fig. 6.8 the effect of deviation from the resonant frequency may clearly be seen. The 11-th harmonic

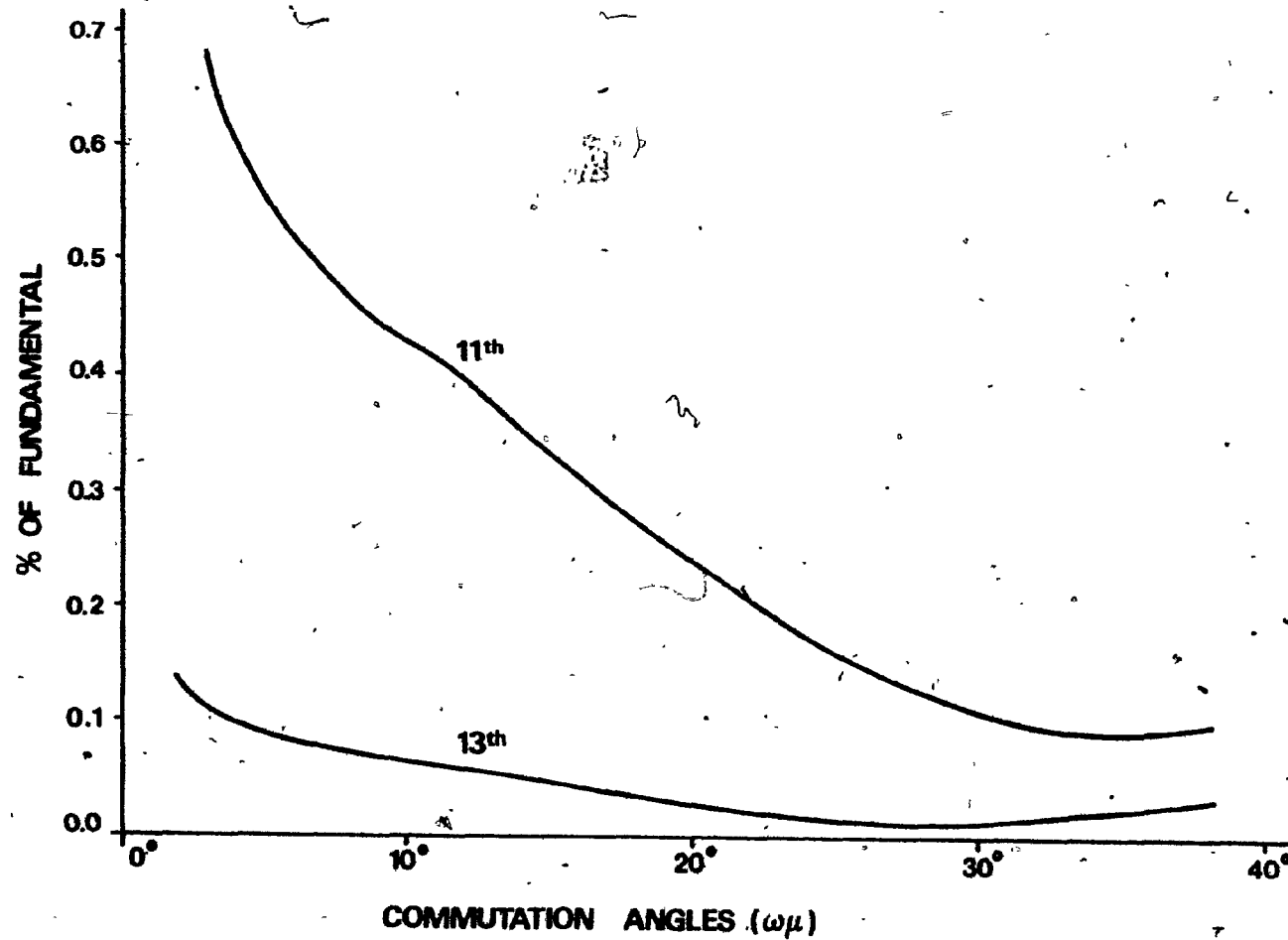


FIGURE 6.8 11-th and 13-th harmonic currents as percentages of the fundamental for range of commutation angle

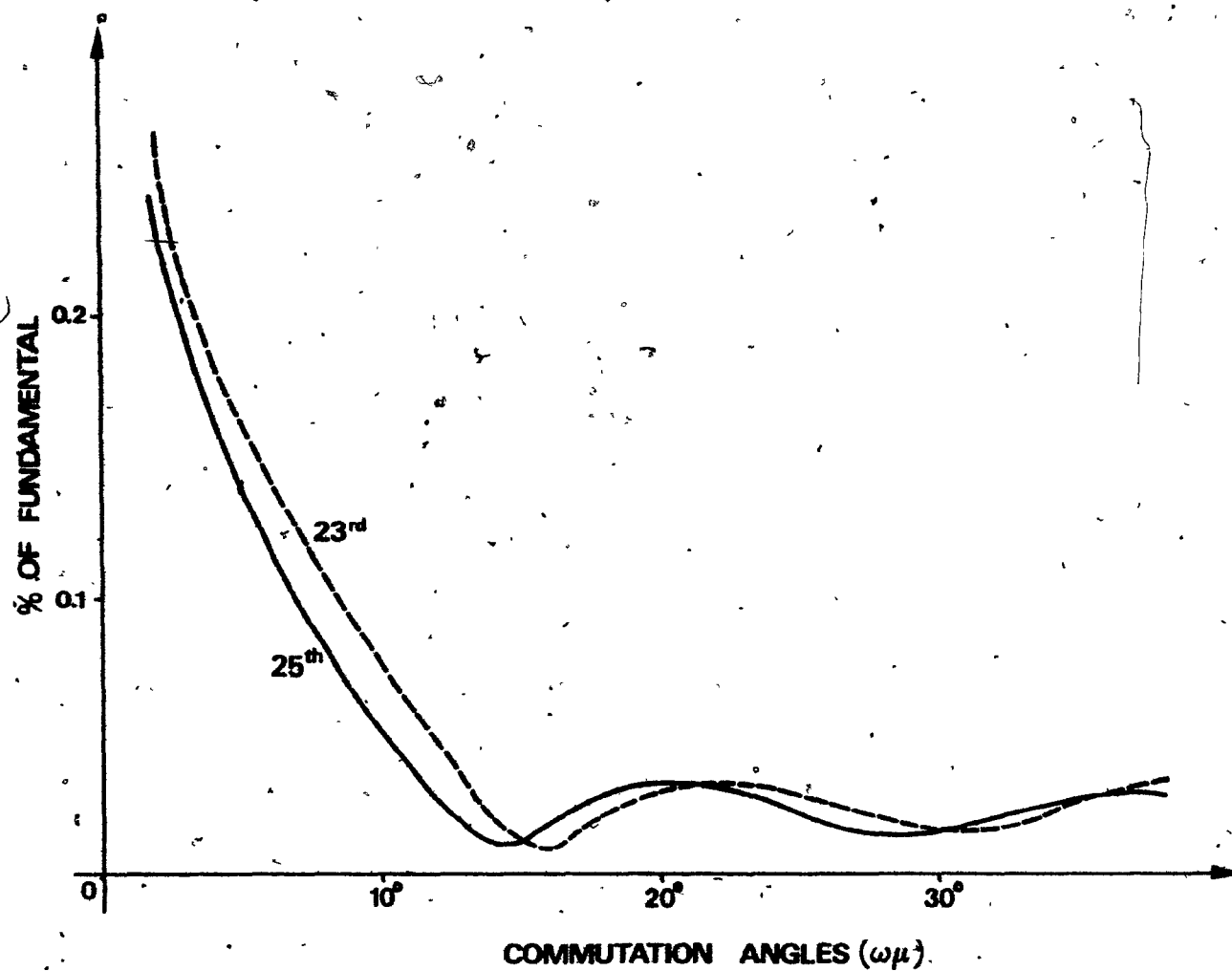


FIGURE 6.9 23-rd and 25-th harmonic currents as percentages of the fundamental for range of commutation angle

filter is poorly tuned and as a consequence the stator phase current contains relatively large components of the 11-th harmonic current for the entire range of commutation angles.

Fig. 6.9 plots the next largest pair of characteristic harmonics generated by the twelve-pulse converter, the 23-rd and 25-th components.

Both graphs display the advantage, in terms of harmonic reduction, achieved by operating the bridges with large commutation angles.

6.4 Numerical Aspects of Results

The examples of Sections 6.2 and 6.3 have shown that the program converges rapidly to the steady-state values. With equal commutation angles in the wye and delta bridges, convergence is usually achieved in three or four iterations. In configurations where the two angles have different values the tolerance is met within seven or eight steps. In both cases the rapidity of convergence with the Newton algorithm is dependent on the initial guess used.

As an example of the performance of the program in arriving at the steady-state results, a simple system with only one shunt element per phase was studied. The dimension of the state vectors for non-commutating sub-intervals for this system are equal to four.

Using the AMBAHL V7A Model 470 computer the program required .71 seconds to compile and .69 seconds to execute. The object code required 76 kbytes of storage while 7 kbytes were needed for array storage. Clearly, for larger systems time requirements increase rapidly due to the eigenvalue calculations and matrix manipulations. However significant savings can be achieved in the study of systems by compiling the [A] and [B] matrices and calculating and storing the eigenvalue solution matrices separately. The amount of time required to calculate results for a fixed configuration with changing inputs could thus be greatly reduced.

The main sub-routines used to study the system of Section 6.2.1 are listed in Appendix B. The eigenvalue evaluation and linear equation solution routines used are from the IMSL subroutine library [27].

CHAPTER 7CONCLUSIONS7.1 Conclusions

A piece-wise linear approach is applied to the analysis of the twelve-pulse converter. Further, by fully exploiting the symmetry properties of the time-varying converter topology, the complexities of the defining equations are significantly reduced. Applying Newton's method to the solution of the final non-linear equations, rapid convergence to the steady state values is achieved.

Significant achievements presented in this thesis, beyond material already presented in the literature, include:

- (1) A simple approach is presented for modelling the winding current distributions in the wye-delta transformer during bridge operation.
- (2) The number of state variables required to model each sub-network is reduced by taking into account the three-phase symmetry of the AC section of the converter.
- (3) The analysis of the converter is resolved into four separate problems corresponding to various combinations of the two bridge commutation angles in the range, $\omega\mu_1 < 60^\circ$, $\omega\mu_2 < 60^\circ$.
- (4) For each range of commutation angles a pair of non-linear equations are derived in terms of μ_1 and μ_2 .

During solution the commutation time iterates are used to specify which pair of equations are to be used in the subsequent iteration.

- (5) Analytical equations are developed for the determination of the frequency distribution in piece-wise linear configurations.

7.2 Suggestions for Further Investigation

Since much of the analysis of power networks involves the determination of steady-state values, the algorithms and programs developed in this thesis have a number of applications. Further research in this field could include investigation of the following topics:

- (1) Incorporation of a more detailed modelling of the DC section of the converter including the DC line filtering elements and transmission line equivalents could allow for detailed steady-state analysis of multi-terminal HVDC connections. Such studies would be particularly useful in analysing control strategies applied to such configurations.
- (2) Re-definition of the system forcing functions and equations in terms of terminal power values would allow for the inclusion of these programs in hybrid load-flow analyses. The programs are particularly economical for these applications since only modifications to the source vectors are required between iterations.

- (3) The programs frequency domain output makes it a potentially useful tool in analysing strategies to reduce characteristic harmonics. In particular the routines could be included as part of a general program for the selection of optimal filter components and configurations subject to constraints such as cost.
- (4) The general approach presented in this thesis for handling piece-wise linear configurations could be used in conjunction with a symbolic language handler [28] to generate the defining equations for a variety of switching network configurations.

BIBLIOGRAPHY

- [1] H. Martensson, T. Adielson, "Simulator Studies of Multi-Terminal HVDC Systems", in "High Voltage DC Transmission", IEE Conf. Rep. Ser. 22, 1966, pp.115-118.
- [2] L. Bergstrom, L.E. Juhlin, G. Liss, G.A. Nunan, "Simulator Study of Multi-Terminal HVDC System Performance", IEEE Trans., Vol. PAS-97, No.6, NOV./DEC. 1978, pp.1057-1067.
- [3] J.B. Bowles, H.L. Nakra, A.B. Turner, "A Small Series Tap on an HVDC Line", IEEE Trans., Vol. PAS-100, FEB. 1981, pp.857-862.
- [4] H.A. Peterson, P.C. Krause, Jr., J.F. Luini, C.H. Thomas, "An Analog Computer Study of a Parallel AC and DC Power System", IEEE Trans., Vol. PAS-85, pp.191-209.
- [5] P.C. Krause, D.P. Carroll, "A Hybrid Computer Study of a DC Power System: I", IEEE Trans., Vol. PAS-87, No.4, APR. 1968, pp.970-978.
- [6] N.G.H. Hingorani, R.H. Kitchin, J.L. Hay, "Dynamic Simulation of HVDC Power Transmission Systems on Digital Computers - Generalized Mesh Analysis Approach", IEEE Trans., Vol. PAS-87, No.4, APR. 1968, pp.989-996.
- [7] J.L. Hay, N.G. Hingorani, "Dynamic Simulation of Multi-Converter HVDC Systems by Digital Computer", IEEE Trans., Vol. PAS-80, No.2, FEB. 1970, pp.218-228.
- [8] G.N. Revankar, S.A. Mahajan, "Digital Simulation for Mode Identification in Thyristor Circuits", Proc. IEE, Vol.120, No.2, FEB. 1973, pp.269-272.
- [9] G.N. Revankar, "Topological Approach to Thyristor Circuit Analysis", Proc. IEE, Vol.120, No.11, NOV. 1973, pp.1403-1405.

- [10] G.N.Revankar, P.K. Srivastava, R.N. Jawle, "Digital Computation of SCR Chopper Circuits", IEEE Trans., Vol.IECI-20, No.1, FEB. 1973, pp.20-23.
- [11] G.N. Revankar, "Computer Analysis of SCR Circuits", IEEE Trans., Vol.IECI-22, No.1, FEB. 1975, pp.48-55.
- [12] H. Haneda, T. Maruhashi, S. Kusumoto, "A General Thyristor-Circuit Analysis Program NETCAP Based on the Network Tableau Approach", Proc. of 1979 International Symposium on Circuits and Systems, pp.112-115.
- [13] H. Haneda, T. Maruhashi, S. Kusumoto, "Digital Simulation of Thyristor Circuits via Tableau Approach", JIEE Japan, Vol.99-B, No.7, July, 1979
- [14] H. Foch, C. Reboulet, J. Schonek, "A General Digital Computer Simulation Programme for Thyristor Static Converters (Programme SACSO) Application Examples", Proc. 2nd IFAC Symposium on Control in Power Electronics and Electrical Drives, 1977.
- [15] A. Coffetti, G. Petrecca, A. Savini, "A Digital Simulation of Converter Circuits", Proc. 2nd IFAC Symposium on Control in Power Electronics and Electrical Drives, 1977.
- [16] T.A. Lipo, "The Analysis of Induction Motors with Voltage Control by Symmetrically Triggered Thyristors", IEEE Trans., Vol.PAS-90, No.2, MAR./APR. 1971, pp.515-525
- [17] M.L. Liou, "Exact Analysis of Linear Circuits Containing Periodically Operated Switches with Applications", IEEE Trans., Vol.CT-19, No.2, MAR. 1972, pp.146-154
- [18] B.T. Ooi, N. Menemenlis, H.L. Nakra, "Fast Steady-State Solution for HVDC Analysis", IEEE Trans., Vol.PAS-99, No.6, NOV./DEC. 1980, pp.2453-2459
- [19] S.C. Kapoor, J. Reeve, "Analysis of a Pole-to-Pole Short-Circuit on Bipolar HVDC Converters", IEEE Trans., Vol.PAS-92, MAY./JUN. 1973, pp.886-892.

- [20] B.T. Ooi, R. Zhen, J.C.H. Lee, "Dynamic Digital Simulation of HVDC System by Piece-Wise Linear System Theory", Paper presented at the Canadian Communications and Energy Conference, OCT. 1982.
- [21] N. Menemenlis, "A Semi-Analytical Method for Steady-State Solution in HVDC Analysis", Master of Engineering Thesis, McGill University, MAR. 1980.
- [22] S.B. Dewan, A. Straughen, "Power Semiconductor Circuits", Wiley-Interscience, 1975.
- [23] E.W. Kimbark, "Direct Current Transmission", Vol.1, Wiley Interscience, 1971.
- [24] Ibid , pp.81-87.
- [25] Ibid , pp.305-318.
- [26] N. Balabanian, T.A. Bickart, "Electrical Network Theory", Wiley, New York, 1969.
- [27] "IMSL Library Reference Manual", Edition 7, IMSL Inc., 1971
- [28] S. Raney, "User's Guide for FORTRAN-FORMAC at NPS", Technical Note, No.0211-23, Naval Postgraduate School, JAN.1973.

APPENDIX 1FORMATION OF SYSTEM MATRICES AND
STATE SOLUTIONS

Applying KVL and KCL to the bridge sub-networks, a system of first-order differential equations may be written in terms of the network constants.

$$[L_n] \dot{x}_n(t) + [R_n] x_n(t) = [G_n] u_n(t) \quad (1-1)$$

The system of equations may be re-arranged as,

$$\dot{x}_n(t) = [A_n] x_n(t) + [B_n] u_n(t) \quad (1-2)$$

The state-transition matrix for Eqn. 1-2 is calculated from the expression,

$$[\Phi_n(t)] = [M_n] e^{[\Lambda_n]t} [M_n]^{-1} \quad (1-3)$$

where $[M_n]$ is the matrix of eigen-vectors for the $[A_n]$ matrix and $[\Lambda_n]$ is the diagonal which satisfies the matrix relation,

$$[A_n] = [M_n] [\Lambda_n] [M_n]^{-1} \quad (1-4)$$

Eigenvalues and vectors are calculated numerically using the subroutine EIGRF from the IMSL subroutine library.

For the specific application of the bridge converter the forcing function of Eqn. 1-1 takes on the form,

$$u_n(t) = \cos \omega t \underline{a}_n + \sin \omega t \underline{b}_n + \underline{c}_n \quad (1-5)$$

where \underline{a}_n , \underline{b}_n , and \underline{c}_n are constant vectors. Given the forcing function of Eqn. 1-5 the ZSR of Eqn. 1-1 has the general form,

$$x_n^{\text{ZSR}}(t) = \cos \omega t \underline{g}_n + \sin \omega t \underline{h}_n + \underline{d}_n \quad (1-6)$$

Substituting Eqn. 1-6 into the state equations,
Eqn. 1-2, and matching coefficients leads to a matrix
solution for the ZSR.

$$\underline{d}_n = [A_n]^{-1} [B_n] \underline{c}_n \quad (1-7)$$

$$\begin{bmatrix} \underline{a}_n \\ \underline{b}_n \end{bmatrix} = \begin{bmatrix} -[A_n] & [I] \\ -[I] & -[A_n] \end{bmatrix} \begin{bmatrix} [B_n] \underline{a}_n \\ [B_n] \underline{b}_n \end{bmatrix} \quad (1-8)$$

APPENDIX 2COMPUTER SUBROUTINES

The subroutines used to implement the algorithms of Chapters 4 and 5 are listed on the following pages. The subroutines LEQTLF, LEQTLIC and EIGRF are from the IMSL Subroutine Library Package. For further documentation on these subroutines consult reference 27.

$ZAB(I,J) = ZAB(I,J) + ZA(I,L) * ZB(L,J)$
1 CONTINUE
RETURN
END

(


```

T6=1.D0/(6.D1*6.D0)
T12=1.D0/(6.D1*1.2D1)
CALL INTSOL(T0,N1,1,7,13,X1S0)
CALL INTSOL(T12,N2,37,42,47,X2ST12)
CALL INTSOL(T12,N1,19,25,31,X3ST12)
CALL INTSOL(T6,N2,52,57,62,X4ST6)

```

```

C
C FORM COMPATIBILITY MATRIX C4 BETWEEN K=1 AND K=4
C

```

```

DO 11 I=1,N2
DO 11 J=1,N2
11 C4(I,J)=0.D0
C4(1,1)=1.D0
C4(1,2)=1.D0
C4(2,1)=-1.D0
C4(3,4)=-1.D0
C4(4,5)=-1.D0
C4(5,3)=-1.D0

```

```

C
C REMAINDER OF PROGRAM CALCULATES NEW VALUES OF F,G FROM INDEPENDENT
C VARIABLE ITERATES
C

```

```

20 T1=U1/(3.6D2*6.D1)
T12U1=T12-T1

```

```

C
C FORM MODAL MATRICES DEPENDENT ON U1
C

```

```

CALL HMG(T1,N1,1,195,P1)
DO 21 I=1,N2
DO 21 J=1,N1
P2122(I,J)=P1(I+1,J)
IF(J.GT.N2)GO TO 21
P22U1(I,J)=P1(I+1,J+1)
21 CONTINUE
CALL HMG(T12U1,N2,145,207,P2T12U)

```

```

C
C FORM ZSR'S DEPENDENT ON U1
C

```

```

CALL INTSOL(T1,N1,1,7,13,X1SU1)
CALL INTSOL(T1,N2,37,42,47,X2SU1)

```

```

C
C FORM SOLUTION VECTORS AND MATRICES DEPENDENT ON U1
C

```

```

CALL MATMUL(N2,N2,N2,N2,N2,N2,N2,N2,N2,N2,P2T12U,P22U1,BU1)
CALL MATVEC(N2,N1,N2,N1,N1,N2,P2122,X1S0,VW1)
DO 25 I=1,N2
25 VW1(I)=-VW1(I)+AYED*P1(I+1,1)+X1SU1(I+1)-X2SU1(I)
CALL MATVEC(N2,N2,N2,N2,N2,N2,P2T12U,VW1,RAU1)
DO 26 I=1,N2
26 RAU1(I)=RAU1(I)+X2ST12(I)

```

```

C
C GO TO (30,30,40,30),L
C

```

```

C CALCULATE ALL VECTORS AND MATRICES REQUIRING ITERATE OF U2 ONLY

```



```

C
30 T2=U2/(3.6D2*6.0D1)
   T12U2=T12-T2
   T12U2P=T12+T2
C
C FORM MODAL MATRICES DEPENDENT ON U2
C
   CALL HOMG(T2,N1,73,201,Q3)
   DO 31 I=1,N2
   DO 31 J=1,N1
   Q2122(I,J)=Q3(I+1,J)
   IF(J.GT.N2)GO TO 31
   Q22U2(I,J)=Q3(I+1,J+1)
31 CONTINUE
C
C FORM ZSR'S DEPENDENT ON U2
C
   CALL INISOL(T12U2P,N2,52,57,62,X4ST12)
   CALL INISOL(T12U2P,N1,19,25,31,X3S12U)
C
C FORM SOLUTION VECTORS AND MATRICES DEPENDENT ON U2
C
   CALL HOMG(T12U2,N2,145,207,P4T12U)
   CALL MATVEC(N2,N1,N2,N1,N1,N2,Q2122,X3ST12,VW2)
   DO 35 I=1,N2
35 VW2(I)=-VW2(I)+Q3(I+1,1)*AYED+X3S12U(I+1)-X4ST12(I)
   CALL MATVEC(N2,N2,N2,N2,N2,N2,P4T12U,VW2,VW1)
   DO 36 I=1,N2
36 VW1(I)=VW1(I)+X4ST6(I)
   CALL MATVEC(N2,N2,N2,N2,N2,N2,C4,VW1,R3U2)
   CALL MATMUL(N2,N2,N2,N2,N2,N2,N2,N2,C4,P4T12U,ALX)
   CALL MATMUL(N2,N2,N2,N2,N2,N2,N2,N2,ALX,Q22U2,AU2)
C
C COMBINE MATRICES AND VECTORS TO FORM F & G
C
40 CALL MATMUL(N2,N2,N2,N2,N2,N2,N2,N2,N2,AU2,BU1,ALX)
   DO 41 I=1,N2
   DO 41 J=1,N2
   ALX(I,J)=-ALX(I,J)
   IF(I.EQ.J)ALX(I,J)=ALX(I,J)+1.D0
41 CONTINUE
C
   CALL MATVEC(N2,N2,N2,N2,N2,N2,AU2,R4U1,VW1)
   DO 42 I=1,N2
42 VW1(I)=VW1(I)+R3U2(I)
C
   IDGT=5
   CALL LEQ11F(ALX,IVEC,5,5,VW1,IDGT,WK,IER)
C
   VW3(1)=AYED-X1S0(1)
   DO 43 I=1,N2
43 VW3(I+1)=VW1(I)-X1S0(I+1)
   CALL MATVEC(N1,N1,N1,N1,N1,N1,N1,P1,VW3,VECX)
   DO 44 I=1,N1

```

44 VECK(I) = VECK(I) + X1SU1(I)

C
C
C

F = IC1(U1)

F = VECK(1)

C

DO 45 I=1,N2

* 45 VW2(I) = VECK(I+1) - X2SU1(I)
CALL MATVEC(N2,N2,N2,N2,N2,N2,P2T12U,VW2,VW4)
G = X3S12U(1) + AXED*Q3(1,1)

C
C
C

G = IC2(U2+T/12)

DO 51 I=1,N1

G = G - Q3(1,I) * X3ST12(I)

IF(I.GT.N2)GO TO 51

G = G + Q3(1,I+1) * (X2ST12(I) + VW4(I))

51 CONTINUE

RETURN

END

()

```

T12=1.D0/(6.D1*1.2D1)
CALL INTSOL(T0,N1,1,7,13,X1S0)
CALL INTSOL(T12,N1,1,7,13,X1ST12)
CALL INTSOL(T6,N2,52,57,62,X4ST6)
CALL INTSOL(T12,N5,67,74,81,X5ST12)

```

```

C
C FORM COMPATIBILITY MATRIX BETWEEN K=1,4
C

```

```

DO 11 I=1,N2
DO 11 J=1,N2
11 C4(I,J)=0.D0
C4(1,1)=1.D0
C4(1,2)=1.D0
C4(2,1)=-1.D0
C4(3,4)=-1.D0
C4(4,5)=-1.D0
C4(5,3)=-1.D0

```

```

C
CALL HMG(T12,N1,1,195,P1)
DO 12 I=1,N1
DO 12 J=1,N2
12 P122(I,J)=P1(I,J+1)

```

```

C
CALL MATMUL(N1,N2,N1,N2,N2,N2,N1,N2,P122,C4,SK1)
CALL MATVEC(N1,N2,N1,N2,N2,N1,SK1,X4ST6,WV3)
CALL MATVEC(N1,N1,N1,N1,N1,N1,P1,X1S0,WV2)

```

```

C
C FORM CONSTANT SOLUTION VECTOR AND PLACE IN WV2
C

```

```

DO 13 I=1,N1
13 WV2(I)=-WV2(I)+X1ST12(I)+WV3(I)+AYED*P1(I,1)

```

```

C
C REMAINDER OF ROUTINE CALCULATES NEW VALUES OF F,G FOR
C NEW INDEPENDENT VARIABLE ITERATES
C

```

```

20 T1=U1/(3.6D2*6.D1)
TUI12=T1-T12

```

```

C
C FORM MODAL MATRICES DEPENDENT ON U1
C

```

```

CALL HMG(TUI12,N5,212,310,P5U112)
DO 14 J=1,N1
R1222(1,J)=P5U112(1,J+1)
DO 14 I=1,N2
14 R1222(I+1,J)=P5U112(I+2,J+1)

```

```

C
C FORM ZSR'S DEPENDENT ON U1
C

```

```

CALL INTSOL(T1,N1,19,25,31,X3SUI)
CALL INTSOL(T1,N5,67,74,81,X5SUI)

```

```

C
CALL MATVEC(N5,N5,N5,N5,N5,N5,P5U112,X5ST12,WV5)

```

```

C
WV3(1)=X5SUI(1)-WV5(1)-X3SUI(1)+AYED*P5U112(1,1)

```

```

DO 17 I=1,N2
17 WV3(I+1)=X5SU1(I+2)-WV5(I+2)-X3SU1(I+1)+AYED*P5U112(I+2,1)
C
GO TO (30,30,40,30),L
C
CALCULATE ALL VECTORS AND MATRICES REQUIRING U2 ITERATE ONLY
C
30 T2=U2/(3.6D2*6.0D1)
T12U2=T12+T2
T1224=T12-T2
C
FORM MODAL MATRICES DEPENDENT ON U2 ONLY
C
CALL HOMG(T1224,N2,145,207,P2T12U)
CALL MATMUL(N2,N2,N2,N2,N2,N2,N2,N2,N2,N2,C4,P2T12U,WU2)
C
FORM ZSR'S DEPENDENT ON U2 ONLY
C
CALL INTSOL(T12U2,N1,19,25,31,X3S12U)
CALL INTSOL(T12U2,N2,52,57,62,X4S12U)
DO 33 I=1,N2
33 WV1(I)=X3S12U(I+1)-X4S12U(I)
CALL MATVEC(N2,N2,N2,N2,N2,N2,WU2,WV1,WV8)
C
COMBINE U1,U2 VECTORS AND MATRICES AND VECTORS
C
40 T12U12=T12+T2-T1
CALL HOMG(T12U12,N1,73,201,Q3U12)
C
FORM Z4 VECTOR
C
CALL MATVEC(N1,N1,N1,N1,N1,N1,Q3U12,WV3,WV4)
DO 47 I=1,N2
47 WV1(I)=WV4(I+1)
CALL MATVEC(N2,N2,N2,N2,N2,N5,WU2,WV1,WV5)
DO 48 I=1,N2
48 WV5(I)=WV5(I)+WV8(I)
CALL MATVEC(N1,N2,N1,N2,N5,N1,P1222,WV5,XZ4)
DO 49 I=1,N1
49 XZ4(I)=XZ4(I)+WV2(I)
C
FORM (Y4) MATRIX
C
CALL MATMUL(N1,N1,N1,N1,N1,N1,N1,N1,N1,N1,Q3U12,R1222,XMAT1)
DO 57 I=1,N2
DO 57 J=1,N1
57 XMAT2(I,J)=XMAT1(I+1,J)
CALL MATMUL(N2,N2,N2,N2,N2,N1,N1,N1,N1,WU2,XMAT2,P1)
CALL MATMUL(N1,N2,N1,N2,N1,N1,N1,N1,N1,P1222,P1,Y4U12)
C
FORM ( (I) - (Y4U12) ) INV * Z4U12
C
DO 58 I=1,N1
DO 58 J=1,N1

```

```

      Y4U12(I,J)=-Y4U12(I,J)
58 IF(I.EQ.J)Y4U12(I,J)=Y4U12(I,J)+1.DO
C
      IDGT=5
      CALL LEQ1F(Y4U12,IVEC,N1,N1,XZ4,IDGT,WK,IER)
C
C
C      FORM X5(U1)
C
      DO 75 I=1,N1
75 WV5(I+1)=XZ4(I)-X5ST12(I+1)
      WV5(1)=AXED-X5ST12(1)
      CALL MATVEC(N5,N5,N5,N5,N5,N5,N5,N5,P5U112,WV5,WV9)
      DO 76 I=1,N5
76 WV9(I)=WV9(I)+X5SU1(I)
C
C
C      F=IC1(U1)
C
C      F=WV9(2)
C
      WV4(1)=WV9(1)
      DO 77 I=1,N2
77 WV4(I+1)=WV9(I+2)
      G=X3S12U(1)
      DO 78 I=1,N1
78 G=G+Q3U12(1,I)*(WV4(I)-X3SU1(I))
C
C
C      G=IC2(U2+T/12)
C
9999 RETURN
      END

```

SUBROUTINE EQUA3 (U1,U2,L,F,G)

PURPOSE: FORM FUNCTIONS OF COMMUTATION CURRENTS FOR
CASE 2(I)

CALLING PARAMETERS: U1,U2; ITERATE VALUES OF INDEPENDENT VARIABLES
L; =1 FIRST CALL, CALCULATE ALL CONSTANT
VALUES AS WELL AS F,G WITH NEW INDEP.
VARIABLES
=2 CALCULATE F,G WITH BOTH INDEP. VAR.
TAKING ON NEW VARIABLES
=3 CALCULATE F,G WITH U1 TAKING ON NEW VALUE
=4 CALCULATE F,G WITH U2 TAKING ON NEW VALUE

```

MAIN VARIABLES: Q3T12(6,6) MODAL MATRIX K=3 AT T=12
                Q1222(6,5) PARTITION OF Q3T12
                C5(6,7) SUB-INTERVAL COMPATIBILITY MATRIX BETWEEN
                        K=6 AND K=1
                P2T12U(6,6) MODAL MATRIX K=2 AT T=T/12-U1
                R7ZM12(7,7) MODAL MATRIX K=6 AT T=U2-T/12
                P1(6,6) MODAL MATRIX K=1 AT T=U1-U2+T/12
                P2122(5,6) PARTITION OF P1
                XMAT1(7,7), XMAT2(6,6), XMAT3(5,5) WORK MATRICES
                VEC1(6), VEC2(5), VEC3(5), VEC4(7), VEC5(7), VEC6(6),
                VEC8(6), VEC9(6) WORK VECTORS
                X S'S ZSR'S

```

COMMON BLOCKS: CONST; NECESSARY CONSTANTS
MATGRO; WORK MATRICES AND VECTORS

```

IMPLICIT REAL*8(A-H,O-Y),COMPLEX*16(Z)
COMMON /MATGRO/X2ST12(5),X3ST12(6),X7ST6(7),Q3T12(6,6),Q1222(6,5),
.X3ST6(6),C5(6,7),X2SUI(5),X1SUI(6),P2T12U(5,5),X1S212(6),
.X7S212(7),R72M12(7,7),R713(7,6),XMAT1(7,7),XMAT2(6,6),
.P2122(5,6),VEC1(6),VEC2(5),VEC3(5),VEC4(7),VEC5(7),VEC6(6),
.VEC8(6),VEC9(6),GARB(3)
COMMON /CONST/ASORC(4),BSORC(4),CSORC(4),ELS,RS,ELL,RL,ELT1,RT1,
.ELT2,RT2,ELD,EM,ALPHA,AYED,PI,OMEGA,SR3,U10,U20,STEP,EPSI,DEL,REDU
.,N1,N2,IVEC,M,K1,K2,K3,K4,K7,N5
DIMENSION WK(5),P1(6,6),XMAT3(5,5)
GO TO (10,20,20,30),L

```

CALCULATE ALL CONSTANT VECTORS AND MATRICES

```
10 T6=1.D0/(6.D1*6.D0)
   T12=1.D0/(6.D1*1.2D1)
```

```
CALL INTSQL(T12,N2,37,42,47,X2ST12)
CALL INTSQL(T12,N1,19,25,31,X3ST12)
CALL INTSQL(T6,N5,67,74,81,X7ST6)
CALL INTSQL(T6,N1,19,25,31,X3ST6)
```

```
CALL INTSQL(T12,N2,37,42,47,X2ST12)
CALL INTSQL(T12,N1,19,25,31,X3ST12)
CALL INTSQL(T6,N5,67,74,81,X7ST6)
CALL INTSQL(T6,N1,19,25,31,X3ST6)
```

```

      CALL HOMG(T12,N1,73,201,Q3T12)
      DO 11 I=1,N1
      DO 11 J=1,N2
11  Q1222(I,J)=Q3T12(I,J+1)
C
      CALL MATVEC(N1,N1,N1,N1,N1,N1,Q3T12,X3ST12,VEC8)
      DO 12 I=1,N1
12  VEC8(I)=-VEC8(I)+X3ST6(I)+AYED*Q3T12(I,1)
C
      DO 13 I=1,N1
      DO 13 J=1,N5
13  C5(I,J)=0.D0
      C5(1,2)=1.D0
      C5(2,3)=1.D0
      C5(2,4)=1.D0
      C5(3,3)=-1.D0
      C5(4,6)=-1.D0
      C5(5,7)=-1.D0
      C5(6,5)=-1.D0
C
C  REMAINDER OF ROUTINE CALCULATES NEW VALUES OF F,G FOR
C  NEW INDEPENDENT VARIABLE ITERATES
C
20  T1=U1/(3.6D2*6.D1)
      T1ZU1=T12-T1
C
      CALL INTSOL(T1,N2,37,42,47,X2SU1)
      CALL INTSOL(T1,N1,1,7,13,X1SU1)
C
      CALL HOMG(T1ZU1,N2,145,207,P2T1ZU)
C
C  GO TO (30,30,40,30),L
C
C  CALCULATE ALL VECTORS AND MATRICES AND VECTORS REQUIRING U2 ITERATE
C
30  T2=U2/(3.6D2*6.0D1)
      T12P2=T12+T2
      T2M12=T2-T12
C
      CALL INTSOL(T2M12,N1,1,7,13,X1S212)
      CALL INTSOL(T12P2,N5,67,74,81,X7S212)
      CALL HOMG(T2M12,N5,212,310,R72M12)
      DO 31 I=1,N5
      R713(I,1)=R72M12(I,1)
      DO 31 J=1,N2
31  R713(I,J+1)=R72M12(I,J+2)
C
C  FORM U2 SEGMENT OF SOLUTION VECTOR
C
      CALL MATVEC(N5,N5,N5,N5,N5,N5,R72M12,X7ST6,VEC4)
      CALL MATVEC(N5,N1,N5,N1,N1,N5,R713,VEC8,VECS)
      DO 32 I=1,N5
32  VEC5(I)=VECS(I)+X7S212(I)-VEC4(I)

```



```

      CALL MATVEC(N1,N5,N1,N5,N5,N1,C5,VEC5,VEC1)
      DO 33 I=1,N1
33  VEC1(I)=VEC1(I)-X1S212(I)
      CALL MATMUL(N5,N1,N5,N1,N1,N2,N2,N5,N5,R713,Q1222,XMAT1)
      CALL MATMUL(N1,N5,N1,N5,N5,N5,N2,N1,N1,C5,XMAT1,XMAT2)
C
C  CALCULATE VECTORS AND MATRICES REQUIRING BOTH U1 AND U2
C  ITERATES AND COMBINE VECTORS AND MATRICES TO FORM F AND
C  G FUNCTIONS
C
40  T12U12=T1-T2+T12
      CALL HOMG(T12U12,N1,1,195,P1)
      DO 41 I=1,N2
      DO 41 J=1,N1
41  P2122(I,J)=P1(I+1,J)
C
      CALL MATMUL(N2,N1,N2,N1,N1,N1,N2,N5,N5,P2122,XMAT2,XMAT1)
      CALL MATMUL(N2,N2,N2,N2,N5,N5,N2,N2,N2,P2T12U,XMAT1,XMAT3)
      DO 42 I=1,N2
      DO 42 J=1,N2
      XMAT3(I,J)=-XMAT3(I,J)
      IF(I.EQ.J)XMAT3(I,J)=XMAT3(I,J)+1.D0
42  CONTINUE
C
      CALL MATVEC(N2,N1,N2,N1,N1,N2,P2122,VEC1,VEC2)
      DO 43 I=1,N2
43  VEC3(I)=X1SUI(I+1)+VEC2(I)-X2SUI(I)+AYED*P1(I+1,1)
      CALL MATVEC(N2,N2,N2,N2,N2,N2,P2T12U,VEC3,VEC2)
      DO 44 I=1,N2
44  VEC2(I)=VEC2(I)+X2ST12(I)
C
C  FORM X3' (T/12)
C
      CALL LEQTLF(XMAT3,IVC,N2,N2,VEC2,5,WK,IER)
C
C  ADVANCE SOLUTION TO FORM FUNCTIONS
C
      CALL MATVEC(N1,N2,N1,N2,N2,N1,Q1222,VEC2,VEC6)
      CALL MATVEC(N5,N1,N5,N1,N1,N5,R713,VEC6,VEC4)
      DO 51 I=1,N5
51  VEC4(I)=VEC4(I)+VEC5(I)
C
C      G= X2(U2+T/12)
C
      G=VEC4(1)
C
      CALL MATVEC(N1,N5,N1,N5,N5,N1,C5,VEC4,VEC6)
      VEC6(1)=VEC6(1)+AYED
      DO 52 I=1,N1
52  VEC6(I)=VEC6(I)-X1S212(I)
      CALL MATVEC(N1,N1,N1,N1,N1,N1,P1,VEC6,VEC9)
C
C      F= X1(U1)
C

```

F=XLSU1(1)+VEC9(1)

RETURN
END

(

```

      T12=1.D0/(6.D1*1.2D1)
      DO 11 I=1,N1
      DO 11 J=1,N5
11  C5(I,J)=0.D0
      C5(1,2)=1.D0
      C5(2,3)=1.D0
      C5(2,4)=1.D0
      C5(3,3)=-1.D0
      C5(4,6)=-1.D0
      C5(5,7)=-1.D0
      C5(6,5)=-1.D0
      CALL INTSOL(T12,N1,1,7,13,X1ST12)
      CALL INTSOL(T6,N1,34,40,46,X3ST6)
      CALL INTSOL(T6,N5,88,95,102,X7ST6)
      CALL INTSOL(T12,N5,67,74,81,X5ST12)

```

```

C
C  REMAINDER OF ROUTINE DEPENDENT ON ITERATES.
C  CALCULATION FOR CHANGES IN U1 ITERATE ONLY
C

```

```

20  T1=U1/(3.6D2*6.D1)
      TU112=T1-T12
      T6U1=T6-T1
      CALL INTSOL(T1,N1,34,40,46,X3SU1)
      CALL INTSOL(T1,N5,67,74,81,X5SU1)
      CALL HOMG(T6U1,N1,123,402,Q3T6U1)
      CALL HOMG(TU112,N5,195,408,S5T12U)

```

```

C
C  PARTITION (S(U1-T/12)) INTO SUB-MATRIX FOR CALCULATION
C

```

```

      DO 22 J=1,N5
      DO 21 I=1,N2
21  WW1(I+1,J)=S5T12U(I+2,J)
22  WW1(1,J)=S5T12U(1,J)
      CALL MATVEC(N5,N5,N1,N5,N5,N1,WW1,X5ST12,VECA)
      VECA(1)=-VECA(1)+X5SU1(1)+S5T12U(1,1)*AYED-X3SU1(1)
      DO 23 I=1,N2
23  VECA(I+1)=-VECA(I+1)+X5SU1(I+2)-X3SU1(I+1)+AYED*S5T12U(I+2,1)
      CALL MATVEC(N1,N1,N1,N1,N1,N5,Q3T6U1,VECA,VECG)
      DO 24 I=1,N1
24  VECA(I)=VECG(I)+X3ST6(I)
      DO 25 I=1,N1
      DO 25 J=1,N1
25  WW4(I,J)=WW1(I,J+1)
      CALL MATMUL(N1,N1,N1,N1,N1,N1,N5,N5,Q3T6U1,WW4,WW1)

```

```

C
C  VECA, WW1  STORE U1 VECTOR, MATRIX SUBSECTION
C

```

```

      GO TO (30,30,40,30),L

```

```

C
C  CALCULATE ALL VECTORS AND MATRICES REQUIRING U2 ITERATE ONLY
C

```

```

30  T2=U2/(3.6D2*6.0D1)
      TU212=T2-T12
      TU212P=T2+T12

```

```

T6U2=T6-T2
CALL INTSQL (TU212,N1,1,7,13,X1SU12)
CALL INTSQL (TU212P,N5,88,95,102,X7SU12)
CALL HOMG (T6U2,N1,1,391,P1T6U2)
CALL HOMG (TU212,N5,293,415,R7UT12)

```

```

C
C
C PARTITION STATE TRANSITION MATRIX

```

```

DO 33 I=1,N5
  WW2(I,1)=R7UT12(I,1)
  DO 32 J=1,N2
32 WW2(I,J+1)=R7UT12(I,J+2)
33 CONTINUE

```

```

C
C CALL MATMUL (N1,N1,N1,N1,N1,N5,N5,N5,N5,P1T6U2,C5,WW3)

```

```

C
C WW3 = (P1(T/6-U2) (C5)      WW2 = (R1(R3) )
C

```

```

CALL MATVEC (N1,N1,N1,N1,N1,N1,P1T6U2,X1SU12,VECB)
DO 34 I=1,N1
34 VECB(I)=-VECB(I)+X1ST12(I)+AYED*P1T6U2(I,1)
CALL MATVEC (N5,N5,N5,N5,N5,N5,R7UT12,X7ST6,VECD)
DO 35 I=1,N5
35 VECD(I)=-VECD(I)+X7SU12(I)

```

```

C
C WW2,WW3,VECB,VECD STORE U2 VECTOR, MATRIX SUB-SECTION
C

```

```

40 CALL MATVEC (N5,N5,N5,N1,N1,N5,WW2,VECA,VECE)
DO 41 I=1,N5
41 VECE(I)=VECE(I)+VECD(I)
CALL MATVEC (N5,N5,N1,N5,N5,N1,WW3,VECE,VECF)
DO 42 I=1,N1
42 VECF(I)=VECF(I)+VECB(I)

```

```

C
C VECF SOLUTION VECTOR
C

```

```

CALL MATMUL (N5,N5,N1,N5,N5,N5,N1,N1,N1,WW3,WW2,WW4)
CALL MATMUL (N1,N1,N1,N1,N5,N5,N1,N1,N1,WW4,WW1,WW5)

```

```

C
C WW5 SOLUTION MATRIX
C

```

```

DO 43 I=1,N1
DO 43 J=1,N1
  WW5(I,J)=WW5(I,J)
43 IF(I.EQ.J)WW5(I,J)=WW5(I,J)+1.D0

```

```

C
C IDGT=5
CALL LBQTLF (WW5,IVEC,N1,N1,VECF,IDGT,WK,IER)

```

```

C
C VECF = X1(T/12)
C

```

```

VECG(1)=AYED-X5ST12(1)
DO 44 I=1,N1
44 VECG(I+1)=VECF(I)-X5ST12(I+1)

```

```

      CALL MATVEC(N5,N5,N5,N5,N5,N5,S5T12U,VECG,VECH)
      DO 45 I=1,N5
45  VECH(I)=VECH(I)+X5SU1(I)

```

C
C
C

```

      VECB = X5(U1)

```

```

      VECG(1)=VECH(1)-X3SU1(1)
      DO 46 I=1,N2
46  VECG(I+1)=VECH(I+2)-X3SU1(I+1)
      CALL MATVEC(N1,N1,N1,N1,N5,N1,Q3T6U1,VECG,VECJ)
      DO 47 I=1,N1
47  VECJ(I)=VECJ(I)+X3ST6(I)

```

C
C
C

```

      VECJ = X3(T/6)

```

```

      VECG(1)=VECJ(1)-X7ST6(1)
      VECG(2)=-X7ST6(2)
      DO 48 I=1,N2
48  VECG(I+2)=VECJ(I+1)-X7ST6(I+2)
      CALL MATVEC(N5,N5,N5,N5,N5,N5,R7UT12,VECG,VECK)
      DO 49 I=1,N5
49  VECK(I)=VECK(I)+X7SU12(I)

```

C
C
C
C
C
C
C
C

```

      VECK = X7(U2+T/12)

```

```

      F = IC1(U1)
      G = IC2(U2+T/12)

```

```

      F=VECH(2)
      G=VECK(1)
      RETURN
      END

```

```

C
C SUBROUTINE FOURIE(L,NCOEFF,NHAR,D,G,H,ZC,ZL,AI,BI,AI,BI,TI,TI1) C
C
C L = SUB-INTERVAL DIMENSION C
C NCOEFF = NUMBER OF CHARACTERISTIC HARMONICS TO BE EVALUATED C
C D,G,H = PARTICULAR SOLUTION COEFFICIENTS C
C ZC = VECTOR OF COMPLEX COEFFICIENTS OF ZIR C
C ZL = VECTOR CONTAINING EIGENVALUES C
C AI,BI = FOURIER COEFFICIENT SOLUTION VECTOR C
C AI,BI = FOURIER COEFFICIENTS FOR FUNDAMENTAL C
C TI,TI1 = BOUNDARY TIMES FOR EVALUATION C
C
C
C IMPLICIT REAL*8(A-H,O-Y),COMPLEX*16(Z)
C DIMENSION ZC(L),ZL(L),AI(NCOEFF),BI(NCOEFF),XAI(2),XBI(2),
C XAN(2),XBN(2),NHAR(NCOEFF)
C EQUIVALENCE(XAI(1),ZAI),(XBI(1),ZBI),(XAN(1),ZAN),(XBN(1),ZEN)
C PI=4.D0*DATAN(1.D0)
C OMEGA=2.D0*PI*6.D1
C WRITE(6,112)OMEGA
112 FORMAT(1H,/, ' OMEGA=',D15.6)
C TAU=TI1-TI
C
C COMPUTE COEFFICIENTS FOR FUNDAMENTAL
C
C CT1=DCOS(OMEGA*TI1)
C CT=DCOS(OMEGA*TI)
C ST1=DSIN(OMEGA*TI1)
C ST=DSIN(OMEGA*TI)
C
C DA1=D*(ST1-ST)/OMEGA
C GA1=G*((TI1-TI)/2.D0+(DSIN(2.D0*OMEGA*TI1)-DSIN(2.D0*OMEGA*TI))/
C .(4.D0*OMEGA))
C HA1=H*(ST1**2-ST**2)/(2.D0*OMEGA)
C
C DB1=D*(CT-CT1)/OMEGA
C GB1=G*(ST1**2-ST**2)/(2.D0*OMEGA)
C HB1=H*((TI1-TI)/2.D0+(DSIN(2.D0*OMEGA*TI)-DSIN(2.D0*OMEGA*TI1))/
C .(4.D0*OMEGA))
C
C ZAI=DCOMPLX(0.D0,0.D0)
C ZBI=DCOMPLX(0.D0,0.D0)
C DO 10 I=1,L
C ZE=CDEXP(ZL(I)*TAU)
C ZAI=ZAI+ZC(I)*(ZE*(ZL(I)*CT1+OMEGA*ST1)-ZL(I)*CT-OMEGA*ST)/
C .(OMEGA**2+ZL(I)**2)
C ZBI=ZBI+ZC(I)*(ZE*(ZL(I)*ST1-OMEGA*CT1)-ZL(I)*ST+OMEGA*CT)/
C .(OMEGA**2+ZL(I)**2)
10 CONTINUE
C AI=DA1+GA1+HA1+XAI(1)
C BI=DB1+GB1+HB1+XBI(1)
C
C COMPUTE COEFFICIENTS FOR HARMONIC COMPONENTS

```

```

C
DO 100 M=1,NCOEFF
N=NHAR(M)
OMEGAN=OMEGA*N
WRITE(6,113) N,OMEGAN
113 FORMAT(1H ,/, ' N=',I2,' OMEGAN=',D15.6)
OMPLUS=OMEGA*(N+1)
OMINUS=OMEGA*(N-1)
CT1=DCOS(OMEGAN*TI1)
CT=DCOS(OMEGAN*TI)
ST1=DSIN(OMEGAN*TI1)
ST=DSIN(OMEGAN*TI)

C
DAN=D*(ST1-ST)/OMEGAN
GAN=G*((DSIN(OMINUS*TI1)-DSIN(OMINUS*TI))/(2.D0*OMINUS)
.+ (DSIN(OMPLUS*TI1)-DSIN(OMPLUS*TI))/(2.D0*OMPLUS))
HAN=H*((DCOS(OMINUS*TI1)-DCOS(OMINUS*TI))/(2.D0*OMINUS)
.+ (DCOS(OMPLUS*TI1)-DCOS(OMPLUS*TI))/(2.D0*OMPLUS))

C
DBN=D*(CT-CT1)/OMEGAN
GBN=G*((DCOS(OMINUS*TI1)-DCOS(OMINUS*TI))/(2.D0*OMINUS)
.+ (DCOS(OMPLUS*TI1)-DCOS(OMPLUS*TI))/(2.D0*OMPLUS))
HBN=H*((DSIN(OMINUS*TI1)-DSIN(OMINUS*TI))/(2.D0*OMINUS)
.+ (DSIN(OMPLUS*TI1)-DSIN(OMPLUS*TI))/(2.D0*OMPLUS))

C
ZAN=DCOMPLX(0.D0,0.D0)
ZEN=DCOMPLX(0.D0,0.D0)
DO 20 I=1,L
WRITE(6,111) ZL(I)
ZK=OMEGAN**2+ZL(I)**2
WRITE(6,111) ZK
ZE=CDEXP(ZL(I)*TAU)
ZAN=ZAN+ZC(I)*(ZE*(ZL(I)*CT1+OMEGAN*ST1)-ZL(I)*CT-OMEGAN*ST)/
.(OMEGAN**2+ZL(I)**2)
WRITE(6,111) ZAN
ZEN=ZEN+ZC(I)*(ZE*(ZL(I)*ST1-OMEGAN*CT1)-ZL(I)*ST+OMEGAN*CT)/
.(OMEGAN**2+ZL(I)**2)
WRITE(6,111) ZEN
20 CONTINUE
111 FORMAT(1H ,/,2(D15.6,1X))
AI(M)=DAN+GAN+HAN+XAN(1)
BI(M)=DBN+GBN+HBN+ZEN(1)
100 CONTINUE
RETURN
END

```